

Doctoral Thesis

博士論文

A Biosensing Platform Based on G-Quadruplex DNA-  
Functionalized Gold Nanoparticles

(DNA四重鎖修飾金ナノ粒子を用いたバイオセンサーに関する研究)

スラチャダ チュアイチョブ

Surachada Chuaychob

**Doctoral Thesis**

**博士論文**

**A Biosensing Platform Based on G-Quadruplex DNA-  
Functionalized Gold Nanoparticles**

**(DNA四重鎖修飾金ナノ粒子を用いたバイオセンサーに関する研究)**

**スラチャダ チュアイチョブ**

**Surachada Chuaychob**

**Department of Advanced Materials Science**

**Graduate School of Frontier Sciences**

**The University of Tokyo**

**July 2020**

## **Preface**

This dissertation is the collection of the studies, which have been accomplished at the Department of Advanced Materials Science, Graduate School of Frontier Sciences, The University of Tokyo and Bioengineering Laboratory, RIKEN Cluster for Pioneering Research under the direction of Professor Mizuo Maeda from September 2017 to July 2020. I would like to express my sincere appreciation and respect to Professor Mizuo Maeda for his continuous guidance, encouragement, and heartwarming support throughout my work.

I would also like to express my great gratitude to Professor Kae Sato (Japan Woman's University), Professor Yuji Sasaki, Professor Katsuhiko Ariga, and Professor Nubuhiko Hosono for their careful reviewing and helpful suggestions on the thesis.

Over the past years, I appreciated having a chance to collaborate with excellent scientists. I am indebted to Dr. Masahiro Fujita (Senior Research Scientist, Bioengineering Laboratory, RIKEN Cluster for Pioneering Research) for his guidance, assistance, and untiring support. He has imparted to me so much valuable knowledge through his insightful advice that will benefit me a whole lifetime. Moreover, several people have been a source of support and inspiration. I would like to express my sincere thanks to Mr. Takafumi Sako (The University of Tokyo), Mr. Yoshifumi Sakamoto (Tokyo Denki University), for their kind assistance along these years. Without whose cooperation, I would not have been able to conduct this work smoothly.

Furthermore, I would like to express my sincere appreciation to Mr. Li Yu for his kindness and support since my application of a doctoral course until my graduation. I would like to express my sincere gratitude to Ms. Masumi Furumoto, Ms. Kumiko Matsumoto, Ms. Naoko Nakata, Ms. Akiko Nakamura, Ms. Hiromi Ito, Mr. Rodtichoti Wannapob, and all the other members of Bioengineering Laboratory for their support, kindness, and friendship. I also thank the staff at The University of Tokyo, Ms. Yukiko Tan, Ms. Sachie Iimura, and Ms. Kiwa Ito for their kind operation, mainly document works. I am also grateful to Ms. Tomoka Kikitsu and Ms. M. Kikuya (RIKEN Center for Emergent Matter Science) for their technical supports and insightful comments.

Besides, I am greatly indebted to the following scholarship and research funding program for their generous support of my research: the International Program Associate (IPA) Foundation provided by RIKEN and the Academic Research Grant for GSFS Doctor Course Students supplied by The University of Tokyo.

Last but not least, I would like to express my sincere appreciation to my parents, Mr. Chanid and Ms. Yupa Chuaychob, and my brother, Dr. Surachat Chuaychob, for supporting me all this time. Without their continued support, affection, and encouragement, I would not have been able to finish this doctoral thesis. They are the best family one could wish. I also would like to thank my best partner, Mr. Tzung-Ying Yang, for his warmhearted care and support during the whole process.

Surachada Chuaychob

July 2020



## Contents

<b>Chapter 1: General Introduction</b> .....	1
1.1 G-quadruplex DNA (G4 DNA) .....	2
1.2 Gold Nanoparticles (AuNPs) .....	4
1.3 Non-crosslinking Aggregation of DNA-AuNPs .....	4
1.4 Purpose of the Study .....	7
1.5 References .....	9
<b>Chapter 2: G-quadruplex DNA-Functionalized AuNPs for Detection of Hazardous Small Molecule “Cisplatin”</b> .....	12
2.1 Abstract .....	14
2.2 Introduction .....	15
2.3 Experimental Section .....	17
2.3.1 Materials .....	17
2.3.2 Design and Criterion .....	18
2.3.3 Preparation .....	18
2.3.3.1 Preparation of Diaqua-cisplatin, -carboplatin, and -oxaliplatin .....	18
2.3.3.2 Preparation of G4-AuNPs .....	19
2.3.4 Characterization of G4-AuNPs .....	20
2.3.5 Proof of Concept .....	22
2.3.6 Detection Mechanism .....	26
2.4 Results and Discussion .....	28
2.4.1 Optimization of Involving Parameters .....	28

2.4.2	Specificity .....	32
2.4.3	Analytical performance .....	34
2.5	Conclusions .....	36
2.6	References .....	37

### **Chapter 3: G-quadruplex DNA-Functionalized AuNPs for Detection of Macromolecule “Thrombin” .....**

3.1	Abstract .....	44
3.2	Introduction .....	45
3.3	Experimental Section .....	46
3.3.1	Materials .....	46
3.3.2	Design and Criterion .....	48
3.3.3	Preparation .....	49
3.3.3.1	Preparation of Proteins .....	49
3.3.3.2	Preparation of G4-AuNPs .....	49
3.3.4	Characterization of G4-AuNPs .....	49
3.3.5	Proof of Concept .....	51
3.3.6	Detection Mechanism .....	55
3.4	Results and Discussion .....	60
3.4.1	Optimization of Involving Parameters .....	60
3.4.2	Specificity .....	71
3.4.3	Analytical performance .....	73
3.4.4	Real Sample Analysis .....	75
3.5	Conclusions .....	79

3.6	References	80
<b>Chapter 4:</b>	<b>Non-crosslinking Aggregation via Inter-stranded Partial Hybridization</b>	<b>84</b>
4.1	Abstract	85
4.2	Introduction	86
4.3	Experimental Section	89
4.3.1	Materials	89
4.3.2	Design and Criterion	89
4.3.3	Preparation	92
4.3.3.1	Preparation of G4–AuNPs	92
4.3.4	Characterization of pH-induced Structural Arrangement	93
4.3.5	Characterization of G4-AuNPs	93
4.3.6	Proof of Concept	95
4.3.7	Detection Mechanism	97
4.4	Results and Discussion	100
4.4.1	Optimization of Involving Parameters	100
4.5	Conclusions	108
4.6	References	109
<b>Chapter 5:</b>	<b>General Conclusions and Perspective</b>	<b>111</b>
<b>Bibliography</b>		<b>113</b>

## **Chapter 1**

### **General Introduction**

## 1.1 G-quadruplex DNA (G4 DNA)

G-quadruplex (G4) DNA is the most famous structure of DNA that forms highly ordered structures. G4 DNA is a sequence containing many Guanine bases, or Guanine-rich sequence<sup>1</sup>. In the guanine-rich (G-rich) sequence, the discrete four-stranded structures formed by the stacking of planar guanines (G-tetrad) via Hoogsteen hydrogen bonding. The G-tetrad structure is stabilized by monovalent cation ( $M^+$ ), most frequently potassium or sodium cations, which connected by electrostatic interactions on the guanine carbonyls<sup>2-4</sup>. In the G4 sequence, a number of guanine shows the number of layers and other bases between guanine bases are denoted as loops, which can be any bases. For example, thrombin-binding aptamer<sup>5-6</sup> (TBA) G4 consists of two-layer of G-tetrads and contains thymine (T) and guanine (G) on the loops, as shown in Fig. 1.1.

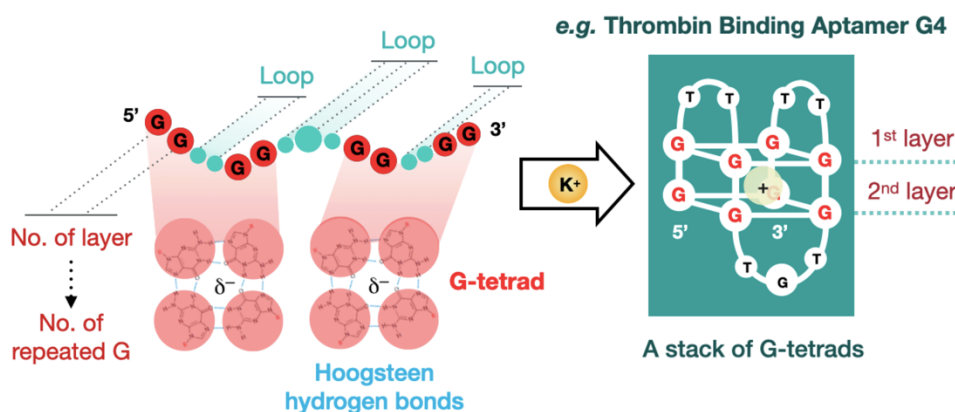
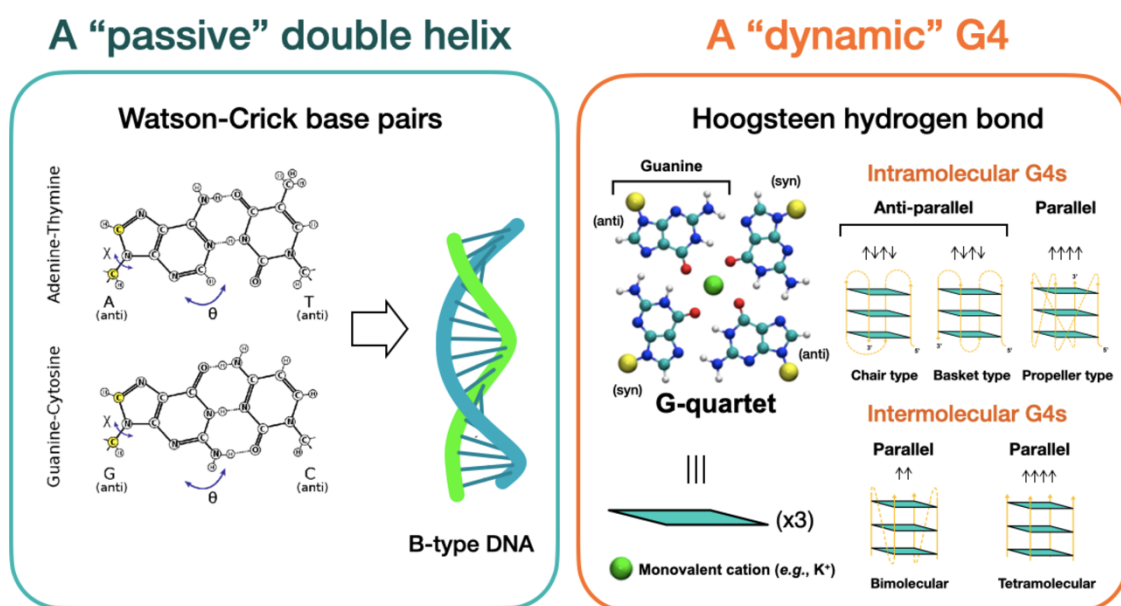


**Figure 1.1** Structural components of G4 DNA: repeated guanines, loops, G-tetrad, Hoogsteen hydrogen bond (blue dash line), and a cation.

Generally, the iconic image of DNA is recognized as a “passive” double-helical structure<sup>7-8</sup>, as shown in Fig. 1.2. It is, however, evident that DNA is a very “dynamic”

molecule capable of forming many arrangements from recent experiments. On top of that, ~3% of the human genome, which is expressed in protein, may adopt non-canonical secondary structures<sup>9</sup> that are functionally important, including G4 DNA. G4 shows a variety of topologies<sup>10</sup> such as chair type, basket type, and propeller type, regarding the various possible combinations of strand direction (parallel and antiparallel) as well as variations of loop size and sequence (Fig. 1.2). G4 DNA can also act as an aptamer<sup>11</sup>, which recognizes with high-affinity specific targets such as proteins, small molecules, and ions. Thus, G4 aptamer is expected to be used as a promising molecular tool targeted toward biologically important ligands.



## 1.2 Gold Nanoparticles (AuNPs)

Gold nanoparticles (AuNPs) possess remarkable optical properties and are widely used in colorimetric detection. Regarding, colorimetric sensors have gained much attention in recent years because they are suitable for simple, fast, and on-site detection.<sup>12</sup> AuNPs have localized surface plasmon resonance in the visible region with a high extinction coefficient.<sup>13</sup> Colloidal AuNPs with a diameter of a few tens of nanometres is vivid red in color. Because the plasmon resonance depends on interparticle plasmon coupling in addition to particle size, the particle aggregation causes a bathochromic shift from red to purple-blue.<sup>14-16</sup> Owing to this unique optical property, target-induced aggregation of AuNPs is a critical event for colorimetric sensing.<sup>17</sup> The aggregation is achieved primarily by a chemical interaction between the modified AuNPs, *e.g.*, binding of a recognition element to target analytes such as sugar, heavy metal, cancerous cells, etc.<sup>18-20</sup>

## 1.3 Non-crosslinking Aggregation of DNA–AuNPs

Principally, there are two aggregation behaviors of DNA-functionalized gold nanoparticles (DNA-AuNPs); crosslinking<sup>21</sup> and non-crosslinking<sup>22</sup> aggregations, which the red color of colloidal solution change to purple takes place within several minutes afterward. Generally, the target of interest acts as a crosslinker between AuNPs, resulting in cross-linking aggregation. The discovery of crosslinking aggregation of DNA-AuNPs<sup>21</sup> was proposed by Mirkin and coworker in 1996 (Fig. 1.3a). AuNPs immobilization with single-stranded DNA (ssDNA-AuNPs) shows the high colloidal stability due to the

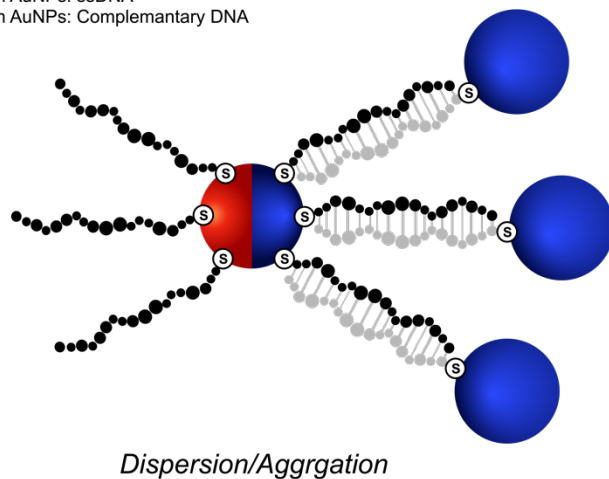
generation of interparticle electrostatic and steric repulsions resulting from the properties of ssDNA. Notably, if AuNPs are hybridized with target DNAs, the particles aggregate under this condition due to the DNA duplex-linked particle aggregation. The crosslinking system requires a period of time for a complete hybridization due to the dominant kinetic based on random collisions between the NPs with relatively slow Brownian motion<sup>23</sup>.

Non-cross-linking aggregation, on the other hand, has been reported a decade ago by Maeda and coworker<sup>22</sup>. In the first proposal, ssDNA is grafted on AuNPs (Fig. 1.3b). Regarding the negative charge and flexibility of DNA strands, ssDNA-AuNPs stably dispersed by the electrostatic and steric repulsions on particle surface in the colloidal system with high salt concentration. After complementary hybridization in perfect sequence and chain length, the colloidal stability of ssDNA-AuNPs was disturbed by the reduction of entropic effect—that is, the conformational change from highly flexible ssDNA to rigid double-stranded DNA (dsDNA)—in addition to the salt screening. Interestingly, if duplex has a single-base mismatch at the 5' distal end, the particles remain to disperse even at high ionic strength due to the fraying motion of mismatch bases.



**(a) Crosslinking Aggregation of ssDNA-AuNPs**

Probe 1 on AuNPs: ssDNA  
Probe 2 on AuNPs: Complementary DNA



**(b) Non-crosslinking Aggregation of ssDNA-AuNPs**

Probe on AuNPs: ssDNA  
Target: Complementary DNA

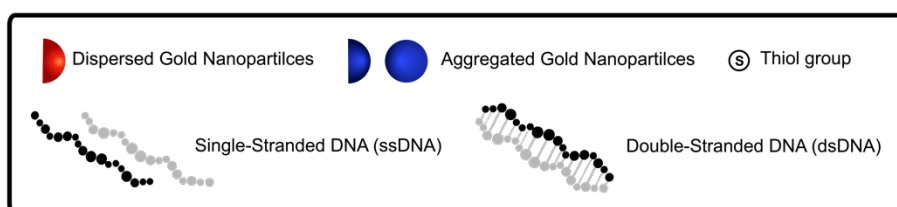
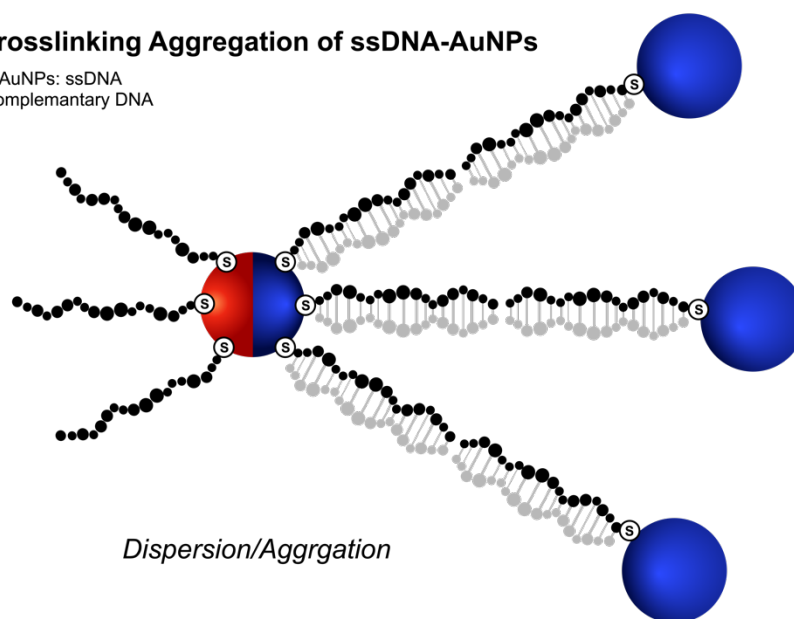


**Figure 1.3** Cross-linking (a) and non-crosslinking aggregations (b) of ssDNA-AuNPs.

Remarkably, the change in the physical properties on the particle surfaces highlights as a key concept for the non-crosslinking system, which is driven by the London–van der Waals attractive force between the NPs when the repulsive interaction is greatly reduced by the formation of duplexes on their surfaces.

Fig. 1.3 shows some samples of such systems, for example, DNA-linked particle aggregation, in which complementary DNA targets act as a crosslinker between the particles as well as DNA non-crosslinked particle, in which DNA targets does not act as a crosslinker between the particles, on the contrary. The colorimetric change of red to purple-blue places the advantages, *i.e.*, simplicity, rapidity, and tunability, on a non-crosslinking approach over the crosslinking. Besides, the colloidal stability of DNA-AuNP based on non-crosslinking aggregation varies depending on DNA structure.

#### **1.4 Purpose of the Study**

Assuming that the change in DNA structure is a key role for non-cross-linking aggregation, other DNA conformational transitions could also induce the change of colloidal stability, or non-cross-linking aggregation. The highly polymorphic G4s are an outstanding candidate because the conformational change is expected to occur in response to binding with specific target molecules or environmental changes such as pH and temperature. The author attempts to prepare various G4 DNA-functionalized AuNPs and examine their colloidal stabilities depending on the conformational change of G4 structure. On the basis of the results, the author optimizes the colloidal system for biosensing applications of interest.

In this present study, the author had developed a new sensing element for molecular detections; (i) a small molecule “cisplatin”, and (ii) a macromolecule “thrombin”, that could be utilized as a novel sensing platform in sensing application. Besides, a new aggregation mechanism of non-crosslinking behavior was firstly proposed using G4-AuNPs, so-called “partial hybridization-induced non-crosslinking aggregation”. In this regard, the characteristics and properties of G4-AuNPs as aforementioned was described in chapters 2, 3, and 4, which is the main body of this thesis.

## 1.5 References

- (1) Pearson, C.E.; Sinden, R.R. Trinucleotide Repeat DNA structures: Dynamic Mutations from Dynamic DNA. *Curr. Opin. Struct. Biol.* **1998**, *8*, 321–330.
- (2) Huppert, J. L. Hunting G-quadruplexes. *Biochimie* **2008**, *90*, 1140–1148.
- (3) Huppert, J. L. Structure, location and interactions of G-quadruplexes. *FEBS J.* **2010**, *277*, 3452–3458.
- (4) Keniry, M. A. Quadruplex Structures in Nucleic Acids. *Biopolymers* **2001**, *56*, 123–146.
- (5) Bock, L. C.; Griffin, L. C.; Latham, J. A.; Vermaas, E. H.; Toole, J. J. Selection of Single-Stranded DNA Molecules That Bind and Inhibit Human Thrombin. *Nature* **1992**, *359*, 710–713.
- (6) Macaya, R. F.; Schultze, P.; Smith, F.W.; Roe, J. A.; Feigon, J. Thrombin-Binding DNA Aptamer Forms a Unimolecular Quadruplex Structure in Solution. *Proc. Natl. Acad. Sci. USA* **1993**, *90*, 3745–3749.
- (7) Yakovchuk, P.; Protozanova, E.; Frank-Kamenetskii, M. D. Base-Stacking and Base-Pairing Contributions into Thermal Stability of the DNA Double Helix. *Nucleic Acids Res.* **2006**, *34*, 564–574.
- (8) Watson, J. D.; Crick, F. H. C. Molecular Structure of Nucleic Acids; A Structure for Deoxyribose Nucleic Acid. *Nature* **1953**, *171*, 737–738.
- (9) Branislav, R.-N.; Jiri, K.; Lukas, N.; Darina, M.; Rene, K.; Vojtech, Adam. G Quadruplexes as Sensing Probes. *Molecules* **2013**, *18*, 14760–14779.
- (10) Burge, S.; Parkinson, G. N.; Hazel, P.; Todd, A. K.; Neidle, S. Quadruplex DNA: Sequence, topology and structure. *Nucleic Acids Res.* **2006**, *34*, 5402–5415.

- (11)Roxo, C.; Kotkowiak, W.; Pasternak, A. G-Quadruplex-Forming Aptamers—Characteristics, Applications, and Perspectives. *Molecules* **2019**, *24*, 3781.
- (12)Sankoh, S.; Thammakhet, C.; Numnuam, A.; Limbut, W.; Kanatharana, P.; Thavarungkul, P. 4-mercaptophenylboronic acid functionalized gold nanoparticles for colorimetric sialic acid detection. *Biosens. Bioelectron.* **2016**, *85*, 743–750.
- (13)Liu, X.; Atwater, M.; Wang, J.; Huo, Q. Extinction coefficient of gold nanoparticles with different sizes and different capping ligands. *Colloids Surf. B. Biointerfaces* **2007**, *58*, 3–7.
- (14)Su, K. H.; Wei, Q. H.; Zhang, X.; Mock, J. J.; Smith, D. R.; Shultz, S. Interparticle coupling effects on plasmon resonances of nanogold particles. *Nano Lett.* **2003**, *3*, 1087–1090.
- (15)Huang, X.; El-Sayed, M. A. Gold nanoparticles: Optical properties and implementations in cancer diagnosis and photothermal therapy. *J. Adv. Res.* **2010**, *1*, 13–28.
- (16)Yeh, Y. C.; Creran, B.; Rotello, V. M. Gold nanoparticles: preparation, properties, and applications in bionanotechnology. *Nanoscale* **2012**, *4*, 1871–1880.
- (17)Saha, K.; Agasti, S. S.; Kim, C.; Li, X.; Rotello, V. M. Gold nanoparticles in chemical and biological sensing. *Chem. Rev.* **2012**, *112*, 2739–2779.
- (18)Daniel, M. C.; Astruc, D. Gold nanoparticles: assembly, supramolecular chemistry, quantum-size-related properties, and applications toward biology, catalysis, and nanotechnology. *Chem. Rev.* **2004**, *104*, 293–346.
- (19)Laderman, E. I.; Whitworth, E.; Dumauual, E.; Jones, M.; Hudak, A.; Hogrefe, W.; Carney, J.; Groen, J.; Rapid, sensitive, and specific lateral-flow immunochromatographic point-of-care device for detection of herpes simplex virus

- type 2-specific immunoglobulin G antibodies in serum and whole blood. *Clin. Vaccine Immunol.* **2008**, 15, 159–163.
- (20) Qin, L.; Zeng, G.; Lai, C.; Huang, D.; Zhang, C.; Xu, P.; Hu, T.; Liu, X.; Cheng, M.; Liu, Y.; Hu, L.; Zhou, Y. A visual application of gold nanoparticles: Simple, reliable and sensitive detection of kanamycin based on hydrogen-bonding recognition. *Sens. Actuators B* **2017**, 243, 946–954.
- (21) Mirkin, C. A.; Letsinger, R. L.; Mucic, R. C.; Storhoff, J. J. A DNA-based Method for Rationally Assembling Nanoparticles into Macroscopic Materials. *Nature* **1996**, 382, 607–609.
- (22) Sato, K.; Hosokawa, K.; Maeda, M. Rapid Aggregation of Gold Nanoparticles Induced by Non-Cross-Linking DNA Hybridization. *J. Am. Chem. Soc.* **2003**, 125, 8102–8103.
- (23) Lin, Y.-W.; Liu C.-W.; Chang, H.-T. DNA Functionalized Gold Nanoparticles for Bioanalysis. *Anal. Methods*, **2009**, 1, 14–24.

**Chapter 2**

**G-quadruplex DNA-Functionalized AuNPs for Detection of Hazardous  
Small Molecule “Cisplatin”**

Inspired by the unique architecture of G4 DNA in the human genome and their important reaction to drug treatment and biological processes in the human body, the G-quadruplex-grafted gold nanoparticles were proposed as a new powerful sensing element. The proposed nano-biosensor was evaluated the performance using two types of the target of significant difference in molecular size; “small molecule”, *e.g.*, cisplatin, and “macromolecule”, *e.g.*, thrombin protein. The targets may unfold and destabilize G-quadruplexes or bind and stabilize G4s (Fig. 2.1), leading to a decrease or an increase in the detection signal. Conditions of detection can be optimized to be compatible with the applications of interest, which became a prospective cohort study.

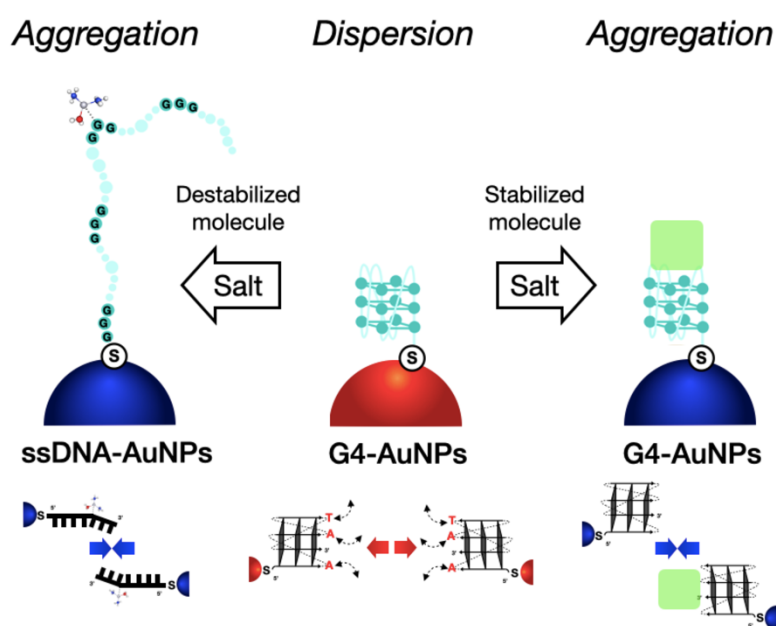


**Figure 2.1** Non-crosslinking aggregations of G4-AuNPs.



## 2.1 Abstract

A novel colorimetric sensor based on G-quadruplex-functionalized gold nanoparticles (G4-AuNPs) for a hazardous small molecule “cisplatin” through non-crosslinking aggregation was demonstrated. In this study, the G4 DNA and AuNPs were utilized as a sensing probe and a signal enhancer, respectively. The modification of AuNPs with G4 strands stably dispersed in the colloidal system, resulting in a red color solution. In the existence of cisplatin, the color of the colloidal solution changed to purple-blue in a short time due to the colloidal aggregation, so-called a colorimetric detection. The cisplatin coordinates at N7 guanine base of G4 as cisplatin-DNA adduct formation. The stability of G4-AuNPs significantly disturbed by the adduct formation that probably caused a reduction in steric repulsion. It is corresponded to the unfolding of the G4 strand, inducing the non-crosslinking aggregation of the particles. The maximum absorption wavelength shifts increasing from the aggregation, which is the degree of colorimetric change, varied with the cisplatin concentration. At room temperature, the developed sensor provided the linearity in the range of 15.0 to 30.0  $\mu\text{M}$  and the detection limit of 12.9  $\mu\text{M}$  with a correlation coefficient greater than 0.99. Besides, this sensor was found to response to cisplatin faster than other analogues such as carboplatin and oxaliplatin, suggesting that this system has a high specificity for cisplatin detection.

## 2.2 Introduction

The Food and Drug Administration (FDA) approved cisplatin as antineoplastic drugs in 1978<sup>1,2</sup>. Cisplatin is the first platinum-based drug in alkylating agent group, that has the smallest molecule (11 atoms) among other drugs. In clinical treatment, cisplatin can use alone and administer in combination with other medications. The primary target of cisplatin is genomic DNA, specifically the N7 position of guanine bases. Cisplatin-DNA adduct is a product of cisplatin, positively charged active diaquated  $[\text{Pt}(\text{NH}_3)_2(\text{H}_2\text{O})_2]^{2+}$ , coordinated with one (mono-adduct) or two guanine bases (di-adduct)<sup>3-5</sup> to afford an intrastrand crosslink. The mono-adduct formation occurs rapidly than the di-adduct, which forms and binds predominantly to the dsDNA target.<sup>3,4,6</sup> The formation of these adducts deforms the helices and disrupts DNA replication, resulting in programmed cell death. A high concentration of cisplatin (800  $\mu\text{M}$ ), however, induces cell necrosis, giving rise to severe side effects, although a low concentration (8  $\mu\text{M}$ ) can cause cell apoptosis.<sup>7</sup> Cisplatin is suspect of being carcinogenic and categorized in a group 2A carcinogen by international agency for research on cancer (IARC). The side effects of cisplatin have been well-documented because it has non-selective mechanism of action<sup>8</sup>, affecting both cancerous and non-cancerous cells. The contamination of cisplatin in environment, *e.g.*, in patients' urine, has also been a serious problem.<sup>9,10</sup> Thus, a reliable method capable of detecting cisplatin at relevant levels is required.

Nowadays, cisplatin has been detected by a variety of analytical methods—that is, chromatography,<sup>11</sup> spectrometry,<sup>12</sup> fluorometry,<sup>13</sup> and electrochemistry<sup>14</sup>. Those approaches have, however, been shown the limit of complicated and/or long processes for sample preparation, and used the expensive equipment. In this study, the author proposes a simple and rapid colorimetric sensor with high specificity for cisplatin using

G-quadruplex (G4) DNA and non-crosslinking aggregation of AuNPs. The author follows unfolding of the G4 structure to single-stranded DNA (ssDNA) after cisplatin binds to the N7 atom of guanine, which stabilizes the G-quartet via Hoogsteen hydrogen bonding.<sup>15-18</sup>, or the formation of cisplatin-DNA adduct. The structural change might induce the reduction of the colloidal stability, leading to non-crosslinking aggregation of the particle (Fig. 2.2). Thus, it is possible to realize cisplatin detection by colorimetric change in a short time.

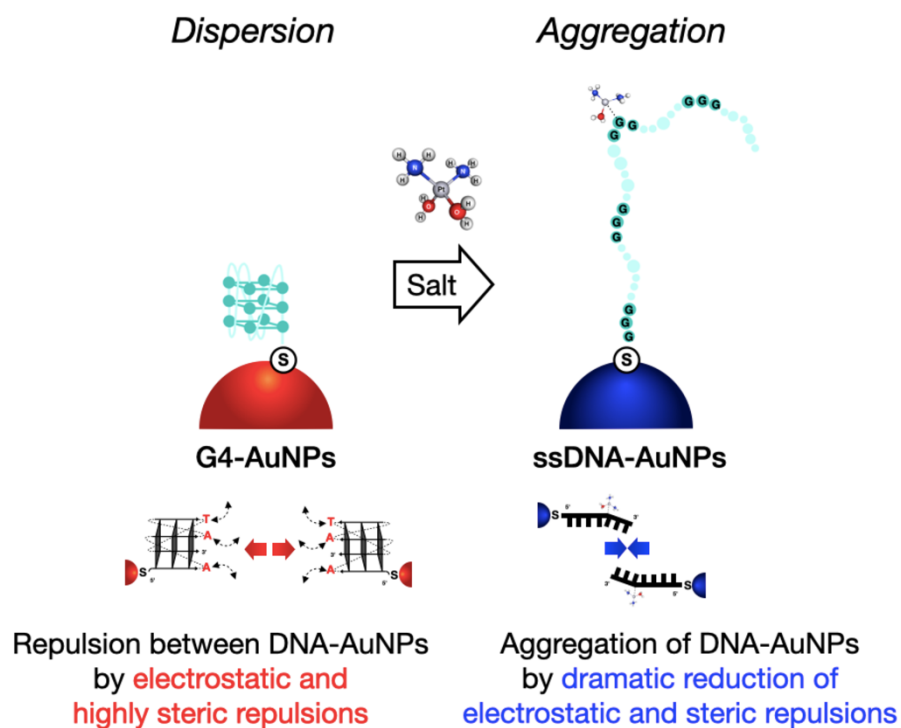


**Figure 2.2** Non-crosslinking aggregation of G4-AuNPs induced by cisplatin-DNA adduct formation.

## 2.3 Experimental Section

### 2.3.1 Materials

15 or 40 nm in diameter of AuNPs were purchased from British Biocell International (Cardiff, UK). The estimation of the real sizes of AuNPs was done by transmission electron microscopy (TEM) (JEM-1230, JEOL, Tokyo) operated at 80 kV (Fig. 2.7). The mean radii of 15 and 40 nm AuNPs were 7.47 ( $\pm$  0.37) and 19.0 ( $\pm$  1.6) nm, respectively. A sulfhydryl group at their 5'-end modified oligo-DNA were purchased from Eurofins Genomics K.K. (Tokyo), and purified by an affinity column (oligonucleotide purification cartridge (OPC); Thermo Fisher Scientific, Waltham, MA) prior to use. Three different types of G4 conformation were used—the chair- (21CTA), basket- (22AG), and propeller-type (35B1 (Kras)) conformations—which incorporated 21, 22, and 35 nucleotides (nt).<sup>19-22</sup> Fig. 2.10 shows these conformations and Table 2.1 shows the list of their sequences. Cisplatin (pharmaceutical secondary standard grade), oxaliplatin (European Pharmacopoeia Reference Standard), silver nitrate ( $\text{AgNO}_3$ ), ethylenediaminetetraacetic acid (EDTA), dithiothreitol (DTT), and carboplatin (analytical grade) were purchased from Sigma-Aldrich (St. Louis, MO). Phosphoric acid ( $\text{H}_3\text{PO}_4$ ) was purchased from Junsei Chemical (Tokyo). Dipotassium hydrogen phosphate ( $\text{K}_2\text{HPO}_4$ ) and sodium nitrate ( $\text{NaNO}_3$ ) were purchased from Wako Pure Chemical Industries (Osaka, Japan). Milli-Q water (resistivity greater than 18.2 M $\Omega$  cm) was used for all experiments.

### 2.3.2 Design and Criterion

Three different types of G4 topology were examined; 21, 22, and 35-nucleotide (nt) for chair-, basket-, and propeller-type conformations, respectively. The sequences of G4s are shown in Table 2.1.

**Table 2.1** DNA sequences of G4 used in this study.

Name	Sequence (from 5' to 3')	Length (base)
21CTA (Chair-type)	HS-(CH <sub>2</sub> ) <sub>6</sub> - <u>GGGCTAGGGCTAGGGCTAGGG</u>	21
22AG (Basket-type)	HS-(CH <sub>2</sub> ) <sub>6</sub> - <u>AGGGTTAGGGTTAGGGTTAGGG</u>	22
35B1 (Kras) (Propeller-type)	HS-(CH <sub>2</sub> ) <sub>6</sub> - <u>AGGGCGGTGTGGGAAGAGGGAAGAGGGGAGGCAG</u>	35

Note: GGG involved in folding the G4.

### 2.3.3 Preparation

#### 2.3.3.1 Preparation of Diaqua-cisplatin, -carboplatin, and -oxaliplatin

To generate the active diaqua-form of cisplatin, cisplatin dichloro-form (1.0 equivalent) added into 2.0 equivalents of AgNO<sub>3</sub> in aqueous media for hydrolysis at room temperature for 15 h in the dark.<sup>16</sup> In this step, the precipitation of silver chloride (AgCl) was formed by chloride anions dissociation from cisplatin, preventing the reversible reaction of cisplatin into the dichloro-form (Fig. 2.3). After 15-h incubation at 25 °C, AgCl was removed by two centrifugations at 15,000 rpm for 10 min at 4 °C. The diaqua-cisplatin solution was kept in the dark at 4 °C before use. The hydrolysis forms of

carboplatin and oxaliplatin were obtained by dissolving them in water, and these solutions were also kept in the dark at 4 °C before use.

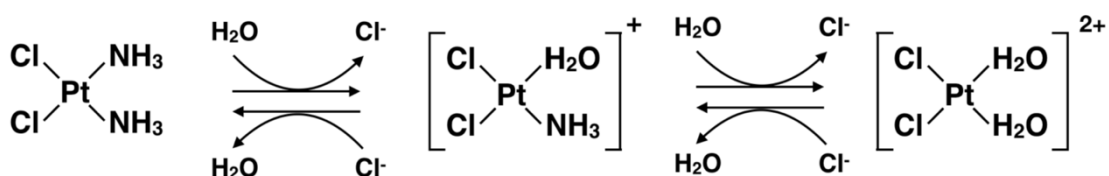


**Fig. 2.3** Hydrolysis of cisplatin dichloro-form (inactive species) to diaqua-form (active species)<sup>6</sup>.

### 2.3.3.2 Preparation of G4-AuNPs

3 nmol of the purified DNAs for 35-nt G4 or 6 nmol of the purified DNAs for 21- and 22-nt G4s was added to an aqueous solution of AuNPs with a concentration of  $2.3 \times 10^{-9}$  of 15 nm AuNPs or  $1.5 \times 10^{-10}$  M 40 nm AuNPs (one optical density (OD) at 520 nm). After incubation in the dark overnight at 50 °C, the solvent was replaced with 10 mM phosphate buffer ( $\text{K}_2\text{HPO}_4 / \text{H}_3\text{PO}_4$ ) (PB) (pH 5.0) containing 1.5 mM EDTA. Then the solution was kept at 50 °C overnight further. The potassium ion is necessary for the formation of quadruplex. Next,  $\text{NaNO}_3$  was added at a final concentration of 0.1 M to facilitate the immobilization of DNA strands. It should be noted that G4 remains in the initial conformation in the coexistence of potassium and sodium ions while some local details of the structure vary.<sup>23</sup> The resulting solution was kept at 50 °C for another day. The solution was centrifuged at 15,000 rpm for 30 min at 4 °C to remove unbound DNA

and re-dispersion of the precipitate was done in the same buffer. The G4-AuNP concentration was adjusted to about 1.0 OD at 520 nm, unless otherwise noted.

#### **2.3.4 Characterization of G4-AuNPs**

Prior to evaluate the DNA density, the compact structure of G4 has to unwind to single-stranded DNA (ssDNA) by removing the cation inside G-tetrad as follows. The G4-AuNP solution was heated at 95 °C for 10 min to deform the G4 structure, then the resulting solution was cooled down and holded at 4 °C for 10 min in EDTA solution (1.5 mM). EDTA chelated the cations to prevent reformation of G4. To quantify the number of grafted G4 strands on the surface of AuNP, a commercial assay was used. DTT was added to a final concentration of 1.0 M to release the strands from the particles.<sup>24</sup> After centrifugation at 15,000 rpm for 30 min (4 °C), the supernatant was treated using an OliGreen ssDNA Quantitation Assay Kit (Thermo Fisher Scientific, Waltham, MA). The resulting supernatant was measured fluorescence with a spectrofluorometer (FP-6500; JASCO, Tokyo). On the basis of a calibration line, the number of G4 strands was then estimated. The dispersion/aggregation or colloidal stability was estimated by UV-vis spectroscopy (UV-2550; Shimadzu, Kyoto, Japan) at 25 °C by scanning of the extinction spectra from 300 to 800 nm. The size and zeta potential of G4-AuNPs were measured with a Zetasizer Nano-ZS instrument (Malvern Instruments, Malvern, UK) at 25 °C.

The examination of size and the aggregation behavior of G4-AuNPs was measured using small angle X-ray scattering (SAXS). The SAXS measurements were performed at BL45XU RIKEN Structural beamline I of SPring-8, Japan. The wavelength ( $\lambda$ ) of X-ray was 0.1 nm. The camera length, calibrated using a silver behenate standard, was about 3.5 m. SAXS images were recorded with a PILATUS 3×2M detector (Dectris,

Baden, Switzerland) at 25 °C. The images were converted into one-dimensional intensity profiles by circular-averaging, as a function of scattering vector  $q = (4\pi \sin\theta) / \lambda$ , where  $2\theta$  is the scattering angle. The data were converted to the absolute intensity according to a published method.<sup>25</sup> The scattering intensity  $I(q)$  is usually expressed by

$$I(q) \propto P(q)S(q) \quad (1)$$

where  $P(q)$  and  $S(q)$  are the form and structure factors of the scattering object, respectively. If the objects disperse without interfering with each other,  $S(q)$  is equal to one. For a spherical particle with a radius  $R$ , the form factor is given by

$$P(q) \propto \int \left[ \frac{3\{\sin(qR) - qR \cos(qR)\}}{(qR)^3} \right]^2 D(R) dR \quad (2)$$

where  $D(R)$  is the distribution function of  $R$ . In this study, Gaussian distribution was applied as  $D(R)$ . The mean radius of G4-AuNPs was evaluated by curve fitting with Eq. 2. The structure factor  $S(q)$  is associated with the interference between the particles. The author obtained the experimental  $S(q)$  by dividing  $I(q)$  of the aggregated particles by that of the dispersed particles. Curve fitting with the calculated  $S(q)$  on the basis of paracrystalline theory was performed using a similar method as in our previous study.<sup>26</sup> A detailed description of the theoretical  $S(q)$  is found in Refs. 27 and 28. By analyzing  $S(q)$ , the author derived structural information such as the interparticle distance in the aggregates.



### 2.3.5 Proof Concept

The graft density for the G4 strands on AuNP with a diameter of 40 nm—that is, 98, 104, and 89 for the 21-, 22- and 35-nt G4s, respectively—was found to be lower than the case of ssDNA.<sup>26,29</sup> The G4-AuNPs showed a stable colloidal dispersion due to the electrostatic stability of the negative charge of the DNA phosphate group, and the steric stability of G4 structure, especially loop part in this case. The stability of G4-AuNPs decreased after cisplatin addition in the colloidal system because the formation of cisplatin-DNA adduct disrupts Hoogsteen hydrogen bond of G-tetrad, resulting in the reduction of the colloidal stability. The colloidal stability did not result in any change (Fig. 2.4a) after the addition of cisplatin at a low concentration of 0.1 M NaNO<sub>3</sub>. This caused a slight decrease in surface potential (Fig. 2.5, blue bars), suggesting cisplatin-DNA adduct formation. Interestingly, the plasmonic peak shifted to longer wavelength after cisplatin addition at a high salt concentration of 1.0 M, where the electrostatic repulsion is known to be subtle. This indicated the reduction of colloidal stability at high ionic strength, associating with the color change of colloidal solution to purple-blue with cisplatin concentration (Fig. 2.4b).

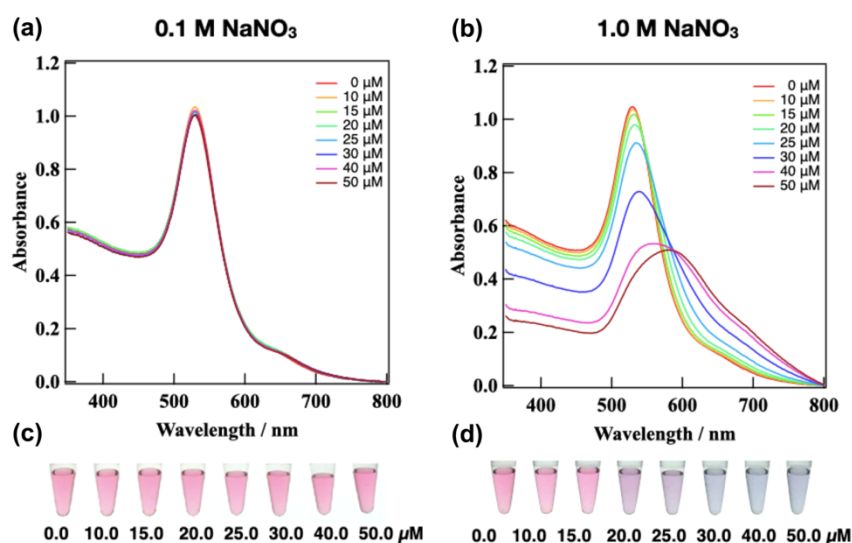


**Fig 2.4** UV-vis spectra of 35-nt G4-AuNPs in 10 mM PB (pH 5.0) containing 1.5 mM EDTA at 0.1 M (a) 1.0 M NaNO<sub>3</sub> (b), varied with cisplatin concentration. All data were gathered at 10 min after adding cisplatin. The corresponding 35-nt G4-AuNPs solutions at 0.1 M (c) 1.0 M NaNO<sub>3</sub> (d) at the various cisplatin concentrations: (a) 0, (b) 10, (c) 15, (d) 20, (e) 25, (f) 30, (g) 40, and (h) 50 μM.

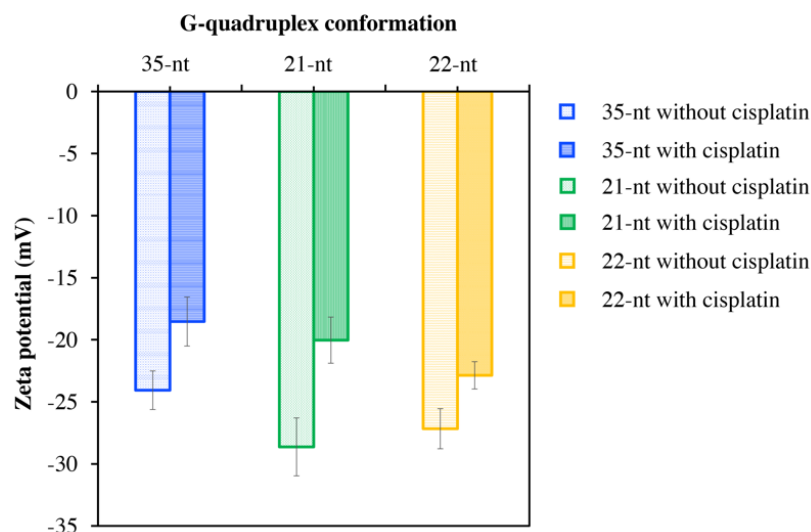


**Fig 2.5** Zeta potential data of 1.0 OD G4-AuNPs in 10 mM PB (pH 5.0) containing 1.5 mM EDTA and 0.1 M NaNO<sub>3</sub> after overnight incubation with (line-filled bar) and without (dash-filled bar) 150 μM of cisplatin.

The author further investigated the colloidal stability (dispersion/aggregation) of G4-AuNPs with cisplatin by SAXS. The SAXS data of 35-nt G4-AuNPs varied with the cisplatin concentration from 15 to 30  $\mu\text{M}$  (Fig. 2.6). The SAXS intensity profiles under a low (0.1 M) and high salt concentration (1.0 M) supported the notion that the particles remained dispersed and aggregated after cisplatin addition, respectively. At the high salt concentration of 0.1 M  $\text{NaNO}_3$ , the profiles of the dispersed particles were well fitted with Eq. 2, as shown by the solid curves in this figure. The mean radius from the fitting analysis (18.8 nm) agreed well with TEM data (19.0 nm) (Fig. 2.7). Besides, it was also comparable to the hydrodynamic radius  $R_h$  of unmodified AuNP (20.7 nm) rather than that of 35-nt G4-AuNP (24.9 nm), associating with the radius of core AuNP. It has been noted that the scattering by far heavier gold atoms is dominant.<sup>26</sup> At the high salt concentration (1.0 M  $\text{NaNO}_3$ ), Fig. 2.6b shows interference peaks at around  $q = 0.15 \text{ nm}^{-1}$  arose from the particle aggregation. The peak was clearly observed when cisplatin concentration increased. Fig. 2.6c shows the corresponding structure factors, analyzing by the assumption of a disordered face-centered cubic structure of the aggregate.<sup>26</sup> The center-to-center distance between the nearest neighbors was independent to cisplatin concentration. The gap between the particle surfaces due to the existence of the DNA layers was estimated at 13.1 nm. It was found that the height of three layers of G4 strand with the hexamethylene thiol linker of 1.5 nm was too short in comparison with the estimated value of 13.1 nm. This indicated that the large gap was most likely caused by the unfolding of the G4 structure.<sup>15,18</sup>

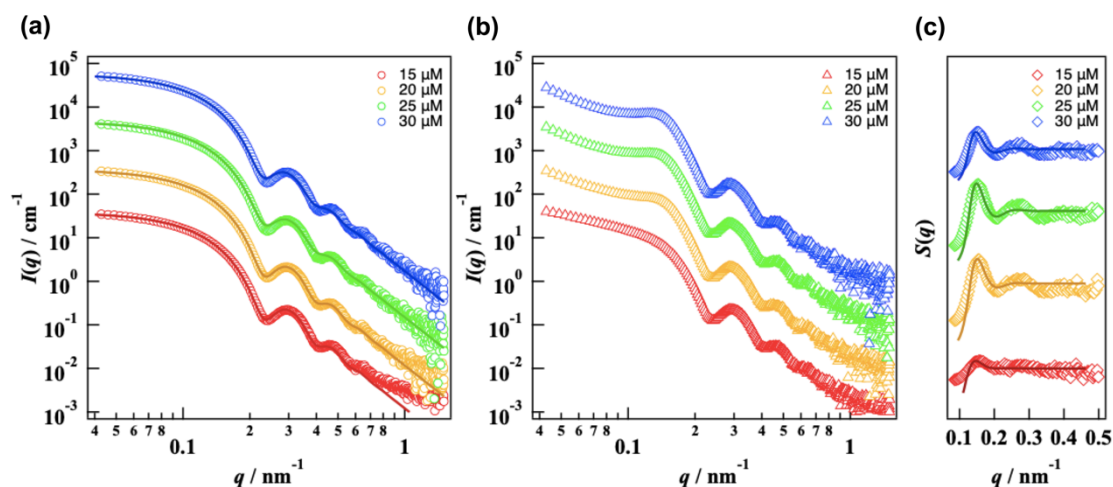


**Fig 2.6** SAXS intensity data for 35-nt G4-AuNPs in 10 mM phosphate buffer (pH 5.0) at 0.1 M  $\text{NaNO}_3$  (a) and 1.0 M  $\text{NaNO}_3$  (b), and the corresponding structure factors (c). The buffer contained 1.5 mM EDTA. The data were taken at various cisplatin concentrations: 15 (red), 20 (orange), 25 (green), and 30  $\mu\text{M}$  (blue). The solid lines in (A) and (C) are the fitting curves of form and structure factors, respectively.

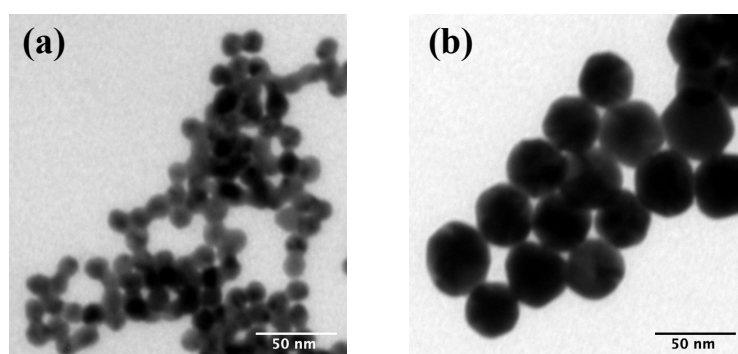


**Fig 2.7** TEM images of 15 nm (a) and 40 nm AuNPs (b). The mean radii and standard deviations for the smaller and larger AuNPs were estimated at  $7.47 \pm 0.37$  nm and  $19.0 \pm 1.6$  nm, respectively, from the TEM observations.

### 2.3.6 Detection Mechanism

On the basis of SAX analysis, there are two plausible styles of particle aggregation could account for the present results. On the one hand, if cisplatin molecules act as a crosslinker between the gold nanoparticles, the formation of cisplatin-DNA adduct, that cisplatin bound the interstrand DNA, would induce the crosslinking aggregation of the particles.<sup>30,31</sup> Previously, it had been reported that cisplatin basically covalently bound to neighboring nucleobases (*e.g.*, guanine-guanine) as intrastrand crosslink, undergoing di-adduct formation while the adducts of interstrand crosslink rarely formed.<sup>3,4</sup> Besides, during a short reaction time like that used here (*ca.* 10 min), most cisplatin molecules bind to only one guanine (*i.e.*, mono-adduct formation).<sup>18</sup> It thus seems extremely unlikely that cisplatin induces the crosslinking aggregation of particles. In fact, the platination of G4 did not drive the particle aggregation without electrostatic screening, as mentioned above (Fig. 2.4a,c and Fig. 2.5).

On the other hand, the reduction in steric repulsion by G4 structure deformation induces the particle aggregation, or non-crosslinking aggregation style.<sup>26,29,32</sup> In comparison, the aggregation of G4-AuNPs appears to against the previous discovery that AuNPs covered with flexible ssDNA show a high colloidal stability because of the entropic effect,<sup>26</sup> since presumably the unfolded DNA strands would be more flexible like ssDNA. The graft density of DNA was taking into account that it might be a key factor to ascribe behavior of the present aggregation. The author notices that the number of grafted G4 strands on AuNP surface was much lower, as mentioned above (90 - 100 strands/particle) than the case of immobilization of the usual oligo-ssDNA strands (*ca.* 400 strands/particle).<sup>26,29</sup> As a result, the particles after the formation of cisplatin-DNA adduct would have a similar appearance to AuNPs covered with a low density of grafted

ssDNA strands. The aforementioned process of non-crosslinking aggregation is schematically illustrated in Fig. 2.8. Even if ssDNA is flexible, such a coarse DNA layer cannot serve as a stabilizer to prevent the particle aggregation. Because the steric effect of coarse layer of the flexible DNA structure is lower than in the case of a rigid DNA structure.<sup>33</sup> The length of 35-nt DNA in an extended manner is *ca.* 15 nm by assuming that the pitch between neighboring nucleotides of ssDNA is 0.43 nm,<sup>34</sup> In fact, however, the DNA strands most likely lie and shrink, as supported by the discovery that the difference in  $R_h$  between the cisplatin-DNA adduct AuNPs and unmodified AuNPs was only 4.0 nm due to the coarse DNA layer. Regarding, the resulting particles might aggregate with the DNA strands being compressed, as shown in Fig. 2.8.

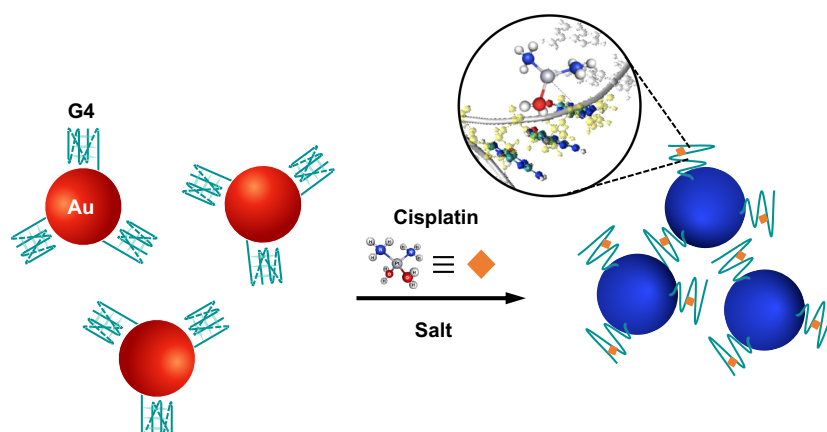


**Fig 2.8** A schematic illustration of cisplatin detection by G4-AuNPs. The deformation of G4 by the formation of cisplatin-monoadduct induces the non-crosslinking aggregation of the colloidal particles.

## 2.4 Results and Discussion

### 2.4.1 Optimization of Involving Parameters

Effect of particle size, G4-conformation, reaction time, and salt concentration was studied to get high performance of G4-AuNPs. The color of the G4-AuNP solution or particles aggregation changed with time after the addition of cisplatin (Fig. 2.9). In the absence of cisplatin, the dispersed particles showed an absorption peak at 529 nm as shown in Fig. 2.4. The degree of color change or progress of particle aggregation was thus investigated by the ratio of the absorption peak at 600 nm to that at 529 nm ( $A_{600} / A_{529}$ ). The time course of the absorption peak ratio is shown in Fig. 2.9a. In this figure, the data for both 15 nm and 40 nm AuNPs grafted with 35-nt G4 strands are shown. The degree of color change depended on AuNP size. The larger the particles, the greater the color change due to a larger van der Waals attraction arising between larger AuNPs. For rapid detection of cisplatin, the use of larger AuNP particles was thus more advantageous. Besides, it was found that the apparent color changes were saturated after 10 - 20 min. The author also investigated hydrodynamic diameter ( $D_h$ ) of such system. As shown in Fig. 2.9b, the apparent  $D_h$  increased over time in presence of cisplatin for any AuNP size, while the G4-AuNP size remained constant in the absence of cisplatin. The degree of colorimetric change and the progress of particle aggregation were corresponded well to each other.

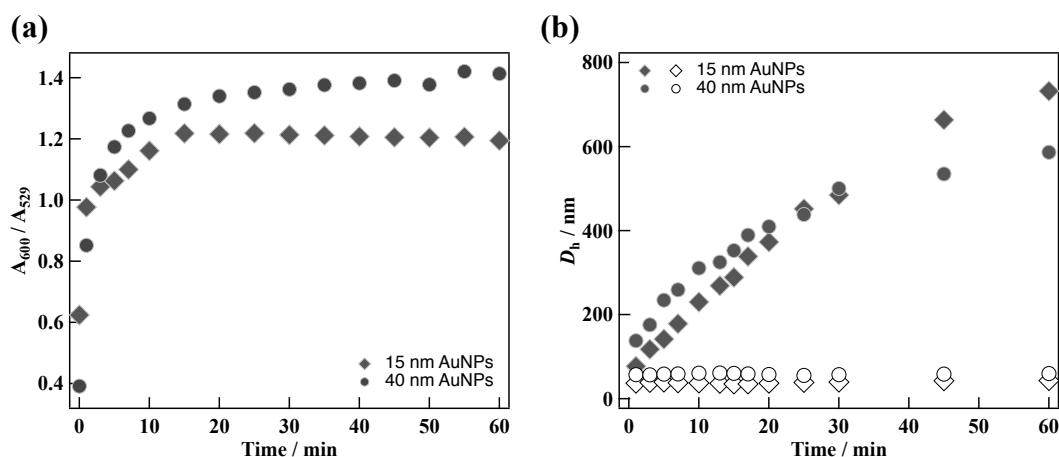


**Fig 2.9** (a) Time course of the absorption peak ratio ( $A_{600} / A_{529}$ ) after adding 50  $\mu\text{M}$  cisplatin for 15 nm and 40 nm AuNPs immobilized with 35-nt G4 in 10 mM PB (pH 5.0) including 1.5 mM EDTA at 1.0 M  $\text{NaNO}_3$ . (b) The corresponding change in hydrodynamic diameter is indicated with the filled symbols. The open symbols indicate data gathered in the absence of cisplatin.

Next, the effect of G4 conformation on the particle stability was investigated. In this study, two different conformations of G4, antiparallel chair-type (21-nt G4) and antiparallel basket-type (22-nt G4), were examined in addition to 35-nt G4 (*see* Fig. 2.10).<sup>20-22</sup> The author hypothesizes that different topologies would respond to cisplatin differently because of G4 structural stability and accessibility to guanine N7. The absorption ratios ( $A_{600} / A_{529}$ ) for 21-, 22-, and 35-nt G4-AuNPs (40 nm) are plotted against the concentration of cisplatin in Fig. 2.11a. The data were taken at 10 min, elapsed from cisplatin addition. The steepest slope was yielded from propeller-type conformation (35-nt G4) in the concentration range of 20 to 40  $\mu\text{M}$  cisplatin, while the chair-type (21-nt G4) and the basket-type (22-nt G4) conformations provided lower slopes but with wider linear ranges (25 to 50  $\mu\text{M}$  of cisplatin) (Fig. 2.11a). The slope is defined as



detection sensitivity, using as the criterion for choosing an optimum value. The resulting sensitivities for 35-nt, 22-nt, and 21-nt G4s are 0.038, 0.033, and 0.024  $\mu\text{M}^{-1}$ , respectively. It is likely because the propeller-type 35-nt G4 exposes a planar guanine tetrad, or so-called G-quartet, into solution (Fig. 2.10a). The chair-type 21-nt and the basket-type 22-nt G4s (Fig. 2.10b), however, protrude two loops consisting of two bases per loop and three bases per loop into solution, respectively.<sup>20-22</sup> More such a loop, more difficult the cisplatin accesses to a planar guanine tetrad of G4. Hence, cisplatin unfolds the propeller-type 35-nt G4 more rapidly than the others, resulting in the highest detection sensitivity.

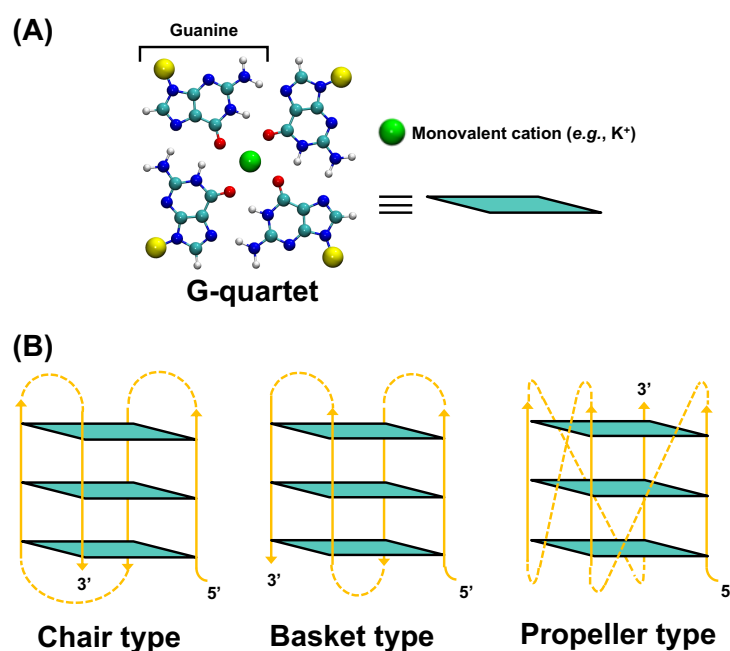


**Fig 2.10** (a) Structure of G-quartet. The yellow and green beads represent the sugar-phosphate residue and the monovalent cation ( $\text{K}^+$ ), respectively. (b) Three different G4 structures with three stacks of G-quartet are illustrated: the chair-, basket-, and propeller-types, which correspond respectively to 21CTA, 22AG, and 35B1 (Kras) investigated in this study.

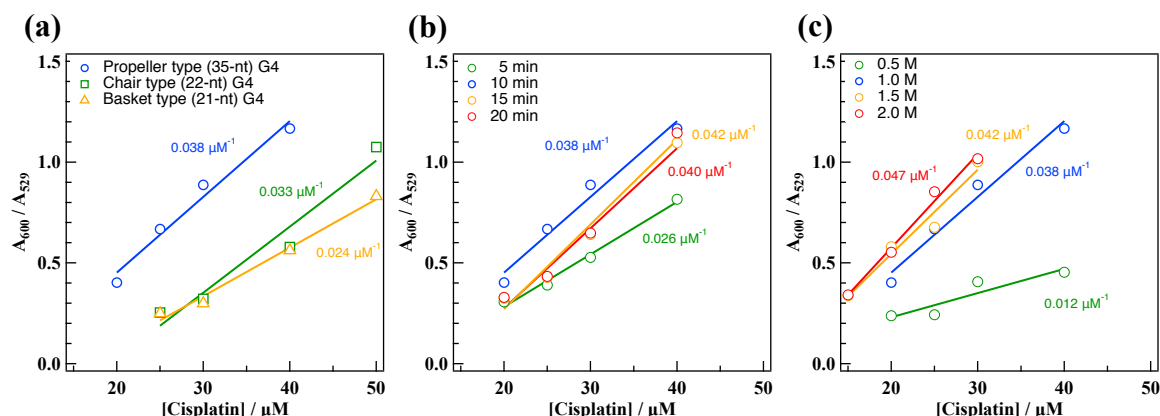


**Fig 2.11** Effects of G4-conformation (a), reaction time (b), and  $\text{NaNO}_3$  concentration (c) on cisplatin detection. In (a), the chair-type (21-nt), basket-type (22-nt), and propeller-type (35-nt) G4 strands were immobilized with 40 nm AuNPs. UV-vis spectra of 35-nt G4-AuNPs in 10 mM PB (pH 5.0) including 1.5 mM EDTA and 1.0 M  $\text{NaNO}_3$  were taken under different cisplatin concentrations. The reaction time was 10 min. The absorption peak ratios ( $A_{600} / A_{529}$ ) were plotted against the cisplatin concentration, together with fitted lines. In (b), the data were evaluated for 35-nt G4-AuNPs (40 nm) in 10 mM PB (pH 5.0) including 1.5 mM EDTA and 1.0 M  $\text{NaNO}_3$ . In (c), the data were evaluated for 35-nt G4-AuNPs (40 nm) in 10 mM PB (pH 5.0) including 1.5 mM EDTA at various  $\text{NaNO}_3$  concentrations. The reaction time was 10 min. In all panels, the values indicate the slopes of the fitted lines, or the sensitivity.

Then the effect of the reaction time after the addition of cisplatin was also investigated, and the detection sensitivity was similarly studied. Fig. 2.11b shows that the sensitivity considerably increased when the reaction time increased from 5 to 10 min. Then the sensitivity remained constant after 10 min. The shortest reaction time with high sensitivity is preferable, and 10 min, thus, was used as the optimum reaction time.

The effect of salt concentration is the last parameter to evaluate for the cisplatin detection. It can be seen that the non-crosslinking aggregation was induced by the addition of salt because of the screening of the electrostatic repulsion. The sensitivity reasonably increased when the concentration of  $\text{NaNO}_3$  increased (Fig. 2.11c). It was found that the sensitivity at 1.0 - 1.5 M  $\text{NaNO}_3$  shown no significant difference with high detection sensitivity. Hence, 1.0 M  $\text{NaNO}_3$  is high enough to detect cisplatin.

#### 2.4.2 Specificity

Cisplatin is the most popular among the platinum-based alkylating agents currently used in clinical treatment. It can be used alone or in combination with other drugs such as carboplatin and oxaliplatin in clinical treatment, as shown in Fig. 2.12.<sup>35</sup>

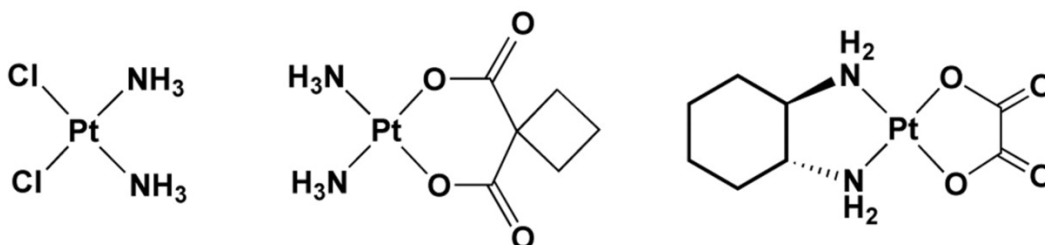


**Fig 2.12** Representation of the platinum-based alkylating agents: (left) cisplatin (11 atoms with two leaving chloride ( $\text{Cl}^-$ ) atoms), (middle) carboplatin (17 atoms with a leaving cyclobutane-1,1-dicarboxylate ( $\text{C}_6\text{H}_6\text{O}_4^{2-}$ ) group) and (right) oxaliplatin (29 atoms with a leaving oxalate ( $\text{C}_2\text{O}_4^{2-}$ ) group).

There are same reaction mechanism of adduct formation among the platinum-based cancer drugs because their structures share some similarities. The specificity was investigated using 40 nm AuNPs functionalized with 35-nt G4 under the optimum

condition of 1.5 M NaNO<sub>3</sub> within 10 min. The degree of color change or the sensitivity for the platinum-based drugs and the corresponding image were shown in Fig. 2.13. It was found that only cisplatin induced the color change to purple-blue or the particle aggregation of 35-nt G4-AuNPs while carboplatin and oxaliplatin did not show any color change. This figure also shows the data for the mixture of three drugs with a molar ratio of 1:1:1. As expected, the sensor can distinguish cisplatin even in the existence of equal concentrations of possible interfering agents.

The same types of adducts at the same sites, *e.g.*, neighboring G-G on DNA<sup>35-37</sup> seem to form by the platinum-based drugs used here. Nevertheless, the author found that the present system of 35-nt G4-AuNP shows a high specificity for cisplatin because of the difference in the kinetics of adduct formation.<sup>36-41</sup> In comparison, the rate constants for monoadduct formations for cisplatin ( $1.96 \times 10^{-3} \text{ s}^{-1}$ ) is much faster than for carboplatin ( $1.88 \times 10^{-5} \text{ s}^{-1}$ ) and oxaliplatin ( $5.76 \times 10^{-6} \text{ s}^{-1}$ ).<sup>39-41</sup> At the short reaction time of 10 min, it is considered that the dispersion of 35-nt G4-AuNPs remained for carboplatin and oxaliplatin. Accordingly, the analogues-induced particle aggregation would occur if the reaction time was much longer.

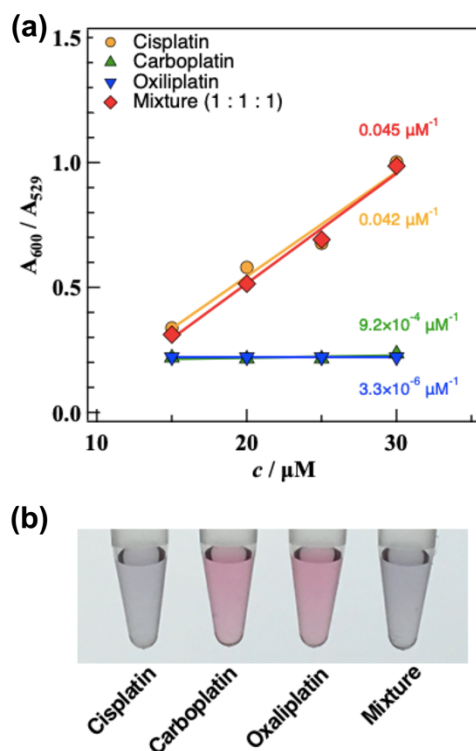


**Fig 2.13** (a) Absorption peak ratio ( $A_{600} / A_{529}$ ) for three platinum-based drugs: cisplatin, carboplatin, and oxaliplatin. UV-vis measurements of 35-nt G4-AuNPs (40 nm) in 10 mM PB (pH 5.0) including 1.5 mM EDTA and 1.5 M  $\text{NaNO}_3$  were performed by varying the drug concentration ( $c$ ). The reaction time was set at 10 min. In this figure, the data for the mixture with a 1:1:1 ratio (plaid-filled) are also shown. The values indicate the slopes of the fitted lines, or the sensitivity. (b) The corresponding image at  $c = 30 \mu\text{M}$ .

### 2.4.3 Analytical Performance

The limit of detection was evaluated based on UV-Vis absorption measurements of G4-AuNPs. The linear range was between 15.0 to 30.0  $\mu\text{M}$  with a slope of  $0.040 \pm 0.0016 \mu\text{M}^{-1}$  from a plot of  $A_{600} / A_{529}$  as a function of wavelength as shown in Fig. 2.14. The lower limit of detection  $y_{\text{LOD}}$  was investigated from the equation  $y_{\text{LOD}} = y_{\text{blank}} + 3\sigma_{\text{blank}}$ , where  $y_{\text{blank}}$  and  $\sigma_{\text{blank}}$  are the mean signal value and its standard deviation of blank sample.<sup>42</sup> The cisplatin concentration yielding the lower detection limit was estimated at 12.9  $\mu\text{M}$  (Fig. 2.14). Compared with the conventional techniques, the G4-AuNP system

shows a little bit lower sensitivity but sufficient detection performance to identify cisplatin in urine samples because the normal level of cisplatin in urine for chemotherapy patients administered 50 mg/m<sup>2</sup> cisplatin is between 54.3 and 321  $\mu$ M.<sup>11,12</sup>

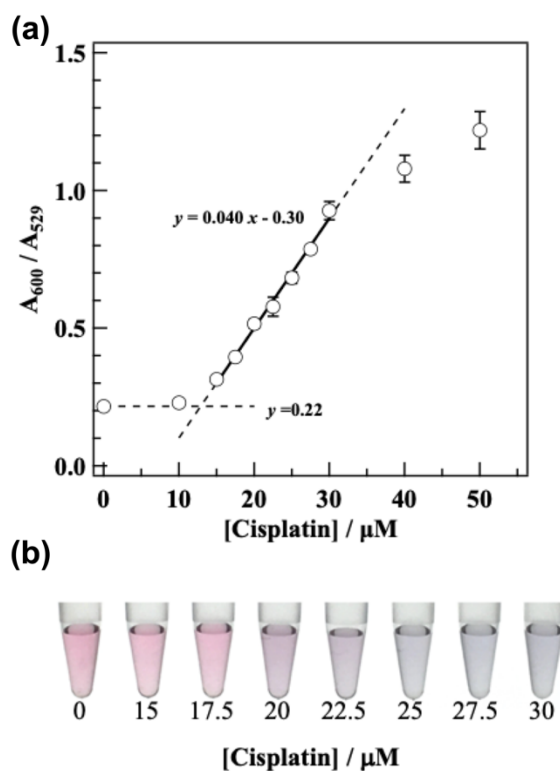


**Fig 2.14** (a) Cisplatin detection using 1.0 OD 35-nt G4-AuNPs in 10 mM PB containing 1.5 mM EDTA (pH 5.0) at 1.5 M NaNO<sub>3</sub>. Data were gathered 10 min after the addition of cisplatin. The regression line ( $y = 0.040x - 0.30$ ) in the dynamic range and LOD ( $y = 0.22$ ) are shown.<sup>58</sup> The intersection point of the lines yielded  $x = 12.9$ . (b) The corresponding images of 35-nt G4-AuNPs solutions.

## 2.5 Conclusions

The cisplatin-induced aggregation of G4-AuNPs is demonstrated as a simple, rapid and selective colorimetric sensor. G4 DNA was used as a sensing probe together with non-crosslinking aggregation of AuNPs. The parallel propeller-type of 35-nt G4 immobilization on the surface of AuNP with a diameter of 40 nm was promising as a cisplatin sensor. The colloidal stability of the functionalization of AuNPs with G4 strands was high and showed vivid red color of the solution. Cisplatin binding to G4 strands was found to induce the aggregation of G4-AuNPs, resulting in the color change of the colloidal solution from red to blue-purple. At about 10 min, the color change was clearly recognized after adding cisplatin to the colloidal system. As expected, the conformation of G4 changes to ssDNA-cisplatin adducts so that non-crosslinking aggregation occurs. It is likely because of the mono-adduct formation of cisplatin, or at most, intrastrand di-adduct formation. Cisplatin is thus detected by the color change of the colloidal solution, or so-called colorimetric cisplatin detection. Besides, this system shows a high specificity for cisplatin detection, noticed from the response of color change to cisplatin being faster than other analogues such as carboplatin and oxaliplatin. The work<sup>43</sup> - Reproduced by permission of The Royal Society of Chemistry.

## 2.6 References

- (1) Kelland, L. The resurgence of platinum-based cancer chemotherapy. *Nat. Rev. Cancer* **2007**, 7, 573–584.
- (2) S. Dasari, P. B. Tchounwou, Cisplatin in cancer therapy: molecular mechanisms of action, *Eur. J. Pharmacol.*, 2014, **740**, 364–378.
- (3) Fichtinger-Schepman, A. M. J.; van der Veer, J. L.; den Hartog, J. H.; Lohman, P. H. M.; Reedijk, J. Adducts of the antitumor drug *cis*-diamminedichloroplatinum(II) with DNA: formation, Identification, and Quantitation. *Biochemistry* **1985**, 24, 707–713.
- (4) Takahara, P. M.; Frederick, C. A.; Lippard, S. J. Crystal structure of the anticancer drug cisplatin bound to duplex DNA. *J. Am. Chem. Soc.* **1996**, 118, 12309–12321.
- (5) Baik, M. H.; Friesner, R. A.; Lippard, S. J. Theoretical study of cisplatin binding to purine bases: why does cisplatin prefer guanine over adenine? *J. Am. Chem. Soc.* **2003**, 125, 14082–14092.
- (6) Legendre, F.; Bas, V.; Kozelka, J.; Chottard, J. C. A complete kinetic study of GG versus AG plantination suggests that the doubly aquated derivatives of cisplatin are the actual DNA binding species. *Chem. Eur. J.* **2000**, 6, 2002–2010.
- (7) Liberthal, W.; Triaca, V.; Levine, J. Mechanisms of death induced by cisplatin in proximal tubular epithelial cells: Apoptosis vs. necrosis. *Am. J. Physiol.* **1996**, 270, F700–F708.
- (8) L. K. Gorsic, A. L. Stark, H. E. Wheeler, S. S. Wong, H. K. Im, M. E. Dolan, EPS8 inhibition increases cisplatin sensitivity in lung cancer cells, *PLoS One*, 2013, 8, e82220.



- (9) Lenz, K.; Koellensperger, G.; Hann, S.; Weissenbacher, N.; Mahnik, S. N.; Fuerhacker, M. Fate of cancerostatic platinum compounds in biological wastewater treatment of hospital effluents. *Chemosphere* **2007**, 69, 1765–1774.
- (10) Curtis, L.; Turner, A.; Vyas, N.; Sewell, G. Speciation and reactivity of cisplatin in river water and seawater. *Environ. Sci. Technol.* **2010**, 44, 3345–3350.
- (11) Riley, C. M.; Sternson, L. A.; Repta, A. J.; Siegler, R. W. High-performance liquid chromatography of platinum complexes on solvent generated anion exchangers. III. Application to the analysis of cisplatin in urine using automated column switching. *J. Chromatogr.* **1982**, 229, 373–386.
- (12) Anilamert, B.; Yalçın, G.; Ariöz, F.; Dölen, E. The spectrophotometric determination of cisplatin in urine, using o-phenylenediamine as derivatizing agent. *Anal. Lett.* **2001**, 34, 113–123.
- (13) Yang, H.; Cui, H.; Wang, L.; Yan, L.; Qian, Y.; Zheng, X. E.; Wei, W.; Zhao, J. A label-free G-quadruplex DNA-based fluorescence method for highly sensitive, direct detection of cisplatin. *Sens. Actuator B-Chem.* **2014**, 202, 714–720.
- (14) Petrlova, J.; Potesil, D.; Zehnalek, J.; Sures, B.; Adam, V.; Trnkova, L.; Kizek, R. Cisplatin electrochemical biosensor. *Electrochim. Acta* **2006**, 51, 5169–5173.
- (15) Ju, H. P.; Wang, Y. Z.; You, J.; Hou, X. M.; Xi, X. G.; Dou, S. X.; Li, W.; Wang, P. Y. Folding kinetics of single human telomeric G-quadruplex affected by cisplatin. *Acs Omega* **2016**, 1, 244–250.
- (16) Garnier, I. O.; Bombard, S. GG sequence of DNA and the human telomeric sequence react with cis-diammine-diaquaplatinum at comparable rates. *J. Inorg. Biochem.* **2007**, 101, 514–524.

- (17) Heringova, P.; Kasparkova, J.; Brabec, V. DNA adducts of antitumor cisplatin preclude telomeric sequences from forming G quadruplexes. *J. Biol. Inorg. Chem.* **2009**, 14, 959–968.
- (18) Viglasky, V. Platination of telomeric sequences and nuclease hypersensitive elements of human c-myc and PDGF-A promoters and their ability to form G-quadruplexes. *FEBS J.* **2009**, 276, 401–409.
- (19) de la Faverie, A. R.; Guédin, A.; Bedrat, A.; Yatsunyk, L. A.; Mergny, J. L. Thioflavin T as a fluorescence light-up probe for G4 formation. *Nucleic Acids Res.* **2014**, 42, e65.
- (20) Cogoi, S.; Xodo, L. E. G-quadruplex formation within the promoter of the KRAS proto-oncogene and its effect on transcription. *Nucleic Acids Res.* **2006**, 34, 2536–2549.
- (21) Lim, K. W.; Alberti, P.; Guedin, A.; Lacroix, L.; Riou, J. F.; Royle, N. J.; Mergny, J. L.; Phan, A. T. Sequence variant (CTAGGG)<sub>n</sub> in the human telomere favors a G-quadruplex structure containing a G·C·G·C tetrad. *Nucleic Acids Res.* **2009**, 37, 6239–6248.
- (22) Wang, Y.; Patel, D. J. Solution structure of the human telomeric repeat d[AG<sub>3</sub>(T<sub>2</sub>AG<sub>3</sub>)<sub>3</sub>] G-tetraplex. *Structure* **1993**, 1, 263–282.
- (23) Hud, N. V.; Smith, F. W.; Anet, F. A. L.; Feigon, J. The selectivity for K<sup>+</sup> versus Na<sup>+</sup> in DNA quadruplexes is dominated by relative free energies of hydration: A thermodynamic analysis by <sup>1</sup>H NMR. *Biochemistry* **1996**, 35, 15383–15390.
- (24) Demers, L. M.; Mirkin, C. A.; Mucic, R. C.; Reynolds III, R. A.; Letsinger, R. L.; Elghanian, R.; Viswanadham, G. A fluorescence-based method for determining the

- surface coverage and hybridization efficiency of thiol-capped oligonucleotides bound to gold thin films and nanoparticles. *Anal. Chem.* **2000**, 72, 5535–5541.
- (25) Orthaber, D.; Bergmann, A.; Glatter, O. SAXS experiments on absolute scale with Kratky systems using water as a secondary standard. *J. Appl. Crystallogr.* **2000**, 33, 218–225.
- (26) Fujita, M.; Katafuchi, Y.; Ito, K.; Kanayama, N.; Takarada, T.; Maeda, M. Structural study on gold nanoparticle functionalized with DNA and its non-cross-linking aggregation. *J. Colloid Interface Sci.* **2012**, 368, 629–35.
- (27) Matsuoka, H.; Tanaka, H.; Hashimoto, T.; Ise, N. Elastic scattering from cubic lattice systems with paracrystalline distortion. *Phys. Rev. B* **1987**, 36, 1754–1765.
- (28) Matsuoka, H.; Tanaka, H.; Iizuka, N.; Hashimoto, T.; Ise, N. Elastic scattering from cubic lattice systems with paracrystalline distortion. II. *Phys. Rev. B* **1990**, 41, 3854–3856.
- (29) Sato, K.; Hosokawa, K.; Maeda, M. Rapid aggregation of gold nanoparticles induced by non-cross-linking DNA hybridization. *J. Am. Chem. Soc.* **2003**, 125, 8102–8103.
- (30) Mirkin, C. A.; Letsinger, R. L.; Mucic, J. J. A DNA-based method for rationally assembling nanoparticles into macroscopic materials. *Nature* **1996**, 382, 605–609.
- (31) Rosi, N. L.; Mirkin, C. A. Nanostructure in biodiagnostics. *Chem. Rev.* **2005**, 105, 1547–1562.
- (32) Mori, T.; Maeda, M. Stability change of DNA-carrying colloidal particle induced by hybridization with target DNA. *Polym. J.* **2002**, 34, 624–628.
- (33) Zhao, W.; Chiuman, W.; Lam, J. C. F.; McManus, S. A.; Chen, W.; Cui, Y.; Pelton, R.; Brook, M. A.; Li, Y. DNA Aptamer folding on gold nanoparticles: From colloid chemistry to biosensors. *J. Am. Chem. Soc.* **2008**, 130, 3610–3618.

- (34) Tinland, B.; Pluen, A.; Sturm, J.; Weill, G. Persistence length of single-stranded DNA. *Macromolecules* **1997**, 30, 5763–5765.
- (35) Johnstone, T. C.; Park, G. Y.; Lippard, S. J. Understanding and Improving Platinum Anticancer Drugs – Phenanthriplatin. *Anticancer Res.* **2014**, 34, 471–476.
- (36) Knox, R. J.; Friedlos, F.; Lydall, D. A.; Roberts, J. J. Mechanism of cytotoxicity of anticancer platinum drugs: Evidence that cis-diamminedichloroplatinum(II) and cis-diamine-(1,1-cyclobutanedicarboxylato)platinum(II) differ only in the kinetics of their interaction with DNA. *Cancer. Res.* **1986**, 46, 1972–1979.
- (37) Blommaert, F. A.; van Dijk-Knijnenburg, H. C. M.; Dijt, F. J.; den Engelse, L.; Baan, R. A.; Berends, F.; Fichtinger-Schepman, A. M. J. Formation of DNA adducts by the anticancer drug carboplatin: Different nucleotide sequence preferences in vitro and in cells. *Biochemistry* **1995**, 34, 8474–8480.
- (38) Saris, C. P.; van de Vaart, P. J. M.; Rietbroek, R. C.; Blommaert, F. A. In vitro formation of DNA adducts by cisplatin, lobaplatin and oxaliplatin in calf thymus DNA in solution and in cultured human cells. *Carcinogenesis* **1996**, 17, 2763–2769.
- (39) Hah, S. S.; Stivers, K. M.; de Vere White, R. W.; Henderson, P. T. Kinetics of carboplatin-DNA binding in genomic DNA and bladder cancer cells as determined by accelerator mass spectrometry. *Chem. Res. Toxicol.* **2006**, 19, 622–626.
- (40) Kim, Y. S.; Shin, S.; Cheong, M.; Hah, S. S. Mechanistic Insights into in vitro DNA adduction of oxaliplatin. *Bull. Korean Chem. Soc.* **2010**, 31, 2043–2046.
- (41) Bancroft, D. P.; Lepre, C. A.; Lippard, S. J. Platinum-195 NMR kinetic and mechanistic studies of cis- and trans-diamminedichloroplatinum(II) binding to DNA. *J. Am. Chem. Soc.* **1990**, 112, 6860–6871.

- (42)Thomsen, V.; Schatzlein, D.; Mercurio, D. Limits of detection in spectroscopy. *Spectroscopy* **2003**, 18, 112–114.
- (43)Chuaychob, S.; Thammakhet-Buranachai, C.; Kanatharana, P.; Thavarungkul, P.; Buranachai, C.; Fujita, M.; Maeda, M. A Nanobiosensor for the Simple Detection of Small Molecules using Non-Crosslinking Aggregation of Gold Nanoparticles with G-quadruplexes. *Anal. Methods*. **2020**, 12, 230–238.

**Chapter 3**

**G-quadruplex DNA-Functionalized AuNPs for Detection of  
Macromolecule “Thrombin”**

### 3.1 Abstract

G-quadruplex-grafted gold nanoparticles (G4-AuNPs) based on non-crosslinking aggregation principles were sought out as a new platform for a real-time biomolecule sensor. Superior colorimetric assay of on-demand turnability to the target of interest may be achieved with the sensors that are highly stable until a specific target binding by the specific potential of G4 aptamers and by the promising role of gold nanoparticle aggregation. The use of DNA G-quadruplexes in the colorimetric assay are reared, yet hidden by limited studies. Thus, to broaden the applications, the author presents gold nanoparticles immobilizing with highly polymorphic G4s, using thrombin-binding aptamers to proof of concept as a capture probe for thrombin detection. After adding thrombin target, a dramatic reduction of G4-AuNP stability has yielded a specific binding between aptamers and targets that causes the depletion of electrostatic repulsion of the colloidal system, inducing non-crosslinking aggregation. The color of the colloidal solution changed clearly from red to purple-blue within 5 min. The bathochromic peak shift appearing from the aggregation varied with the concentration of thrombin. The properties of needs—these are, the degree of aggregation, the detection sensitivity, and analytical performance—were successfully tuned for an on-demand sensor with linearity of 10.0 to 40.0 nM and limit of detection of 0.72 nM. The sensor showed very high specificity to thrombin targets over major proteins in human serum. Besides, the sensor is applicable to detect thrombin in the serum matrix. Thus, this G4-AuNP sensor is promising for real-time biomolecular detection to broaden colorimetric applications using G-quadruplex-gold nanoparticles.

### 3.2 Introduction

Among various types of protein, *in vivo*, thrombin is an important protein in blood plasma, expressing a strong impact on blood clotting. Apart from this central role, thrombin initiates pro-inflammatory signaling responses, leading to neurodegenerative diseases, *e.g.*, Parkinson's disease and Alzheimer's disease. It is suspected that over-expressing of thrombin from the normal concentration (14  $\mu\text{M}$ ) seems to contribute to signaling in health and disease. Therefore, to monitor abnormal levels of thrombin, this work presents a rapid yet sensitive colorimetric sensor for thrombin detection based on DNA aptamer in G-quadruplex conformation and non-crosslinking aggregation of gold nanoparticles. In this experiment, the author follows target binding and stabilizing G4, which made up the tighter and more rigid structure of G4 on the AuNP surface due to the use of a poly A-modified thrombin-binding aptamer (Poly A-modified TBA) in G4 conformation with AuNPs (Fig. 3.1). The thrombin binding aptamer (TBA)<sup>1-2</sup> is a well-characterized chair-type conformation G4 that binds to thrombin at nanomolar concentrations with high affinity and specificity. The binding of target and G4-AuNP could induce the reduction of particle stability, resulting in an aggregation based on non-crosslinking behavior. Due to the synergistic properties of G4 aptamer and colloidal gold, it is possible to realize thrombin detection by the particle aggregation, resulting in a plasmonic spectra shift and the colorimetric change in several minutes.



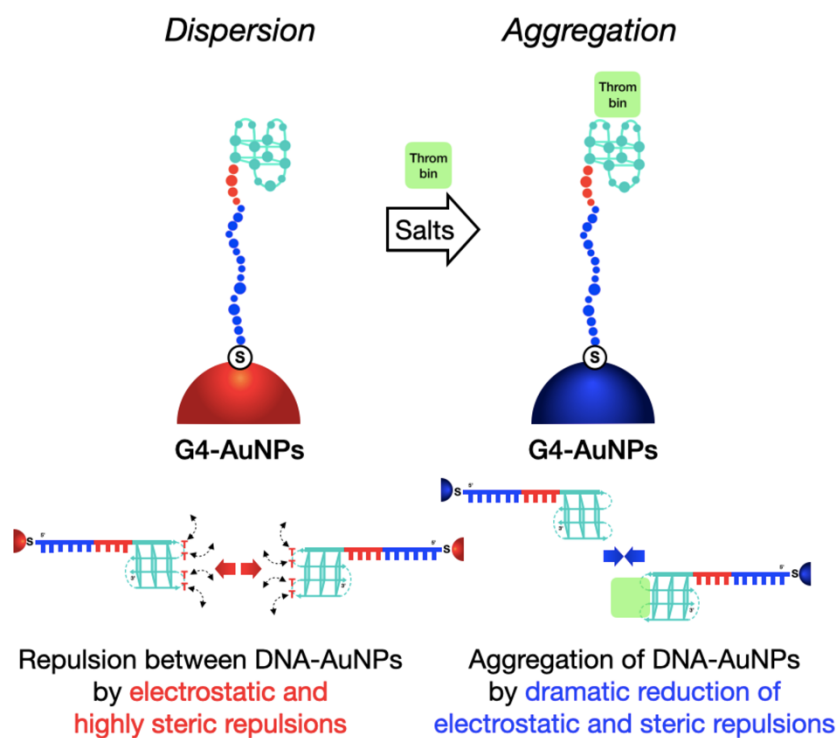


**Figure 3.1** Non-crosslinking aggregations of G4-AuNPs induced by thrombin-stabilized G4-structure.

### 3.3 Experimental Section

#### 3.3.1 Materials

AuNPs with diameters of about 40 nm were purchased from British Biocell International (Cardiff, UK). The aggregation of AuNPs was estimated by transmission electron microscopy (TEM) (JEM-1230, JEOL, Tokyo) operated at 80 kV (Fig. 3.14). Oligo-DNA having a sulfhydryl group at their 5'-end were purchased from Eurofins Genomics K.K. (Tokyo) and purified by an affinity column (oligonucleotide purification cartridge (OPC); Thermo Fisher Scientific, Waltham, MA) prior to use. Thrombin binding aptamer was utilized as G4 conformation which incorporated 15 nucleotides

(nt).<sup>1-2</sup> The chair-type conformation of G4 is shown in Fig. 3.2. The DNA sequences using in this study are listed in Table 3.1. Dithiothreitol (DTT) and potassium chloride (KCl) were purchased from Sigma-Aldrich (St. Louis, MO). Sodium chloride (NaCl) and sodium nitrate (NaNO<sub>3</sub>) were purchased from Wako Pure Chemical Industries (Osaka, Japan). Trizma<sup>®</sup> hydrochloride solution pH 7.4 (BioPerformance Certified), human serum (from human male AB plasma), thrombin (from human serum), albumin (from human serum),  $\gamma$ -globulin (from human serum), and immunoglobulin G (from human serum) were purchased from Sigma (St. Louis, MO). 11-mercapto-1-undecanol (C<sub>11</sub>H<sub>24</sub>OS) was purchased from Aldrich (Milw, WI). Calcium chloride (CaCl<sub>2</sub>) was purchased from Kanto Chemical (Tokyo). Magnesium chloride hexahydrate (MgCl<sub>2</sub>·6H<sub>2</sub>O) was purchased from Kokusan chemical (Tokyo). Milli-Q water (resistivity greater than 18.2 M $\Omega$  cm) was used for all experiments.

**Table 3.1** DNA sequences of G4 used in this study.

Name	Sequence (from 5' to 3')	Length (base)
Poly-A5 G4	HS-(CH <sub>2</sub> ) <sub>6</sub> -AAAAATCTCGGTTGGTGTGGTTGG	24
Poly-A10 G4	HS-(CH <sub>2</sub> ) <sub>6</sub> -(AAAAA) <sub>2</sub> TCTCGGTTGGTGTGGTTGG	29
Poly-A15 G4	HS-(CH <sub>2</sub> ) <sub>6</sub> -(AAAAA) <sub>3</sub> TCTCGGTTGGTGTGGTTGG	34
Poly-A30 G4	HS-(CH <sub>2</sub> ) <sub>6</sub> -(AAAAA) <sub>6</sub> TCTCGGTTGGTGTGGTTGG	49
Poly-A45 G4	HS-(CH <sub>2</sub> ) <sub>6</sub> -(AAAAA) <sub>9</sub> TCTCGGTTGGTGTGGTTGG	64
Poly-A60 G4	HS-(CH <sub>2</sub> ) <sub>6</sub> -(AAAAA) <sub>12</sub> TCTCGGTTGGTGTGGTTGG	79

Note: GG involved in folding the G4.

### 3.3.2 Design and Criterion

Among a large number of G4 aptamers, thrombin-binding aptamer (TBA), the first and the most well-known anticoagulant aptamer, discovered by Bock in 1992<sup>1</sup>, is considerably selected as an aptamer probe to proof-of-concept in this study. Minor modification on the TBA sequence is considerably designed in order to tune additional functions. The DNA sequence is functionally defined to be four residues: (i) an “aptamer” chain at the 3’ end, composes of 15 nucleotide (nt), that is responsible for binding the target “thrombin”; (ii) a “linker”, 4-nt connected to an aptamer, that reduces the electrostatic repulsion of an aptamer from the particle surface and makes an aptamer lining up on the surface of particles; (iii) a “spacer poly-adenine (poly-A)” residues, attached to the linker, that has highest adsorption affinity among homo-oligonucleotides<sup>3-4</sup> on the gold surface; (iv) a hexamethylene thiol linker moiety at the 5’ end, that plays a major role as a linker on the gold surface as shown in Fig. 3.2

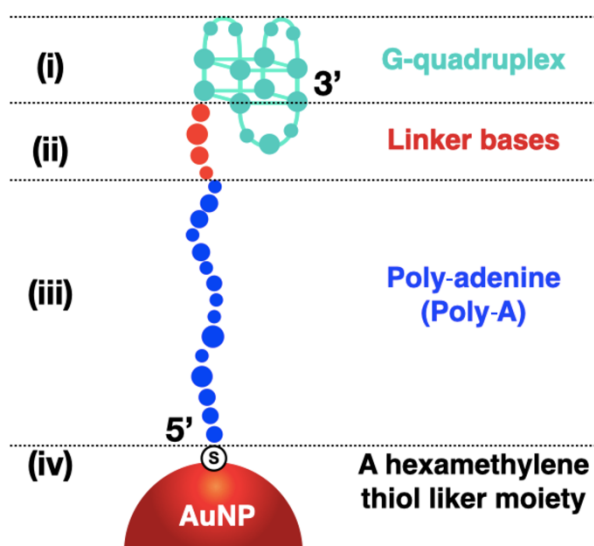


**Figure 3.2** AuNPs functionalization with four residues of DNA: (i) an “aptamer” (ii) a “linker” (iii) a “spacer poly-adenine (poly-A)” and (iv) a hexamethylene thiol liker moiety

### **3.3.3 Preparation**

#### **3.3.3.1 Preparation of Proteins**

All proteins were prepared in aqueous media at room temperature, with the exception of preparation of immunoglobulin G in saline media. The solutions were also kept in the at 4 °C before use.

#### **3.3.3.2 Preparation of G4-AuNPs**

In brief, 3 nmol of oligo-DNA was incubated with 1 ml of the gold nanoparticle solution at 50 °C overnight. The solution was changed into 0.01 M K<sup>+</sup> phosphate buffer (pH 7) and kept at 50 °C for another day. Noted, a potassium ion is necessary to stabilize the G4 aptamer structure<sup>5</sup>. Then the necessary salt was added to change solution into 0.1 M NaNO<sub>3</sub> and kept at 50 °C for 2 days. To remove unbound probes, the solution was centrifuged at 15,000 rpm for 30 min at 4 °C, and the supernatant was replaced by 1 ml of the same buffer. After another centrifugation under the same condition, the precipitate was re-dispersed with the same buffer to make a stock solution, which was used for the following experiments after adjusted to about 1.0 OD at 520 nm, unless otherwise noted.

#### **3.3.4 Characterization of G4-AuNPs**

In accordance with a commercial assay, the density of G4 strands on the colloidal surface was investigated. Briefly, the G4-AuNP solution was added into DTT solution with a final concentration of 1.0 M to release the strands from the particles<sup>25</sup>. The bare AuNP was removed from the solution containing DNAs by centrifugation at 15,000 rpm for 30 min (4 °C). For the fluorescence measurement of a number of DNA strand, the

DNA solution was treated using an OliGreen ssDNA Quantitation Assay Kit (Thermo Fisher Scientific, Waltham, MA) and measured fluorescence intensity with a microplate reader spectroscopy (Thermo Scientific Varioskan Lux; Thermo Scientific, Kyoto, Japan), afterward. The number of G4 strands was then evaluated using a calibration curve. In this regard, the grafted number of DNA strands immobilized on AuNP with a diameter of 40 nm was estimated at  $163 \pm 2$ ,  $164 \pm 1$ ,  $162 \pm 2$ ,  $161 \pm 2$ ,  $159 \pm 1$ , and  $156 \pm 1$  for the A5, A10, A15, A30, A45, A60 of poly-A G4s, respectively. The density of G4 strands was wholly lower than the case of ssDNA—that is *ca.* 400 strands/particle—, likely due to the steric bulk of G4 conformation. Compared to the unmodified G4 case (*ca.* 90 strands/particle), interestingly, the author found a moderately higher in G4 density, likely due to the spacer poly-A in the modified G4 case. The colloidal stability of G4-AuNPs (dispersion/aggregation) was estimated by microplate reader spectroscopy (Thermo Scientific Varioskan Lux; Thermo Scientific, Kyoto, Japan) at 25 °C. The absorption spectra were scanned from 300 to 800 nm with a scan rate of 100 sec/scan. The size and zeta potential of G4-AuNPs were measured with a Zetasizer Nano-ZS instrument (Malvern Instruments, Malvern, UK) at 25 °C. The size of the aggregation behavior of G4-AuNPs was also examined by small angle X-ray scattering (SAXS). The SAXS measurements were performed at BL40B2 RIKEN Structural Biology beamline II of SPring-8, Japan. The wavelength ( $\lambda$ ) of X-ray was 0.1 nm. The camera length, calibrated using a silver behenate standard, was about 4.2 m. SAXS images were recorded with a PILATUS  $3 \times 2$ M detector (Dectris, Baden, Switzerland) at 25 °C. The SAXS data analysis was previously ascribed in section 2.3.4 of chapter 2.

### 3.3.5 Proof Concept

According to the G4 aptamer entity, the binding to thrombin with TT loops at the thrombin exosite I as a pincer<sup>6-7</sup> is in charge of G4 stabilization on AuNPs. The pincer-like system makes a rather tighter and more rigid than a flexible structure of G4. This shares similarity in the detection cascade of dsDNA formation on AuNPs of the initial proposal of a non-crosslinking manner<sup>8</sup>. A significant reduction of the entropic effect and electrostatic repulsion was found to happen after the addition of thrombin in working buffer containing high salt concentration. Eventually, the aggregation clearly ascribed from the absorption peak shift to longer wavelength over 2 hours (Fig. 3.3b), and the solution completely turned purple-blue within 10 min, as shown in Fig. 3.3d. However, when thrombin was added in buffer solution, there was no peak shift and no color change over time Fig. 3.3a. Besides, a slight decrease in surface potential was observed from *ca.* -29.8 mV to *ca.* -24.7 mV (Fig. 3.3c), suggesting the binding of the thrombin and G4 aptamer. Also, the author investigated the absorption peak under such conditions without thrombin, the maximum absorption peak was observed at 535 nm (Fig. 3.4), and the colorimetric image remained a clear red color, indicating the high stability of G4-AuNPs under the high salt concentration.

Furthermore, the evidence of the dissociation constant (KD) of thrombin and G4 supported such behaviors of the G4-AuNPs in each system. The KD was found to depend on the ionic strength of working buffer (Fig. 3.5)—that is, the higher ionic strength, the greater the binding affinity was observed ( $KD = 4.61 \pm 0.07$  nM), associating with the previous report<sup>9</sup>—due to the subtraction of charge-charge repulsion between an aptamer and a substance. The lower one showed a much higher KD of  $929.50 \pm 0.47$  nM. Noted, the KD is disproportional to binding affinity. This highlighted a crucial role of salts to

increase the binding affinity of the aptamer and to induce a non-crosslinking aggregation. Thus, the experiments should carry on in the sufficiently high salt solution, where the electrostatic effect is known to be subtle, to overcome the steric stabilization of the colloidal stability of G4-AuNPs. As a result, the analyte trigs particle aggregation under the non-crosslinking aggregation concept.

The author further confirmed the results using dynamic light scattering (DLS) in order to trace the aggregation transition path. As expected, Fig. 3.3d showed the hydrodynamic diameter ( $D_h$ ) of aggregated particles (*ca.* 379 nm) much bigger than the dispersed ones (*ca.* 55 nm) as a result of a clear change in color of the solution from red to purple-blue. Also, the zeta-potential of salt-adding systems clearly showed the net negative charge of particles decreased from *ca.* -16 mV of the dispersed state to *ca.* -14 mV after reaching the aggregated state (Fig. 3.3c). For all results, the experiments had conducted at 10 minutes of reaction time. This confirmed that thrombin induced the non-crosslinking aggregation of G4-AuNPs in the buffer, containing high salt concentration as expected.

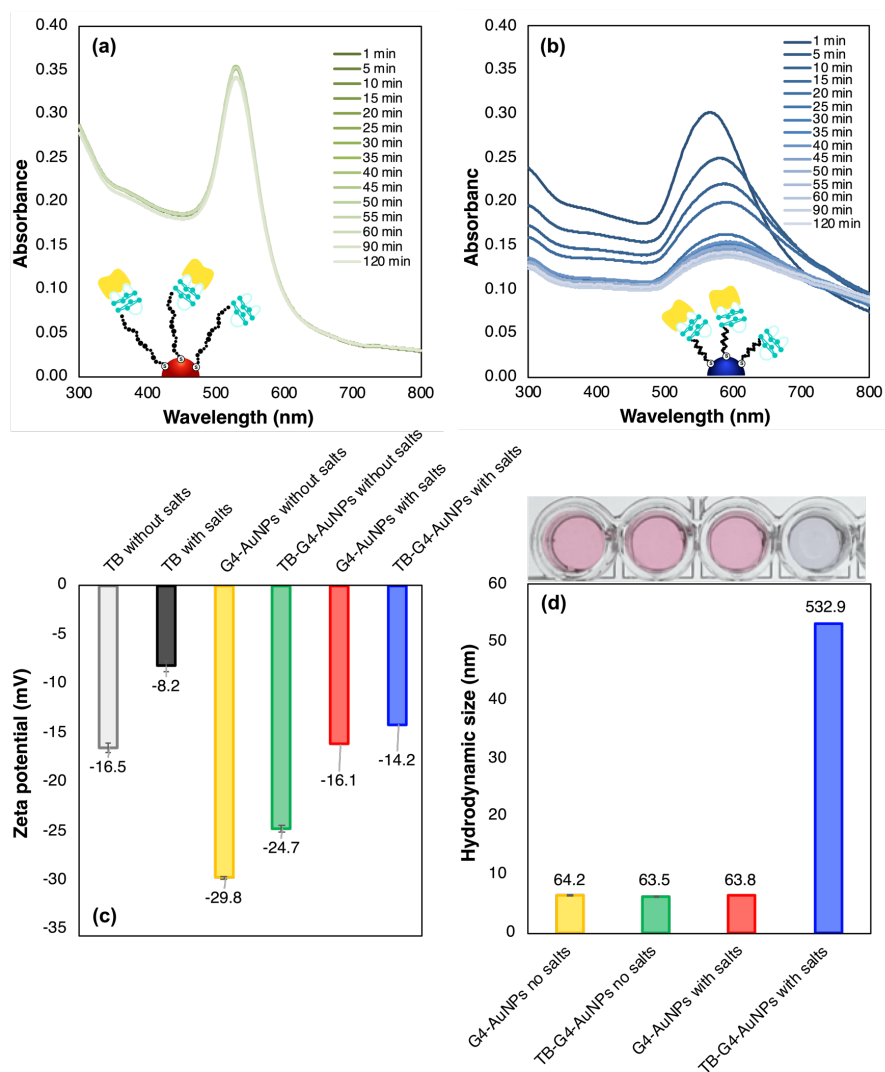


**Figure 3.3** Time course of the absorption spectra of 1.0 OD poly-A15 G4-AuNPs in 20 mM Tris-HCl (pH 7.4) without (a) and with 140 mM NaCl, 5 mM KCl, 1 mM CaCl<sub>2</sub> and 1 mM MgCl<sub>2</sub> (b) after adding 50 nM thrombin. (c) Zeta potential data of 50 nM free thrombin and 50 nM thrombin detection using 1.0 OD G4-AuNPs in 20 mM Tris-HCl (pH 7.4) with and without the mixer of salts after 10 min incubation. (d) The corresponding hydrodynamic diameter ( $D_h$ ) and colorimetric image of the particles for thrombin detection. The significant surface potential and  $D_h$  change of the aggregated particles, induced by thrombin addition were shown.



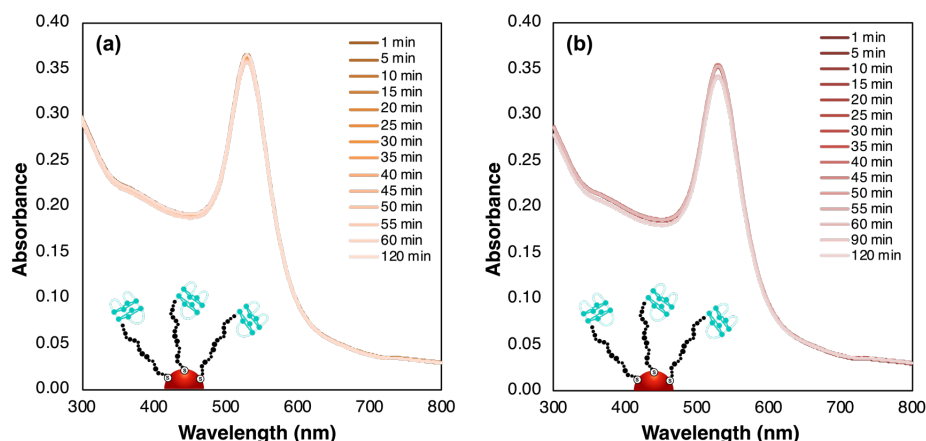


**Figure 3.4** Time course of the absorption spectra of 1.0 OD poly-A15 G4-AuNPs in 20 mM Tris-HCl (pH 7.4) without (a) and with 140 mM NaCl, 5 mM KCl, 1 mM CaCl<sub>2</sub> and 1 mM MgCl<sub>2</sub> (b). Data were gathered without adding thrombin. No peak shift was observed overtime in such systems. The particles remained dispersed over 120 min.

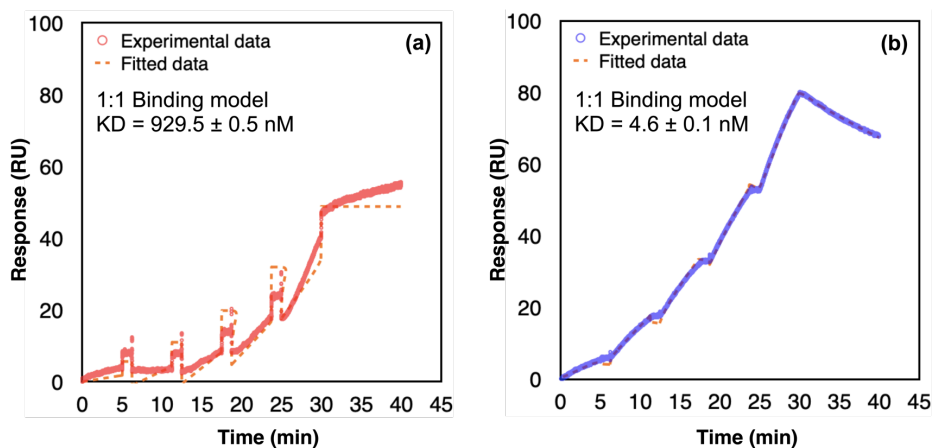


**Figure 3.5** Sensorgram of the binding between target thrombin and thrombin binding aptamer G4 in 20 mM Tris-HCl (pH 7.4) (a) and in 20 mM Tris-HCl (pH 7.4) containing 140 mM NaCl, 5 mM KCl, 1 mM CaCl<sub>2</sub> and 1 mM MgCl<sub>2</sub> (b). The dissociation constant (KD) from 1:1 binding model is shown.

### 3.3.6 Detection Mechanism

The author decided to clarify the aggregation mechanism under non-crosslinking cascade using small angle X-ray scattering (SAXS) technique whether the functionalization of AuNPs with the designed G4 DNA probe could be achieved for various aspects: (i) interparticle distance between surface of the aggregated AuNPs; (ii) behavior of DNA after aggregation; and (iii) ratio of binding stoichiometry between thrombin and G4 aptamer.

The thrombin concentration-dependency of G4-AuNPs had been investigated with various poly-A lengths (A5, A10, A15, A30, A45, A60) from the intensity profiles and the fitting analysis of SAXS. As expected, the intensity profiles of the colloidal solution without thrombin support the notion that particles remained dispersed since the profiles were well fitted, as shown in the red solid curves in Fig. 3.6. By regarding the target thrombin-induced aggregation process of G4-AuNPs as a nucleation and growth process, the scattering profiles of a spherical particle with a radius  $R$  could be fitted with Eq. 1 (section 2.3.4 of chapter 2) The mean radius of gold colloid was calculated from Eq. 1 about 19.1 nm and  $R_h$  of bare AuNPs (20.4 nm). This agreed well to the radius of AuNPs because the dominant scattering noticeably belongs to heavier gold atoms<sup>5</sup>. In the existence of thrombin in the G4-AuNPs solution, the aggregation was clearly noticed from the interferent peak arising, dependent on thrombin (Fig. 3.7a-f). The peak position at  $q$  (nm<sup>-1</sup>) steadily shifted from 0.16 to 0.11 with the length of DNA (Fig. 3.7g), implying the larger interparticle distance between NPs at aggregation state. For analysis of SAXS profiles at this state, the author considered the interference between the particles in terms of the structure factor  $S(q)$ , as shown in Eq. 2 (section 2.3.4 of chapter 2).

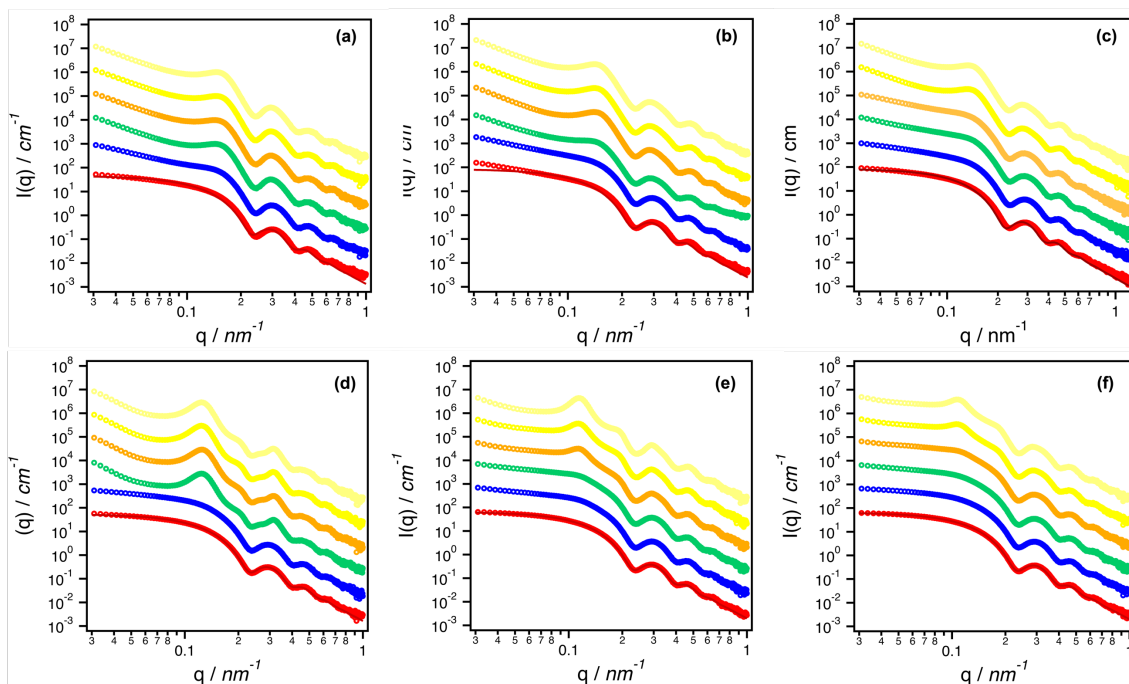


**Figure 3.6** SAXS intensity data for 1.0 OD poly-A (a) A5, (b) A10, (c) A15, (d) A30, (e) A45 and (f) A60 in 20 mM Tris-HCl (pH 7.4) containing 140 mM NaCl, 5 mM KCl, 1 mM CaCl<sub>2</sub> and 1 mM MgCl<sub>2</sub>. The data were taken at various thrombin concentrations: 0 (red), 10 (blue), 20 (green), 30 (orange), 40 (yellow) and 50 nM (pale-yellow). The red solid lines in (a-f) are the fitting curves of form factor.

If the objects, *e.g.*, AuNPs, aggregate with interfering with each other,  $S(q)$  must deviate from one, principally. To obtain the experimental  $S(q)$ ,  $I(q)$  of the aggregated particles is divided by that of the dispersed particles<sup>10-11</sup>. Then curve fitting with the calculated  $S(q)$  was performed based on paracrystalline theory, followed by the reported method in the previous study<sup>5</sup>.

On the basis of paracrystalline theory, Fig. 3.7a-f shows the corresponding structure factors, which were analyzed by assuming that the aggregate adopts a disordered face-centered cubic structure<sup>5</sup>. The center-to-center distance between the nearest neighbors did not seem to depend on the thrombin concentration. The mean value was calculated from fitting analysis, and thus the gap between the particle surfaces was estimated. Noted, the gap generated from the existence of the DNA layers, which prevent the further approach of the particles. Respectively, the comparison of gap values between SAXS data and theoretical calculation was examined to predict the behavior of DNA on AuNP core and the binding ratio between thrombin and G4 aptamer, afterward. In comparison, the non-linear relationship of the gap between the particle surfaces was observed when the poly-A chain increases (Fig. 3.7h). This definitely confirmed the adsorption and shrinkage characteristic of DNA inside the gap. For example, the estimated values of A5 and A10 seem to be associated with the principle values from the calculation, supporting the aforementioned adsorption of a poly-A spacer on the surface of AuNPs. More interestingly, the shrinkage of DNA strands was declared in the case of A15, A30, A45, A60, because the estimated gaps are narrower rather wider with DNA length, independent with the number of adenine. Hence, the DNA probes were found to adsorb and/or shrink between particle surfaces after an aggregation if the colloidal gold was grafted with the well-designed G4 probe.

For the ratio of binding stoichiometry between thrombin and G4 aptamer, the author paid more attention to the gap between NPs, length of DNA, and size of target thrombin. In particular, the occupied area per strand on colloidal gold (40 nm size in diameter) is around 25 nm<sup>2</sup> if the particle was covered with ~160 strands of G4. It was assumed that the number of nucleotides that could be fit in 25 nm<sup>2</sup> is about 8-nt (3.4 nm)

at most. An illustration of the aggregation process was explained using the representative poly-A5 G4-AuNPs (Fig. 3.7i). Looking into each segment of the sensor, the height of a G4 strand with two layers of G-tetrad and a TCTC-linker is only about 0.5 nm and 1.7 nm, respectively, and even if the length of the hexamethylene thiol linker is taken into consideration, the DNA layer would still be only about 2.2 nm high. The gap was estimated at 9.4 nm as of poly-A5 G4-AuNPs. From PBD library<sup>12</sup>, thrombin size is about 4.5 nm x 4.5 nm x 5.0 nm. Hence, if a molecule of thrombin involved inside the gap, the author could get such a perfect assumption of an aggregation process under a non-crosslinking manner, as shown in Fig. 3.7i.

**Table 3.2** Hydrodynamic diameter ( $D_h$ ) and zeta potential data of poly-A modified G4-AuNPs.

Name	$D_h$ (nm)		Zeta potential (mV)	
	Without Thrombin	With Thrombin	Without Thrombin	With Thrombin
Poly-A5 G4-AuNPs	50.0±1.1	373.5±2.0	-16.2±0.6	-13.5±1.1
Poly-A10 G4-AuNPs	52.3±1.4	378.8±10.9	-16.3±0.2	-13.2±1.3
Poly-A15 G4-AuNPs	55.4±0.9	379.0±5.9	-16.9±0.7	-14.1±0.7
Poly-A30 G4-AuNPs	62.5±0.3	381.5±0.8	-16.9±0.4	-14.8±1.2
Poly-A45 G4-AuNPs	65.1±0.2	410.2±17.3	-16.8±0.7	-14.1±0.6
Poly-A60 G4-AuNPs	68.9±1.1	440.3±23.6	-17.0±0.4	-14.9±0.9

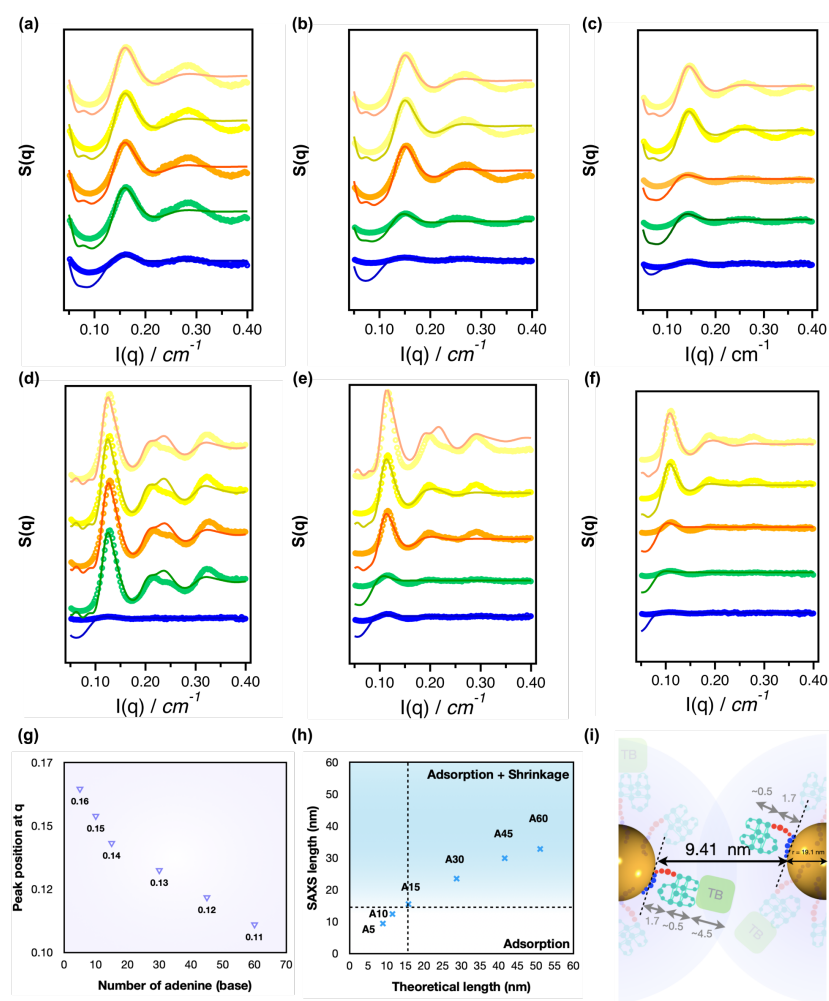


**Figure 3.7** SAXS data of structure factor for poly-A: A5 (a), A10 (b), A15 (c), A30 (d), A45 (e), and A60 (f) G4-AuNPs in 20 mM Tris-HCl (pH 7.4), containing 140 mM NaCl, 5 mM KCl, 1 mM  $\text{CaCl}_2$  and 1 mM  $\text{MgCl}_2$ . The data were taken at various thrombin concentrations: 10 (blue), 20 (green), 30 (orange), 40 (yellow), and 50 nM (pale-yellow). The solid lines in (a-f) is the fitting curves of structure factor. (g) The plot of peak position at  $q$  ( $\text{nm}^{-1}$ ) from the fitting analysis of G4-AuNPs with different length of poly-A. (h) The gap between the particle surfaces from SAXS and theoretical data, indicating the adsorption and shrinkage of DNA on particle surfaces, and (i) the corresponding schematic illustration of poly-A5 G4-AuNPs as an example for the prediction of aggregation mechanism.

### 3.4 Results and Discussion

#### 3.4.1 Optimization of Involving Parameters

Excellent biocompatibility of gold nanoparticles with biomolecules, especially interaction with DNAs, has long been presented to know as a key for its stability control of DNA-based AuNPs. Here, the author had especially focused on the interactions of gold nanoparticles with an adenine subunit of DNAs. In this interest, the thiolated strands of G4 DNA are engineered with a residue of poly-adenine (Poly-A) or adenine deoxyribonucleotide (dA) with the difference in base pair chains as a spacer onto G4 aptamer probe due to the dominant adsorption of oligo(dA) over the other oligonucleotides (dA>dG>dC>dT) to AuNP surface in the environment of PBS buffer<sup>13</sup>. Noted, the adsorption affinity of the nucleobases via the keto and imino groups might vary with the experimental conditions. The highest and the lowest affinity was found to be adenine (A) and thymine (T), while the affinity of cytosine (C) and guanine (G) varies from different measurements<sup>3-4,13-15</sup>. Interestingly, the thiol–gold (S–Au) bond (> 200 kJ/mol) was found to have an affinity even stronger than the nucleobase–gold interaction (>100 kJ/mol for each base in a vacuum)<sup>15</sup>.

In the field of molecular sensing, the demand of interested properties, the different controllability needs to be designed on the DNA probe. The aggregation behavior of different sequences-modified AuNPs should be evaluated under the controlled variables of capping agent efficiency on particle stability, for example, the number of G4 probes per particle as for the concentration of G4-AuNPs. In this sense, G4-AuNPs, as a sensor of macromolecular thrombin, show outstanding features of the inherent properties of bulky steric G4 cooperated with the natural properties of thiols and adenine nucleobases

adsorbed onto AuNPs, where G4 conformations were pushed up into the solution for the favor of thrombin capture. Appealingly, the author was able to fabricate the uniformly identical DNA density on the particle (*ca.* 160 strands/particle) for all poly-A (A5, A10, A15, A30, A45, A60)-modified G4-AuNPs. The functionalization of AuNPs with the chain-length independence of G4 DNA is found to contrast to other previous studies of non-G4 DNA-AuNPs that the surface density directly depends on the length of oligonucleotide<sup>16-17</sup>, especially the colloidal system with free of S-Au modification.

For the programmable degree of aggregation, the length of the spacer poly-A was varied from 5-, 10-, 15-, 30-, 45-, and 60-nucleotides to investigate whether short- or long-chained oligonucleotides could potentially stabilize the colloidal stability as a well-designed sensor. It was presumed that the different DNA-capping radii of G4-AuNPs, prevents cluster aggregation differently due to the difference in London-van der Waals force attracted between NPs. The absorption peak ratio (ratio A), expressed as the difference between the initial and final maximum absorption wavelengths of each sequence, was plotted as a function of the concentration of thrombin in Fig. 3.8a-b. The data were taken at 10 minutes after thrombin addition. When the length of poly-A increased, the gradual aggregation was observed (Fig. 3.8a) with a gradual increase in the range of thrombin concentrations. The shorter spacers (A5, A10, A15) was found to provide faster aggregation than the longer spacers (A30, A45, A60). Besides, the nanoconjugates superbly provided a chain-dependent linear range (Fig. 3.8b), which emphasized the ease of adjustability of the aggregation amount toward programmable engineering in a spacer poly-A on G4 probes.



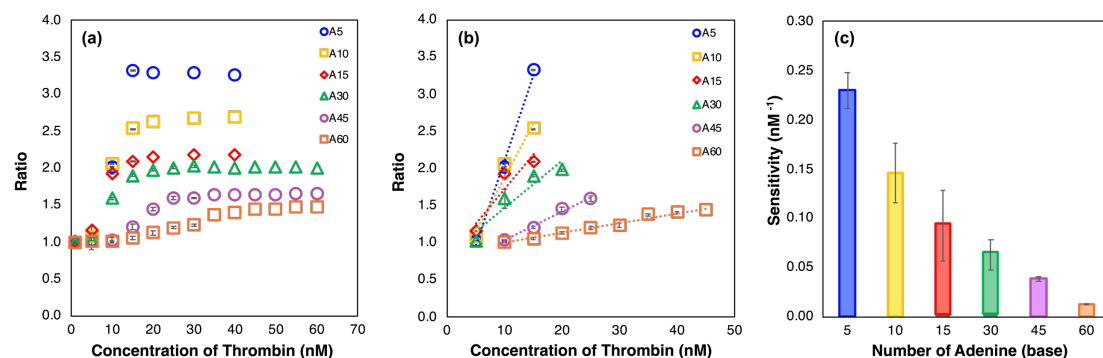


**Figure 3.8** (a) The absorption peak ratio after adding various concentrations of thrombin for poly-A (A5, A10, A15, A30, A45, A60) G4-AuNPs in 20 mM Tris-HCl (pH 7.4), containing 140 mM NaCl, 5 mM KCl, 1 mM  $\text{CaCl}_2$  and 1 mM  $\text{MgCl}_2$ . Data was collected at 10 min after adding thrombin. The corresponding linearities (b) and sensitivity (c) were shown.

The author further investigated the distribution of the particles by dynamic light scattering (DLS). The G4-AuNPs showed the monodispersity of particles in dispersion and aggregation states (Fig. 3.9), indicating the excellent homogenous particle sizes and ease of functionalization. Besides, the hydrodynamic diameter ( $D_h$ ) of such particles were found to perfectly correspond to UV absorption results, showing in Table 3.2. For G4-AuNPs, the longer sequences, the larger  $D_h$  was clearly seen due to the larger layer of DNA ligand covered around AuNPs. In addition to thrombin (50 nM) into the G4-AuNP solution, the significant change in particle size about 6~7 fold was recorded with the consistency of length of poly-A (Table 3.2). In the sake of well-defined G4-AuNPs, the values of surface potential shown no significant difference among sequences, despite showing a slight decrease in surface potential after thrombin addition to imply the binding

of thrombin and G4 aptamer on AuNP surface. As a result, the clear red color of the solution obviously changed to purple-blue, afterward (Fig. 3.10).

Such remarkably controlled surface density of the thiolated poly-A-G4 coated AuNP surface, the poly-A spacer not only suggested the greatly improved aggregation efficiency but also quantitatively controlled the sensitivity of detection as represented in term of the slope of linearity. Fig. 3.8c clearly shows the reduction of the sensitivities with the number of adenine about 18 fold between the shortest (poly-A5) and the longest (poly-A60) lengths. These results suggest that the length of DNA-covered AuNPs is a key factor in preventing aggregation and strongly influences both the degree of aggregation and the detection sensitivity. To be more specific, the introduction of S-Au modification with the poly-A spacer on the G4 DNA underlines the synergistic properties of the highly steric effect of G4, the strong adsorption affinity onto Au of poly-A, and S-Au chemistry that cables to be tuned the property of needs simply by varying the spacer chains. Noted, the choosing criteria could be varied depending on the purpose of applications.

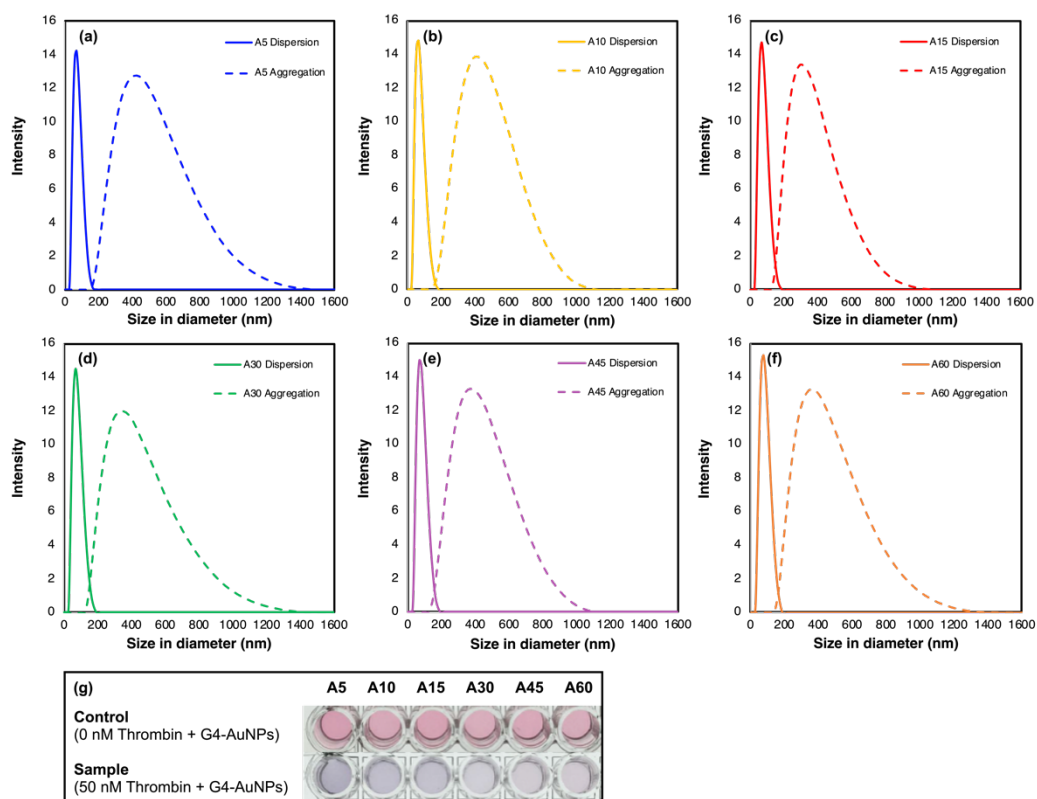


**Figure 3.9** The monodispersity of particles in dispersion (solid line) and aggregation states (dash line). Thrombin detection using 1.0 OD G4-AuNPs with different poly-A length; (a) A5, (b) A10, (c) A15, (d) A30, (e) A45 and (f) A60 in 20 mM Tris-HCl (pH 7.4) containing 140 mM NaCl, 5 mM KCl, 1 mM  $\text{CaCl}_2$  and 1 mM  $\text{MgCl}_2$ . Data were gathered 10 min after the addition of 50 nM thrombin. (g) The corresponding colorimetric change of particles without (control) and with (sample) 50 nM thrombin addition is shown.

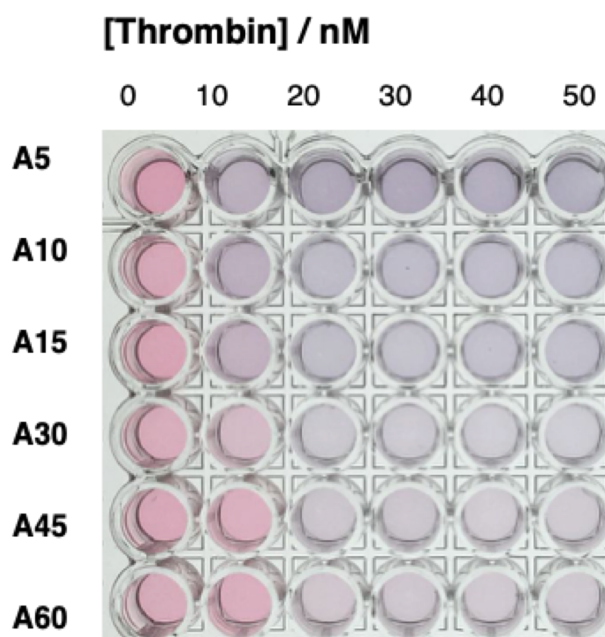


**Figure 3.10** The corresponding images of poly-A (A5, A10, A15, A30, A45, A60) G4-AuNPs solutions with the different concentration of thrombin from 0 to 50 nM in 20 mM Tris-HCl (pH 7.4) containing 140 mM NaCl, 5 mM KCl, 1 mM CaCl<sub>2</sub> and 1 mM MgCl<sub>2</sub>. The image was taken at 10 min after thrombin addition.

In the viewpoint of salt-induced non-crosslinking aggregation, the detection sensitivity relies on the considerably high salt concentration, where the solution supposes to support the formation of the G4 aptamer for binding to the target thrombin via charge-charge interaction. Potassium ions (K<sup>+</sup>) have a favorably effective ionic radius to interact with G4 DNA among the cations<sup>18</sup>, which is essential for G-quadruplex formation, especially thrombin binding aptamer G4.<sup>2</sup> Accordingly, potassium chloride (KCl) was evaluated in this experiment due to its high ability to stabilize the G4 structure. By using the

conjugation of poly-A (A5, A15, A60)-G4 with AuNPs on the basis of UV-Vis absorption measurements, the detection sensitivity (slope of linear) is a criterion to choose the optimum condition. The loading of salt into the solution increased from 5 to 500 mM (Fig. 3.11) with the concentration of thrombin. When  $K^+$  concentration increased, the detection sensitivities of the particles with poly-A5 (shortest length) displayed a subtle change, and The coefficient of determination ( $R^2$ ) was found to be greatly improved (Fig. 3.11). The  $R^2$  of linear regression was improved with potassium concentration. The higher the value of  $R^2$ , the better the fit of the regression to the data set. A value of  $R^2$  near 1 indicates an extremely good fit of the linear regression. Poly-A15 (middle length) shown no significant difference in sensitivities with  $K^+$  concentration as same as the longest poly-A60 (Fig. 3.12a), excluding at the highest  $K^+$ . At 500 mM  $K^+$ , the author could not observe an aggregation of poly-A60 G4-grafted AuNPs after thrombin addition over 7 hr (Fig. 3.13) because the longer the DNAs, the harder binding of thrombin-G4 aptamer occurs in varying high salt concentration. This result is corresponding to the previous report of the effect of electrostatic shielding on destabilization of the thrombin-G4 aptamer complex at high ionic strength<sup>19</sup>.

Under the consideration of a constant  $K^+$  concentration, the inverse relationship between detection sensitivity and poly-A chain was noticed—the sensitivity sharply decreased when the DNA chain was getting longer (Fig. 3.8c)—because of the reduction of aggregation degree. Interestingly, it was found that the surface potential of all sequences is not significantly different, as shown in Table 3.2, indicating the negligibility of electrostatic repulsion of the particles. This additionally implies that only the influence of steric repulsion is a predominant factor in the colloidal stability due to the flexible and bulky steric G4 DNA on the AuNP surface. In addition, TEM images showed the relevant

dispersion and aggregation of G4-AuNPs for thrombin detection (Fig. 3.14), which is corresponding to absorption results. The assay performed under 50 mM of  $K^+$  displayed the significant-high sensitivity with an excess amount of  $K^+$  for G4 stabilization, which was chosen as the optimum value, afterward. Noted, when one parameter was varied, other parameters were kept constant to find out the optimum value.

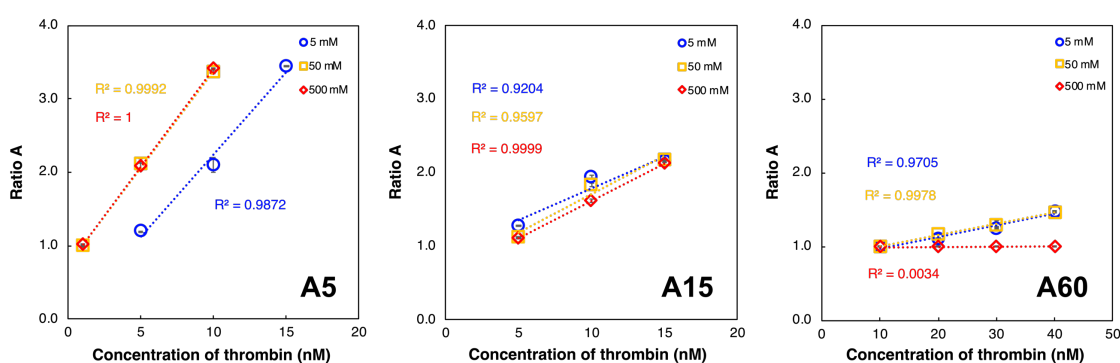


**Figure 3.11** Ratio absorption of 1.0 OD poly-A (a) A5, (b) A15, and (c) A60 G4-AuNPs with the different concentration of potassium ion from 5 to 50 mM in 20 mM Tris-HCl (pH 7.4) containing 140 mM NaCl, 1 mM  $CaCl_2$ , 1 mM  $MgCl_2$ . Data were recorded 10 min after the addition of thrombin.

Respectively, the other factor that indirectly affected the detection sensitivity is incubation time. By using a poly-A60 to get the best performance, the absorption spectra of poly-A60 G4-AuNPs gradually shifted from 535 nm to 560 nm by time (Fig. 3.15). As a comparison, the sensitivity of detection was found to be time-independent (Fig. 3.12b) because of the constant change in the ratio absorbance (ratio A). Noted, the ratio A was defined by the ratio of the shifted peak to that at the original peak, indicating aggregation

amount. Furthermore, the degree of color change depended on thrombin concentration overtime. (Fig. 3.12c). Thus, the shortest time of 5 min, suspended after thrombin addition, was decided as optimum incubation time.

The optimization of involving parameters provides strong evidence that AuNPs with poly-A spacer (A5, A10, A15, A40, A45, A60) exhibit remarkably different stability toward salt-inducing aggregation and suggests ease of tunability for properties of interest—the degree of aggregation and the detection sensitivity. Conditions of detection had been optimized to be compatible with the applications of interest, which became a prospective cohort study.

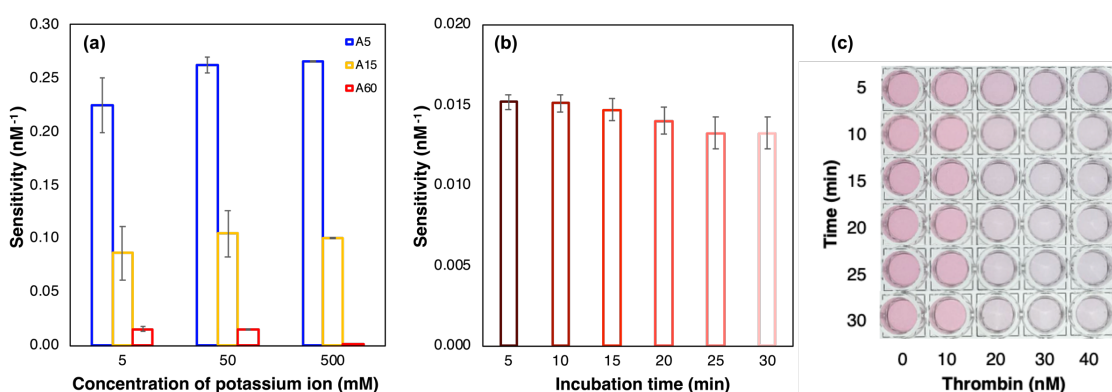


**Figure 3.12** (a) Thrombin detection using 1.0 OD AuNPs immobilized with poly-A: A5 (blue), A15 (yellow), A60 (red) in 20 mM Tris-HCl (pH 7.4) containing 140 mM NaCl, 1 mM CaCl<sub>2</sub> and 1 mM MgCl<sub>2</sub> with varying KCl concentration from 5 to 500 mM. The absorption were measured at 10 min after adding thrombin. The values indicate the slopes of the fitted lines, or the sensitivity. The comparison of sensitivity (b) and corresponding image (c) in various incubation time from 5 to 30 min using poly-A60 G4-AuNPs in 20 mM Tris-HCl (pH 7.4) containing 140 mM NaCl, 50 mM KCl, 1 mM CaCl<sub>2</sub> and 1 mM MgCl<sub>2</sub>.

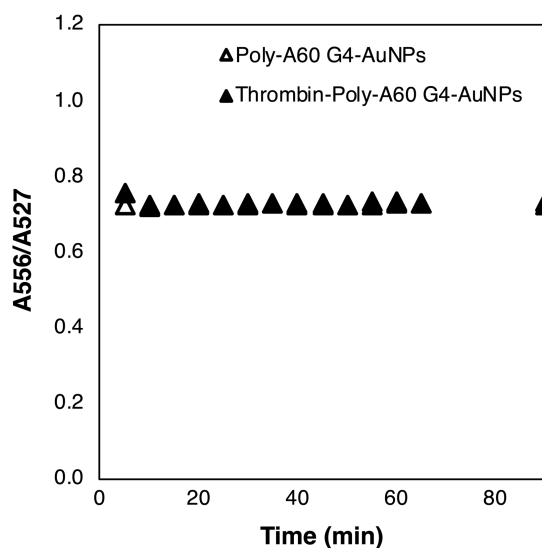


**Figure 3.13** Time-dependent ratio of absorption ( $A_{556}/A_{527}$ ) of 1.0 OD poly-A60 G4-AuNPs in 20 mM Tris-HCl (pH 7.4) containing 140 mM NaCl, 500 mM KCl, 1 mM  $\text{CaCl}_2$ , 1 mM  $\text{MgCl}_2$  with 40 nM thrombin. No aggregation was observed over 420 min due to the effect of electrostatic shielding on destabilization of the thrombin-G4 aptamer complex at high ionic strength.

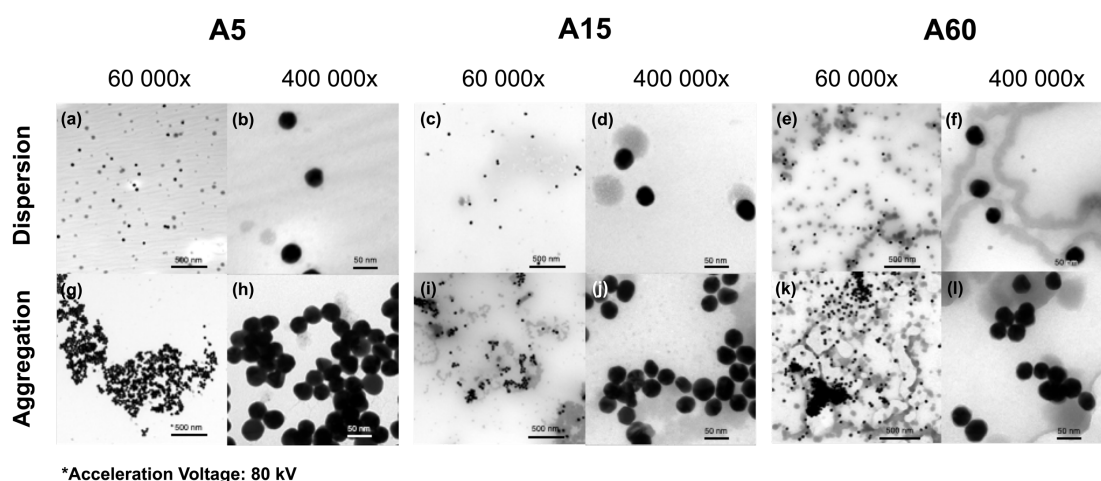


**Figure 3.14** TEM images of poly-A (A5, A15, A60) G4-AuNPs at dispersion/aggregate states under 60 000 and 400 000 magnification.



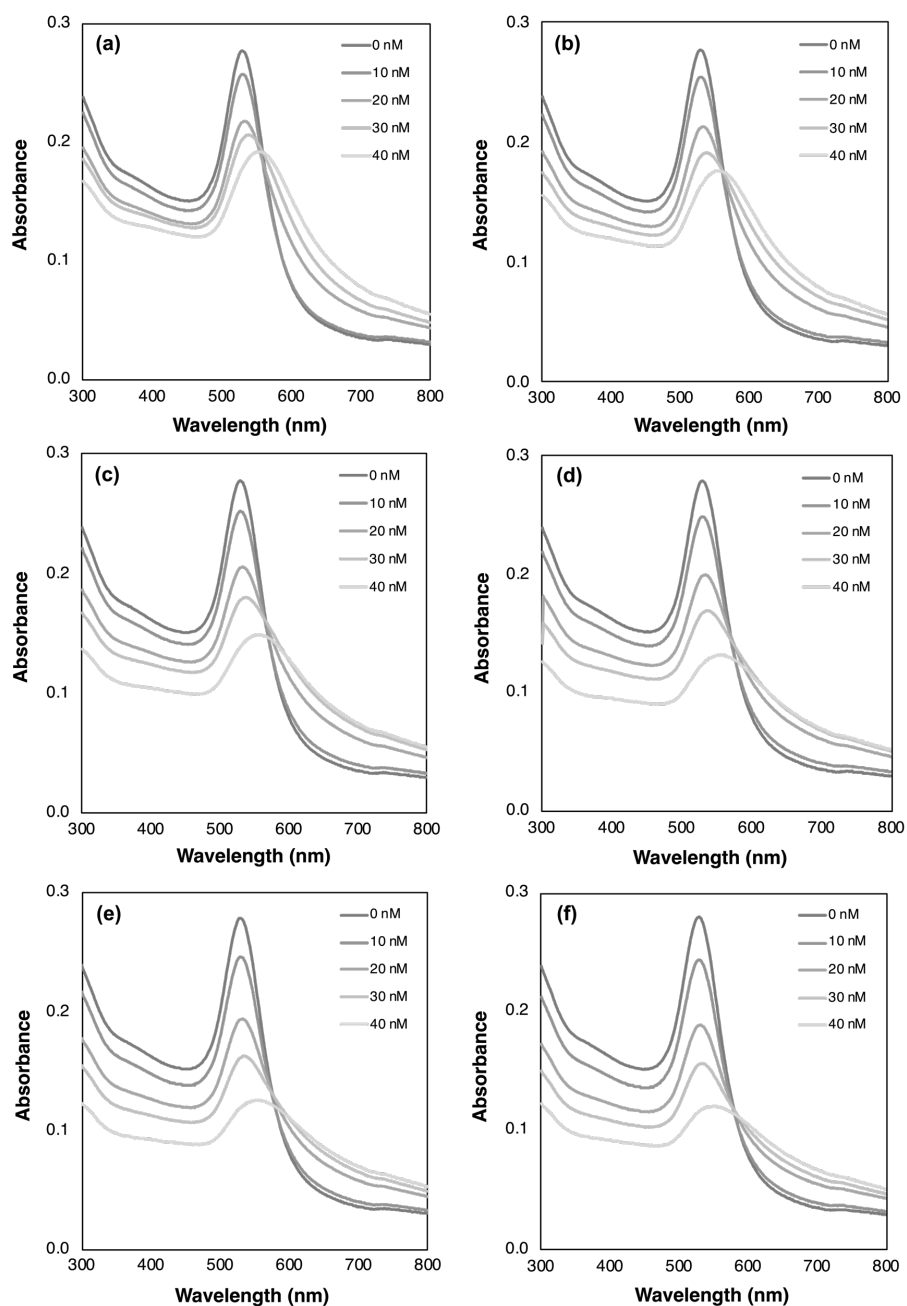


**Figure 3.15** UV-vis spectra of 1.0 OD poly-A60 G4-AuNPs in 20 mM Tris-HCl (pH 7.4), containing 140 mM NaCl, 50 mM KCl, 1 mM CaCl<sub>2</sub>, 1 mM MgCl<sub>2</sub>, under different thrombin concentrations from 0 to 40 nM. The longer in time, the more the aggregation was shown. The sensitivity was obtained with no significant difference at any incubation time: 5 (a), 10 (b), 15 (c), 20 (d), 25 (e), and 30 min (f).

### 3.4.2 Specificity

The specificity of the sensor was studied in order to confirm that the inherent role of G4 aptamer is responsible for binding specifically to the target thrombin at exosite I toward charge-charge interaction between TT of G4 and arginine of thrombin. In addition, the fabricated G4-AuNPs could single out only the protein of interest, thrombin, among other coexisting proteins in blood serum, showing the particles aggregated. The author expected that other proteins do not interfere with the sensor response, showing the particles remained dispersed. To test the specificity, three dominantly abundant proteins—albumin, gamma globulin, and immunoglobulin G—in blood serum were investigated. The investigation of the specificity was performed by comparing  $A_{556}/A_{527}$  after spiking with an interfering agent at 40  $\mu\text{M}$  against 40 nM thrombin.

Using 40 nm AuNPs functionalized with poly-A60 under the optimum condition of 50 mM  $\text{K}^+$  concentration and 5 min reaction time, the proposed sensor shows concrete evidence that our G4-AuNPs are highly specific toward thrombin with the significant response change from the control (Fig. 3.16). The response of other proteins is as same as the response of control. Even if, they were present at a much higher level about 1000 times compared with thrombin. Noted, the specificity is justified if the response of other interferent proteins does not significantly deviate from the control. The color change can observe only for thrombin as the corresponding image shown in Fig. 3.16. This must be due to the outstanding function of the G4 aptamer. Besides, the plasmonic peak shift of poly-A60 G4-AuNPs was induced only by thrombin, indicating this colloidal system has a high specificity for thrombin (Fig. 3.17). Therefore, the G4-AuNP sensor was promising to use for thrombin detection.

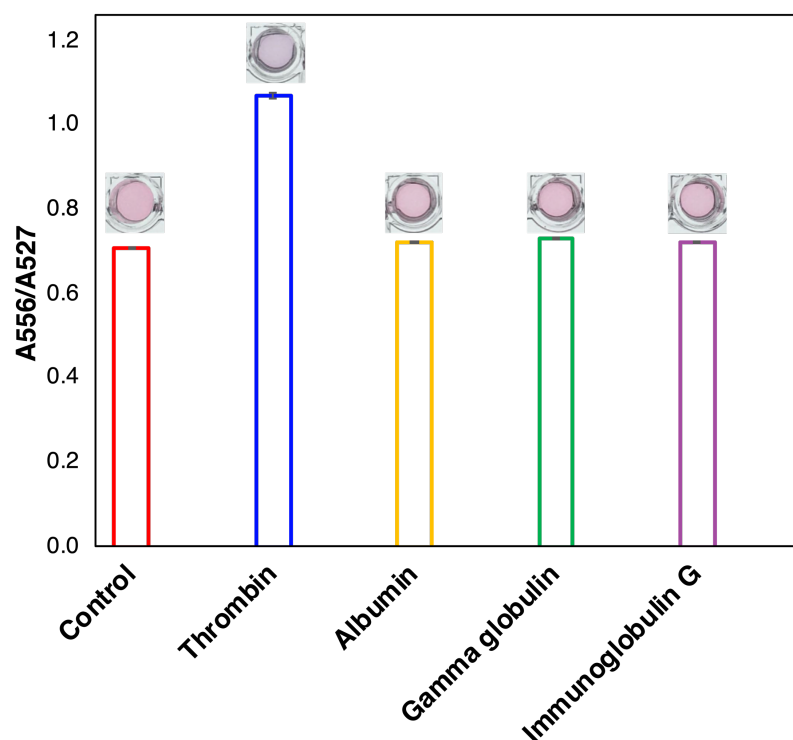


**Figure 3.16** Absorption peak ratio ( $A_{556} / A_{527}$ ) for the detection of different blood proteins: thrombin, albumin, gamma globulin, and immunoglobulin G. UV-vis measurements of poly-A60 G4-AuNPs in 20 mM Tris-HCl (pH 7.4) containing 140 mM NaCl, 50 mM KCl, 1 mM  $\text{CaCl}_2$ , 1 mM  $\text{MgCl}_2$  were performed at 40 nM of thrombin and 40  $\mu\text{M}$  of other proteins. The incubation time was set at 5 min. The corresponding images were shown above each bar.

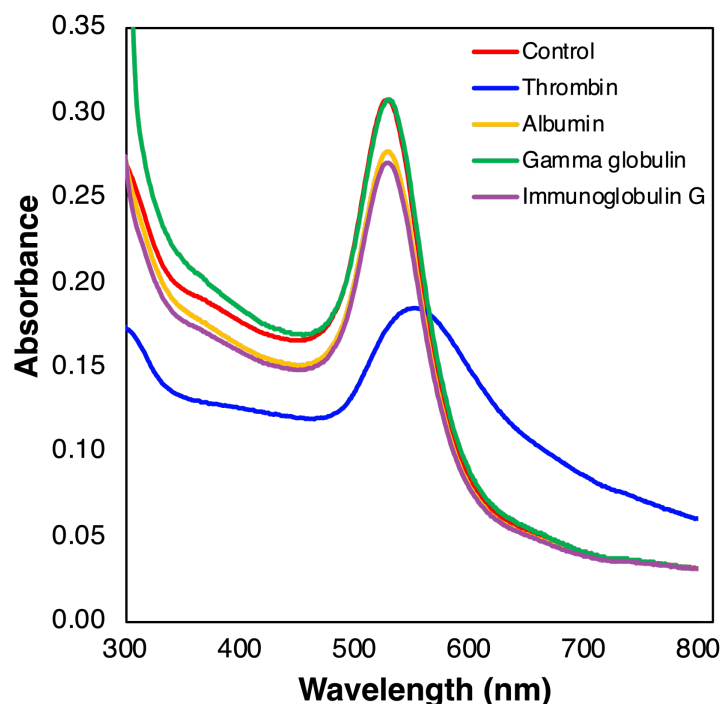


**Figure 3.17** UV-vis spectra of 1.0 OD poly-A60 G4-AuNPs (red) under the addition of 40 nM thrombin (blue), 40  $\mu$ M albumin (yellow), 40  $\mu$ M gamma globulin (green), and 40  $\mu$ M immunoglobulin G (purple) in 20 mM Tris-HCl (pH 7.4) containing 140 mM NaCl, 50 mM KCl, 1 mM  $\text{CaCl}_2$ , 1 mM  $\text{MgCl}_2$ . Data were gathered 5 min after adding thrombin. No peak shift was observed under the addition of any proteins, except thrombin.

### 3.4.3 Analytical Performance

The limit of detection was evaluated on the basis of UV-Vis absorption measurements. Fig. 3.18a shown that the absorption peak shifted to longer wavelengths after thrombin addition. The corresponding linear dynamic range was observed in Fig. 3.18b, and the linearity was obtained between 10.0 to 40.0 nM with a slope of

$0.0164 \pm 0.0007 \text{ nM}^{-1}$ . The lower limit of detection  $y_{\text{LOD}}$  was evaluated from the equation  $y_{\text{LOD}} = y_{\text{blank}} + 3\sigma_{\text{blank}}$ . Noted,  $y_{\text{blank}}$  and  $\sigma_{\text{blank}}$  are the mean signal value and its standard deviation of blank sample<sup>20</sup>. It was found that poly-A G4-AuNPs provided 0.72 nM of the limit of detection. According to the experiment results, it is proof that this sufficient detection performance of this colloidal system, thus cable to detect thrombin in serum samples since the normal level of thrombin in the serum of healthy people is between 1.1 and 1.4  $\mu\text{M}$ .

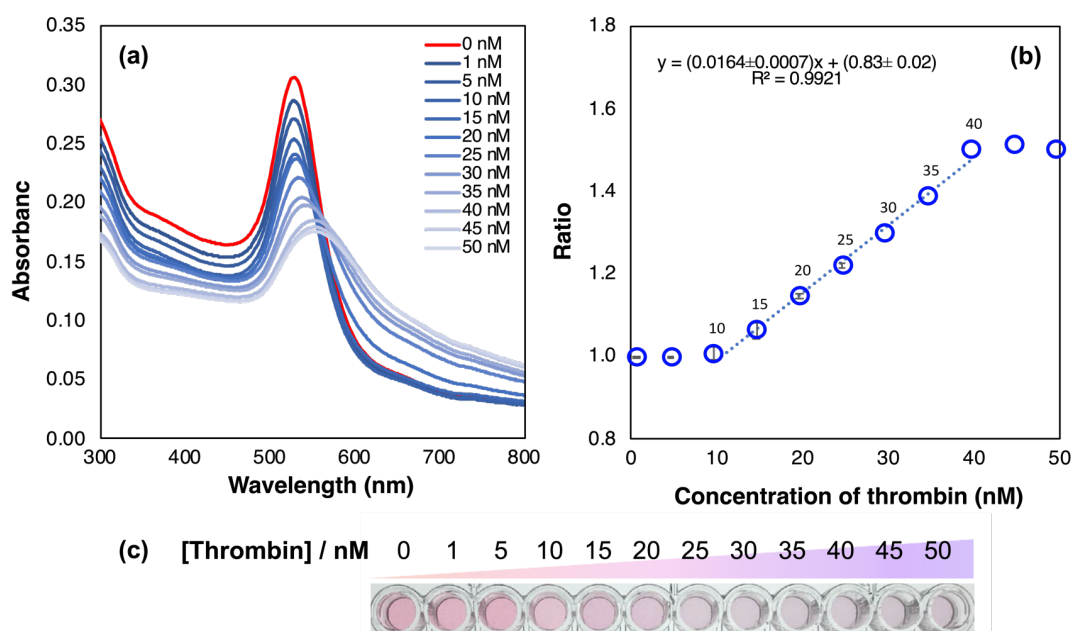


**Figure 3.18** UV-vis spectra (a) and the corresponding linear dynamic range (b) of poly-A60 G4-AuNPs in 20 mM Tris-HCl (pH 7.4) containing 140 mM NaCl, 50 mM KCl, 1 mM  $\text{CaCl}_2$ , 1 mM  $\text{MgCl}_2$ , varied with thrombin concentration. All data were gathered at 5 min after adding thrombin. (c) The corresponding colorimetric image of poly-A60 G4-AuNP solutions at the various thrombin concentrations: 0, 1, 5, 10, 15, 20, 25, 30, 40, 45, and 50 nM.

### 3.4.4 Real Sample Analysis

As on-demand tunable properties of interests, the author applied the excellent performance of poly-A60 G4-AuNPs for the issues concerning the practical thrombin sensor. Therefore, the author further assessed whether G4-AuNPs could provide the specific detection of thrombin in the human serum sample. Prior to measurement, the author complementarily studied the effect of sample dilution in order to use the serum sample under the confidential of no extra signal from the sample itself. With that, 200 fold of dilution was found to overcome the viscosity effect of the sample from the generation of the bubble with the stable dispersion of G4-AuNPs (Fig. 3.19).

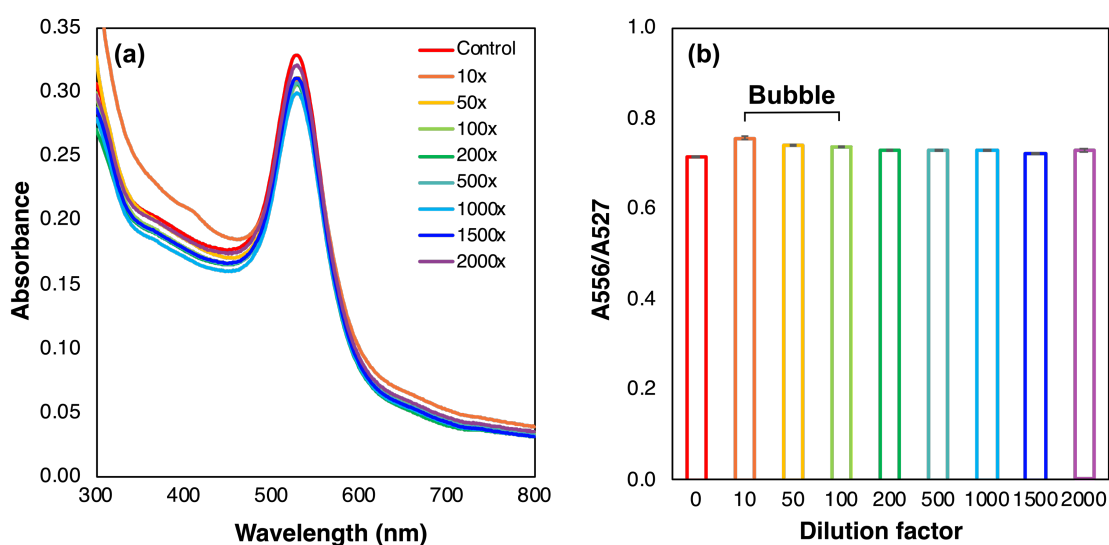


**Figure 3.19** UV-vis spectra (a) and ratio a (b) of 1.0 OD poly-A60 G4-AuNPs (red) in serum sample at different dilution factors from 0 to 2000 fold in 20 mM Tris-HCl (pH 7.4) containing 140 mM NaCl, 50 mM KCl, 1 mM CaCl<sub>2</sub>, 1 mM MgCl<sub>2</sub>. No peak shift was observed at any dilution factors. No effect of serum viscosity from the generation of bubble was observed after 200 fold.

To evaluate the matrix effect in the real serum sample, human serum was spiked with thrombin at various final concentrations. Also, thrombin standard solutions were also prepared at the same final concentrations. On the basis of UV-Vis measurement, the ratio A of the spiked solution and the standard solution were plotted against thrombin concentration to obtain two calibration plots (Fig. 3.20), and slopes of the two curves were compared the variation using two-way ANOVA, afterward.

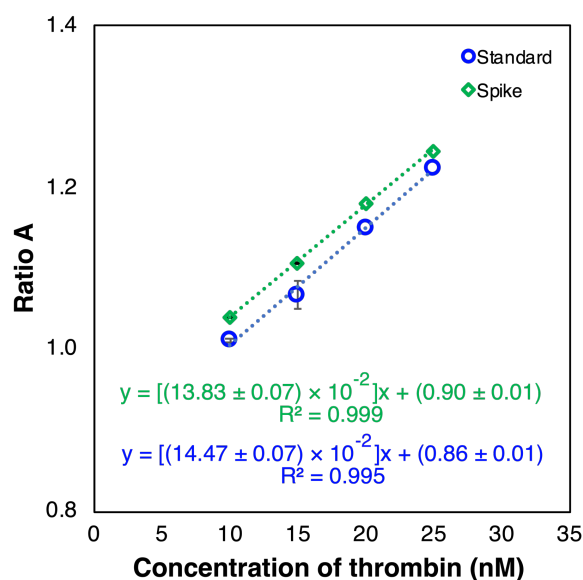


**Figure 3.20** Absorption peak ratio for the spike (matrix-match) (green) and the standard calibration curves (blue). UV-vis measurements of poly-A60 G4-AuNPs in 20 mM Tris-HCl (pH 7.4) containing 140 mM NaCl, 50 mM KCl, 1 mM CaCl<sub>2</sub>, 1 mM MgCl<sub>2</sub> were performed by varying the thrombin concentration. The optimum incubation time at 5 min was used. In this figure, no difference of slopes are also shown. The slopes of the two plots were compared using two-way ANOVA to investigate the variation.

Using a sensor to measure the thrombin concentration under the optimal condition, the author observed a good correlation of the slopes of the matrix-match (spiked) curve with the standard calibration curve. The slopes of the two plots were compared using two-way ANOVA to investigate the variation (Fig. 3.20). It was found that both were not significantly different ( $P>0.05$ ), indicating no matrix effect in the real sample. This verified that the interferences—proteins and chemicals—in the real sample had not generated any significant signal toward thrombin. Importantly, the sensor provided acceptable recoveries in the range of 99 - 101% of the whole concentration of thrombin based on AOAC guideline<sup>21</sup> as shown in Table 3.3. However, the real human serum sample shows a non-detectable concentration of thrombin under 200 fold dilution because the initial concentration of thrombin in blood serum is relatively low compared with the major proteins such as albumin<sup>22-23</sup>, gamma globulin<sup>23</sup>, and immunoglobulin G.<sup>24</sup> Besides, such high specificity of the G4-AuNPs is accompanied by notable precision in the representation of the RSDs. Noted, it is acceptable by AOAC if the recoveries are between 80 - 110%, and the RSDs are less than 7.3 - 15% for analyte concentration of 0.1 - 10 mg. L<sup>-1</sup>. As expected, the sensor can apply to use in real serum matrix with high efficiency and specificity of the thrombin detection. This strongly confirmed the specificity of G4-AuNP to target identification for real sample analysis.



**Table 3.3** Concentration of thrombin found in human serum sample along with % recoveries.

Thrombin in the real sample (nM)	Spiked (nM)	Found (nM)	Recovery $\pm$ r.s.d (%) (n=4)
ND	10.00	10.02	100.16 $\pm$ 0.57
ND	15.00	14.86	99.10 $\pm$ 0.36
ND	20.00	20.22	101.12 $\pm$ 1.40
ND	25.00	24.90	99.59 $\pm$ 1.31

ND is non-detectable (<LOD)

### 3.5 Conclusions

This work presents a rapid yet sensitive colorimetric sensor for thrombin detection based on DNA aptamer in G-quadruplex conformation and non-crosslinking aggregation platform of gold nanoparticles. The aggregation of G4-AuNPs was found to be induced by thrombin binding and stabilizing G4, which made up the tighter and more rigid structure of G4 on the AuNP surface. The quantitative analysis of particle aggregation was measured at 5 min after the addition of thrombin to the colloidal system. The real-time color of the solution change to purple-blue was easily observed with the naked eye within 3 min as of qualitative analysis. Besides, the author has achieved the on-demand tunability of properties of interests—the degree of aggregation and the sensitivity of detection—which allows us to broaden the built-in S-Au chemistry and poly-A functions of the G4-AuNPs for various applications. In this sense, the insertion of short-chain of poly-A on G4 strands offers ultrasensitive aggregation with relatively high sensitivity of detection. On the other hand, the long poly-A-inserted G4s represent the wider dynamic range and the better detection limit. Likewise, the author has illustrated the powerful approach with the highly specific detection despite the existence of the interferences at 1000 times in blood serum. Repetitively, the author successfully utilized the sensor to differentiate thrombin in the human serum sample, where the practitioner of G4-AuNPs was expressed under a non-crosslinking aggregation platform. Finally, the challenge to broaden applications of the functionalization of gold nanoparticle with G-quadruplex DNA have been revealed by the robust benefits of these next-generation G4-AuNPs.

### 3.6 References

- (1) Bock, L. C.; Griffin, L. C.; Latham, J. A.; Vermaas, E. H.; Toole, J. J. Selection of Single-Stranded DNA Molecules That Bind and Inhibit Human Thrombin. *Nature* **1992**, 359, 710–713.
- (2) Macaya, R. F.; Schultze, P.; Smith, F.W.; Roe, J. A.; Feigon, J. Thrombin-Binding DNA Aptamer Forms a Unimolecular Quadruplex Structure in Solution. *Proc. Natl. Acad. Sci. USA* **1993**, 90, 3745–3749.
- (3) Kimura-Suda, H.; Petrovykh, D. Y.; Tarlov, M. J.; Whitman, L. J. Base-Dependent Competitive Adsorption of Single-Stranded DNA on Gold. *J. Am. Chem. Soc.* **2003**, 125, 9014–9015.
- (4) Koo, K. M.; Sina, A. A. I.; Carrascosa, L. G.; Shiddiky, M. J. A.; Trau, M. DNA–Bare Gold Affinity Interactions: Mechanism and Applications in Biosensing. *Anal. Methods*, **2015**, 7, 7042–7054.
- (5) Fujita, M.; Katafuchi, Y.; Ito, K.; Kanayama, N.; Takarada, T.; Maeda, M. Structural Study on Gold Nanoparticle Functionalized with DNA and Its Non-Cross-Linking Aggregation. *J. Colloid Interface Sci.* **2012**, 368, 629–35.
- (6) Paborsky, L. R.; McCurdy, S. N.; Griffin, L. C.; Toole, J. J.; Leung, L. L. K. The Single-Stranded DNA Aptamer-Binding Site of Human Thrombin. *J. Biol. Chem.* **1993**, 268, 20808–20811.
- (7) Pica, A.; Russo Krauss, I.; Merlino, A.; Nagatoishi, S.; Sugimoto, N.; Sica, F. Dissecting the Contribution of Thrombin Exosite I in the Recognition of Thrombin Binding Aptamer. *FEBS J.* **2013**, 280, 6581–6588.

- (8) Sato, K.; Hosokawa, K.; Maeda, M. Rapid Aggregation of Gold Nanoparticles Induced by Non-Cross-Linking DNA Hybridization. *J. Am. Chem. Soc.* **2003**, 125, 8102–8103.
- (9) Trapaidze A.; Hérault, J.-P.; Herbert, J.-M.; Bancaud, A.; Gué, A.-M. Investigation of the Selectivity of Thrombin-Binding Aptamers for Thrombin Titration in Murine Plasma. *Biosens. Bioelectron.* **2016**, 78, 58–66.
- (10) Matsuoka, H.; Tanaka, H.; Hashimoto, T.; Ise, N. Elastic Scattering from Cubic Lattice Systems with Paracrystalline Distortion. *Phys. Rev. B* **1987**, 36, 1754–1765.
- (11) Matsuoka, H.; Tanaka, H.; Iizuka, N.; Hashimoto, T.; Ise, N. Elastic Scattering from Cubic Lattice Systems with Paracrystalline Distortion. II. *Phys. Rev. B* **1990**, 41, 3854–3856.
- (12) Krauss, I. R.; Merlino, A.; Randazzo, A.; Novellino, E.; Mazzarella, L.; Sica, F. High-Resolution Structures of Two Complexes between Thrombin and Thrombin-Binding Aptamer Shed Light on the Role of Cations in the Aptamer Inhibitory Activity. *Nucleic Acids Research* **2012**, 40, 8119–8128.
- (13) Yang, J.; Pong, B.-K.; Lee, J. Y.; Too, H.-P. Dissociation of Double-Stranded DNA by Small Metal Nanoparticles. *J. Inorg. Biochem.* **2007**, 101, 824–830.
- (14) Liu, B.; Wu, P.; Huang, Z.; Ma, L.; Liu, J. Bromide as a Robust Backfiller on Gold for Precise Control of DNA Conformation and High Stability of Spherical Nucleic Acids. *J. Am. Chem. Soc.* **2018**, 140, 4499–4502.
- (15) Zhou, W.; Wang, F.; Ding, J.; Liu, J. Tandem Phosphorothioate Modifications for DNA Adsorption Strength and Polarity Control on Gold Nanoparticles. *ACS Appl. Mater. Interfaces* **2014**, 6, 14795–14800.

- (16) Pei, H.; Li, F.; Wan, Y.; Wei, M.; Liu, H.; Su, Y.; Chen, N.; Huang, Q.; Fan C. Designed Diblock Oligonucleotide for the Synthesis of Spatially Isolated and Highly Hybridizable Functionalization of DNA–Gold Nanoparticle Nanoconjugates. *J. Am. Chem. Soc.* **2012**, 134, 11876–11879.
- (17) Zhu, D.; Chao, J.; Pei, H.; Zuo, X.; Huang, Q.; Wang, L.; Huang, H.; Fan, C. Coordination-Mediated Programmable Assembly of Unmodified Oligonucleotides on Plasmonic Silver Nanoparticles. *ACS Appl. Mater. Interfaces* **2015**, 7, 11047–11052.
- (18) Venczel, E. A.; Sen, D. Parallel and Antiparallel G-DNA Structures from a Complex Telomeric Sequence. *Biochemistry* **1993**, 32, 6220–6228.
- (19) Zhang, J.; Ogorzalek Loo, R. R.; Loo, J. A. Structural Characterization of a Thrombin-Aptamer Complex by High Resolution Native Top-Down Mass Spectrometry. *J. Am. Soc. Mass Spectrom.* **2017**, 28, 1815–1822.
- (20) Thomsen, V.; Schatzlein, D.; Mercuro, D. Limits of Detection in Spectroscopy. *Spectroscopy* **2003**, 18, 112–114.
- (21) AOAC, *Guidelines for standard method performance requirements*. The Association of Official Analytical Chemists International, **2016**, p. 1-18.
- (22) Wang, R. E.; Tian, L.; Chang, Y.-H. A Homogeneous Fluorescent Sensor for Human Serum Albumin. *J Pharm Biomed Anal.* **2012**, 63, 165–169.
- (23) Kasper, D. L.; Fauci, A. S.; Hauser, S. L.; Longo, D. L.; Jameson, J. L.; Loscalzo, J. Harrison's principles of internal medicine. 19th edition. New York: The McGraw-Hill Companies, Inc. **2015**.
- (24) Jolliff, C. R.; Cost, K. M.; Stivrins, P. C.; Grossman, P. P.; Nolte, C. R.; Franco, S. M.; Fijan, K. J.; Fletcher, L. L.; Shriner, H. C. Reference Intervals for Serum IgG,

IgA, IgM, C3, and C4 as Determined by Rate Nephelometry. *Clin Chem.* **1982**, 28, 126–128.

(25) Demers, L. M. ; Mirkin, C. A.; Mucic, R. C.; Reynolds III, R. A.; Letsinger, R. L.; Elghanian, R.; Viswanadham, G. A Fluorescence-based Method for Determining the Surface Coverage and Hybridization Efficiency of Thiol-capped Oligonucleotides Bound to Gold Thin Films and Nanoparticles. *Anal. Chem.* **2000**, 72, 5535–5541.

## **Chapter 4**

### **Non-crosslinking Aggregation via Inter-stranded Partial Hybridization**

## 4.1 Abstract

The newly inter-stranded partial hybridization of DNA duplex on gold nanoparticles (dsDNA-AuNPs) induced non-crosslinking aggregation has discovered the first time using G-quadruplex-functionalized gold nanoparticles (G4-AuNPs) with an additional pH-dependent property. This new phenomenon has efficiency comparable to the previous report of a full-match hybridization manner. The discovery of a partial hybridization concept was found to strike the sensor robustness being more straightforward and more applicable because an aggregation was induced even if the target oligo-DNA hybridized “partially” to the probe with blunt-ended duplex formation. Colloidal stability has yielded by a bulky steric structure of G4 DNA, resulting in the red color of the G4-AuNP solution. After a partial hybridization to DNA target, the colloidal solution color changed to purple-blue in a short time since the formation of DNA duplex destabilized G-tetrad to Watson-Crick base pairings. Besides, G4-AuNPs displayed the structural arrangement depending on pH due to the ability of protonation of DNA subunit in acidic conditions, leading to a pH-dependent aggregation.



## 4.2 Introduction

Regarding the well-known non-crosslinking aggregation of ssDNA-AuNPs (Fig. 4.1a) reported by Maeda and co-work,<sup>1</sup> the complementary DNA target should perfectly match in “sequence” and “chain length” to maintain fully matched duplex formation at considerably high salt concentration, where the probe conformation is tighter and stiffer. Non-crosslinking aggregation was induced, afterward, by  $\pi$ – $\pi$  stacking of nucleobases, leading to the change of color of the colloidal solution from red to purple-blue. Another outstanding point of ssDNA-AuNPs is that a one-base mismatch of DNA target at the end of 5' could not induce an aggregation. The particles remained dispersed due to fraying motion of distal end bases, generating repulsion between NPs. The red color solution of the double-stranded DNA (dsDNA) with a mismatch on the AuNP surface was observed. In this sense, it inspired to improve the robustness of the system for ease of use and applicability under the non-crosslinking concept.

According to the unique features of the non-crosslinking aggregation of no limitation in DNA design, the author takes advantage of a highly polymorphic structure-sensitive colloidal behaviors of G4-AuNPs (Fig. 4.1b). The conformational transition of G4 DNA to dsDNA on AuNP core would significantly affect the colloidal stability, regarding particle aggregation. Besides, It would be more straightforward if the hybridization to some part of the DNA probe, so-called partial hybridization, could induce aggregation in order to broaden an unrevealed mechanism and to create a platform in future applications. In this sense, the author follows the unwinding of G4 to blunt-ended duplex after a partial hybridization to target, which destabilizes the G-quartet to Watson-Crick base pairings<sup>2</sup> (Fig. 4.1b, right). The decrease of G4-AuNP stability might cause by

the G4 structural transition based on a partial hybridization idea, leading to a non-crosslinking aggregation. Hence, it is possible to see the color of the G4-AuNP solution change by driving inter-stranded partial hybridization on the surface of particles. Another interesting point of the design of the DNA sequence in this study is that the particles remained dispersed due to loop-like structure formation in acidic conditions (Fig. 4.1b, left). Moreover, G4-AuNPs provided a structural arrangement over a wide range of pH.

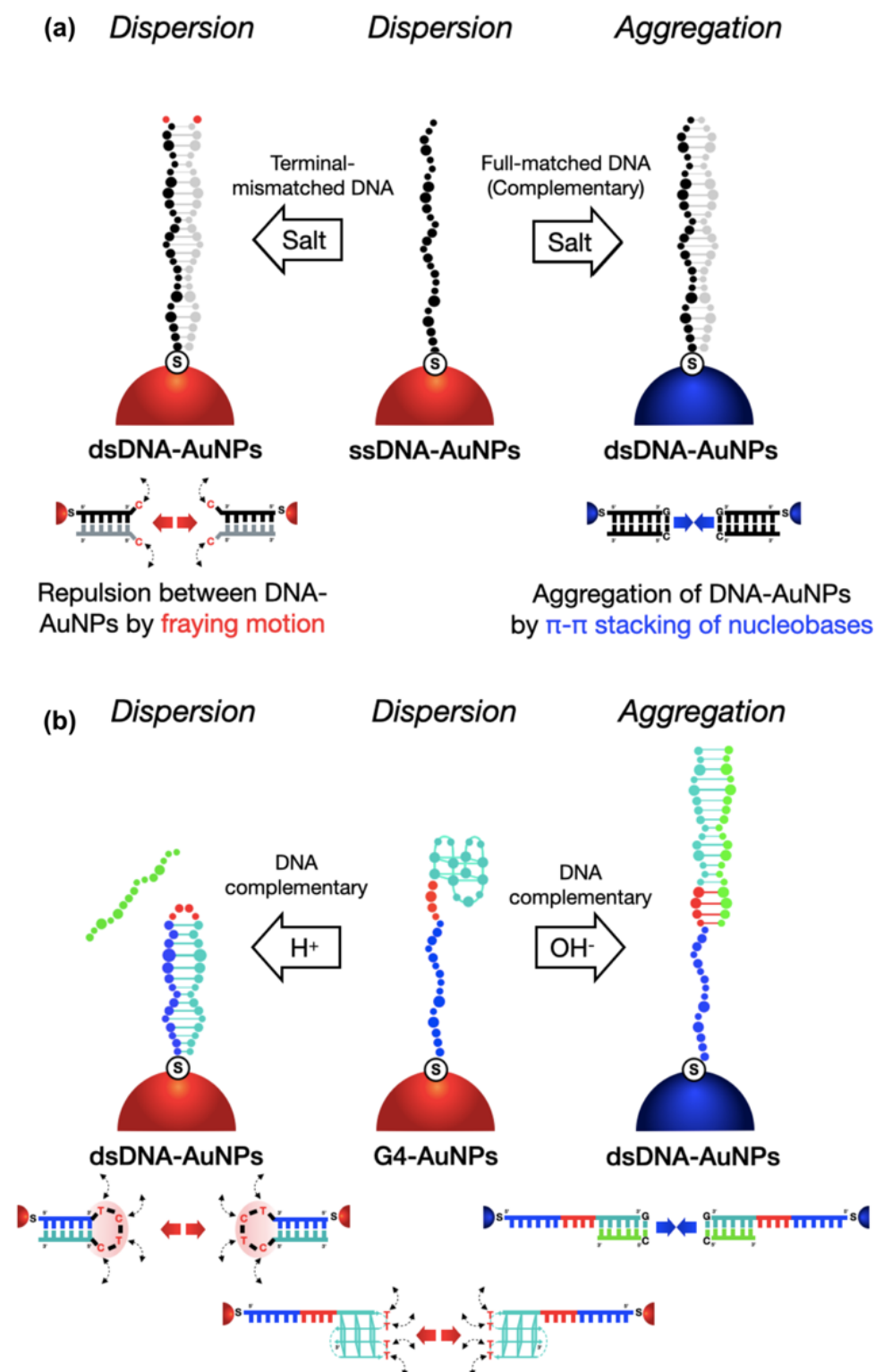


**Figure 4.1** Non-crosslinking aggregations of ssDNA-AuNPs (a) and G4-AuNPs (b) induced by duplex formation.

## **4.3 Experimental Section**

### **4.3.1 Materials**

AuNPs with diameters of about 40 nm were purchased from British Biocell International (Cardiff, UK). Oligo-DNA having a sulfhydryl group at their 5'-end were purchased from Eurofins Genomics K.K. (Tokyo) and purified by an affinity column (oligonucleotide purification cartridge (OPC); Thermo Fisher Scientific, Waltham, MA) prior to use. The DNA sequences using in this study are listed in Table 4.1. Dithiothreitol (DTT) and potassium chloride (KCl) were purchased from Sigma-Aldrich (St. Louis, MO). Sodium acetate ( $\text{CH}_3\text{COONa}$ ), sodium chloride ( $\text{NaCl}$ ), sodium dihydrogenphosphate dihydrate ( $\text{NaH}_2\text{PO}_4 \cdot 2\text{H}_2\text{O}$ ), acetic acid ( $\text{CH}_3\text{COOH}$ ), and sodium nitrate ( $\text{NaNO}_3$ ) were purchased from Wako Pure Chemical Industries (Osaka, Japan). Disodium hydrogenphosphate ( $\text{Na}_2\text{HPO}_4$ ) was purchased from Kanto Chemical (Tokyo). Milli-Q water (resistivity greater than  $18.2 \text{ M}\Omega \text{ cm}$ ) was used for all experiments.

### **4.3.2 Design and Criterion**

The design of oligo-DNAs and its preparation of G4-AuNPs is similar to section 3.3.2 of chapter 3, as shown in Fig. 3.2. Hereby, poly A-modified TBA aims to use as a reversible probe, binding the “oligo-DNA” target instead of thrombin with the potential of multi-structural arrangement in the considerable condition. Poly A-modified TBA on AuNPs could form an intra-stranded hairpin structure in acidic solution while G4 structure could be maintained in basic solution, which allows a complementary DNA target to hybridize fully or partially to G4, resulting to the double helix formation (Fig. 4.1b). Besides, the stem of “poly-A” itself can get partially protonated in acidic conditions,

which induces  $A^+_{(anti)} \bullet G_{(syn)}$  mispairs<sup>2</sup> to stabilize intra-stranded hairpin formation (Fig. 4.2).

**Table 4.1** DNA sequences used in this study.

Name	Sequence (from 5' to 3')	Length (base)
DNA probe-1	HS-(CH <sub>2</sub> ) <sub>6</sub> -A <sub>15</sub> <u>TCTCGGTTGGTGTGGTTGG</u>	34
DNA probe-2	HS-(CH <sub>2</sub> ) <sub>6</sub> -T <sub>15</sub> <u>TCTCGGTTGGTGTGGTTGG</u>	34
DNA probe-3	HS-(CH <sub>2</sub> ) <sub>6</sub> -C <sub>15</sub> <u>TCTCGGTTGGTGTGGTTGG</u>	34
DNA probe-4	HS-(CH <sub>2</sub> ) <sub>6</sub> -G <sub>15</sub> <u>TCTCGGTTGGTGTGGTTGG</u>	34
DNA probe-5	HS-(CH <sub>2</sub> ) <sub>6</sub> -TCAATCGGATCGAAT <u>TCTCGGTTGGTGTGGTTGG</u>	34
DNA probe-6	HS-(CH <sub>2</sub> ) <sub>6</sub> -A <sub>15</sub> <u>TTCTCGGTTGGTGTGGTTGG</u>	33
DNA probe-7	HS-(CH <sub>2</sub> ) <sub>6</sub> -A <sub>15</sub> <u>TCTCGGTTGGTGTGGTTGG</u>	32
DNA probe-8	HS-(CH <sub>2</sub> ) <sub>6</sub> -A <sub>15</sub> <u>TGGTTGGTGTGGTTGG</u>	31
DNA probe-9	HS-(CH <sub>2</sub> ) <sub>6</sub> -A <sub>15</sub> <u>CGGTTGGTGTGGTTGG</u>	31
DNA probe-10	HS-(CH <sub>2</sub> ) <sub>6</sub> -A <sub>15</sub> <u>GGTTGGTGTGGTTGG</u>	30
DNA probe-11	HS-(CH <sub>2</sub> ) <sub>6</sub> -CCAACCACACCAACCGAGA	19
Poly-A-modified TBA	A <sub>15</sub> <u>TCTCGGTTGGTGTGGTTGG</u>	34
cDNA-1	CCAACC	6
cDNA-2	CCAACCACACCA	12
cDNA-3	CCAACCACACCAACC	15

Name	Sequence (from 5' to 3')	Length (base)
cDNA-4	CCAACCACACCAACCGA	17
cDNA-5	CCAACCACACCAACCGAA	18
cDNA-6	CCAACCACACCAACCGAGA	19
cDNA-7	CCAACCACACCAACCGATTTTT	22
cDNA-8	CCAACCACACCAACCGAATTTTT	23
cDNA-9	CCAACCACACCAACCGAGATTTTT	24
cDNA-10	CCAACCACACCAACCGATTTTTTTTTTT	28
cDNA-11	CCAACCACACCAACCGAATTTTTTTTTTT	29
cDNA-12	CCAACCACACCAACCGAGATTTTTTTTTTT	30
cDNA-13	CCAACCACACCAACCGATTTTTTTTTTTTTTT	32
cDNA-14	CCAACCACACCAACCGAATTTTTTTTTTTTTTT	33
cDNA-15	CCAACCACACCAACCGAGATTTTTTTTTTTTTTT	34

Note: GG involved in folding the G4. Italic type , *e.g.*, *TC*, indicated the liker part.

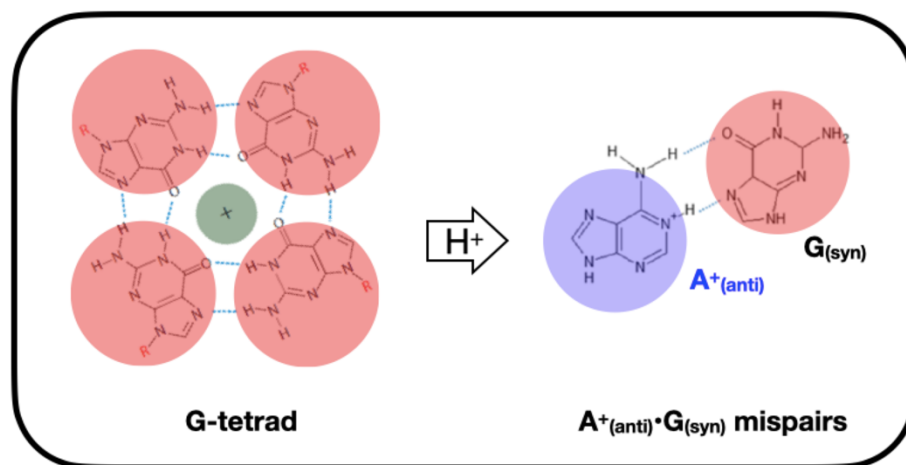


**Figure 4.2** The deformation of G-tetrad of G4 DNA to A<sup>+</sup><sub>(anti)</sub>•G<sub>(syn)</sub> mispairs<sup>2</sup> of intra-stranded hairpin duplex.

### 4.3.3 Preparation

#### 4.3.3.1 Preparation of G4-AuNPs

3 nmol of the oligo-DNAs was added to an aqueous solution of AuNPs with a concentration of one optical density (OD) at 520 nm and then the solution was kept at 50 °C in the dark overnight. Next, the solvent was replaced with 0.01 M K<sup>+</sup> phosphate buffer (pH 7) and was kept at 50 °C for another day. Potassium ion denoted as an essential cation for quadruplex conformation. After subsequent overnight heating at 50 °C, the necessary salt was added to change solution into 0.1 M NaNO<sub>3</sub> and was kept at 50 °C for 2 days. To get rid of the unbound DNA probe, the solution was centrifuged at 15,000 rpm for 30 min at 4 °C, and the precipitate was re-dispersed in the same buffer. The concentration of G4-AuNPs was adjusted to about 1.0 OD at 520 nm, unless otherwise noted.

#### 4.3.4 Characterization of pH-induced Structural Arrangement

The conformations of DNA in various pH were investigated by circular dichroism (CD) spectroscopy (JASCO J-720WI, Tokyo, Japan) at 25 °C. The CD measurements used a 0.1 cm-path cell. The CD spectra were averaged over three scans, and data were obtained with a 2 nm slit width from 220 to 320 nm. CD experiments were carried out on DNA samples at a concentration of 10  $\mu$ M in 0.1 M sodium buffer (pH 4 to 8) with 0.25 M NaCl and 0.01 M KCl.

#### 4.3.5 Characterization of G4-AuNPs

The density of G4 strands on AuNPs was investigated regarding a commercial assay. Briefly, DTT solution with a final concentration of 1.0 M was mixed with the G4-AuNP solution to release the DNA strands from the surface of particles<sup>3</sup>. The G4-AuNP solution was centrifugated at 15,000 rpm for 30 min (4 °C). Then the DNA solution was treated using an OliGreen ssDNA Quantitation Assay Kit (Thermo Fisher Scientific, Waltham, MA) and measured fluorescence intensity with a microplate reader spectroscopy (Thermo Scientific Varioskan Lux; Thermo Scientific, Kyoto, Japan), afterward. The number of G4 strands was then evaluated. The grafted number of DNA strands immobilized on AuNP with a diameter of 40 nm were shown in Table 4.2. The density of G4 strands<sup>4</sup> was also lower than the case of ssDNA<sup>5-6</sup> (*ca.* 400 strands/particle) because of the highly steric G4 conformation. The extinction spectra of G4-AuNPs (dispersion/aggregation) was estimated by microplate reader spectroscopy (Thermo Scientific Varioskan Lux; Thermo Scientific, Kyoto, Japan) at 25 °C. The absorption spectra were scanned from 300 to 800 nm with a scan rate of 100 sec/scan. The hydrodynamic diameter ( $D_h$ ) and zeta potential were measured with a Zetasizer Nano-ZS



instrument (Malvern Instruments, Malvern, UK) at 25 °C. The size and aggregation behavior of G4-AuNPs were also examined by small angle X-ray scattering (SAXS). The SAXS measurements were performed at BL40B2 RIKEN Structural Biology beamline II of SPring-8, Japan. The wavelength ( $\lambda$ ) of X-ray was 0.1 nm. The camera length, calibrated using a silver behenate standard, was about 4.2 m. SAXS images were recorded with a PILATUS 3  $\times$  2M detector (Dectris, Baden, Switzerland) at 25 °C. The SAXS data analysis was previously ascribed in section 2.3.4 of chapter 2.

**Table 4.2** The number of DNA strands per nanoparticle in this study.

Name	Sequence (from 5' to 3')	#DNA strand
DNA probe-1	HS-(CH <sub>2</sub> ) <sub>6</sub> -A <sub>15</sub> <i>TCTCGGTTGGTGTGGTTGG</i>	156 $\pm$ 1
DNA probe-2	HS-(CH <sub>2</sub> ) <sub>6</sub> -T <sub>15</sub> <i>TCTCGGTTGGTGTGGTTGG</i>	157 $\pm$ 1
DNA probe-3	HS-(CH <sub>2</sub> ) <sub>6</sub> -C <sub>15</sub> <i>TCTCGGTTGGTGTGGTTGG</i>	155 $\pm$ 1
DNA probe-4	HS-(CH <sub>2</sub> ) <sub>6</sub> -G <sub>15</sub> <i>TCTCGGTTGGTGTGGTTGG</i>	156 $\pm$ 1
DNA probe-5	HS-(CH <sub>2</sub> ) <sub>6</sub> -TCAATCGGATCGAAT <i>TCTCGGTTGGTGTGGTTGG</i>	158 $\pm$ 1
DNA probe-6	HS-(CH <sub>2</sub> ) <sub>6</sub> -A <sub>15</sub> <i>TTCCGGTTGGTGTGGTTGG</i>	161 $\pm$ 1
DNA probe-7	HS-(CH <sub>2</sub> ) <sub>6</sub> -A <sub>15</sub> <i>TCGGTTGGTGTGGTTGG</i>	155 $\pm$ 1
DNA probe-8	HS-(CH <sub>2</sub> ) <sub>6</sub> -A <sub>15</sub> <i>TGGTTGGTGTGGTTGG</i>	153 $\pm$ 1
DNA probe-9	HS-(CH <sub>2</sub> ) <sub>6</sub> -A <sub>15</sub> <i>CGGTTGGTGTGGTTGG</i>	155 $\pm$ 1
DNA probe-10	HS-(CH <sub>2</sub> ) <sub>6</sub> -A <sub>15</sub> <i>GGTTGGTGTGGTTGG</i>	154 $\pm$ 1

Note: GG involved in folding G4. Italic type, *e.g.*, *TC*, indicated the liker part.

#### 4.3.6 Proof Concept

To proof, an assumption of the pH-induced structural arrangement, the conformations of DNA in various pHs were investigated using CD spectroscopy (Fig. 4.3). For free strand of G4 DNA at a concentration of 10  $\mu$ M without complementary DNA (cDNA), The dominant positive and negative peaks of the loop-like structure at 260 and 240 nm were observed, respectively, in 0.1 M sodium acetate (pH 4) with 0.25 M NaCl and 0.01 M KCl. When the pH of the DNA solutions increased to the basic range, the characteristic of the G4 structure had clearly identified by a gradual peak shift to 290 and 250 nm of positive and negative bands (Fig. 4.3a), respectively. Noted, the thrombin binding aptamer (TBA) adopts a chair type anti-parallel structure in solution<sup>8-9</sup>, that CD spectrum has a positive band near 290 nm and a negative band near 260 nm that is characteristic of an antiparallel structure. The design poly-A modified TBA displayed the corresponding band with the reference TBA. In the existence of cDNA at a concentration of 10  $\mu$ M, the CD spectra have a more pronounced positive band between 260 to 280 nm and deep negative peak near 245 nm (Fig. 4.3b), which is the characteristic band of dsDNA. The indicative wavelength of chair-type G-4, ssDNA, and dsDNA of partial hybridization was shown in table 4.3.

**Table 4.3** CD band of DNA conformations

	Band	
	Positive	Negative
<b>Hairpin (Loop-like)</b>	260	240
<b>G4 (Chair-type)</b>	290	250
<b>dsDNA</b>	260-280	245

Based on duplex-induced non-crosslinking aggregation cascade, the deformation of G4 on AuNP surface is in charge of a duplex formation. The partial hybridization of duplex DNA disturbed the colloidal stability, regarding the color of the solution change to purple-blue with pH (Fig. 4.4a). The corresponding plasmonic peak shift to longer wavelength was found to be happened after the addition of 1.0  $\mu\text{M}$  cDNA in 0.1 M sodium buffer with a wide range of pH from 4 to 8, containing 0.25 M NaCl. It is likely due to the significant reduction of the entropic effect and electrostatic repulsion. The ratio of absorption (ratio A) was expressed as the difference between the initial and final maximum absorption wavelengths (Fig. 4.4b). Eventually, the degree of aggregation of each pH was performed by calculating the ratio A of sample/control where the sample was a solution of G4-AuNPs with complementary DNA (cDNA), denoted dsDNA-AuNPs, and control was a solution of G4-AuNPs (Fig. 4.4c).

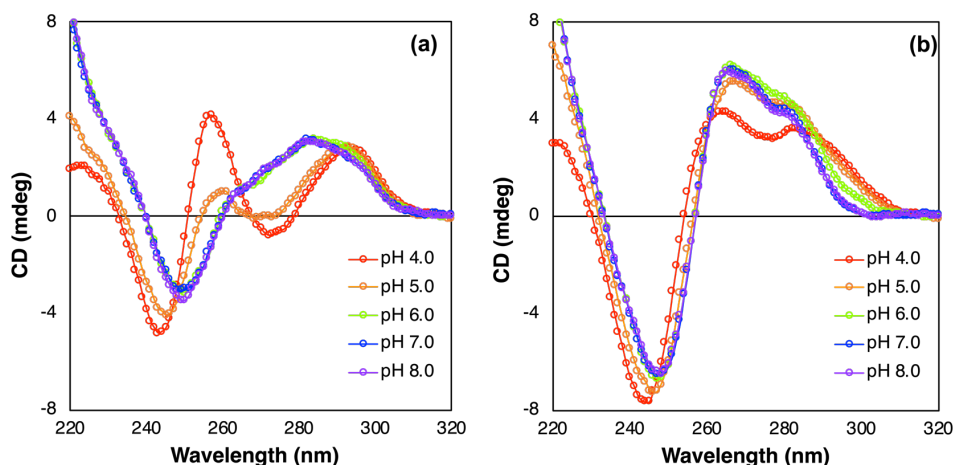


**Figure 4.3** The CD spectrum of d(A<sub>15</sub>TCTCGGTTGGTGTGGTTGG) at a concentration of 10  $\mu\text{M}$  in absence (a), and presence (b) of its 19-nt complementary DNA (cDNA-6) at a concentration of 10  $\mu\text{M}$  in 0.1 M sodium buffer in at various pH from 4 to 8, containing 0.25 M NaCl and 0.01 M KCl.

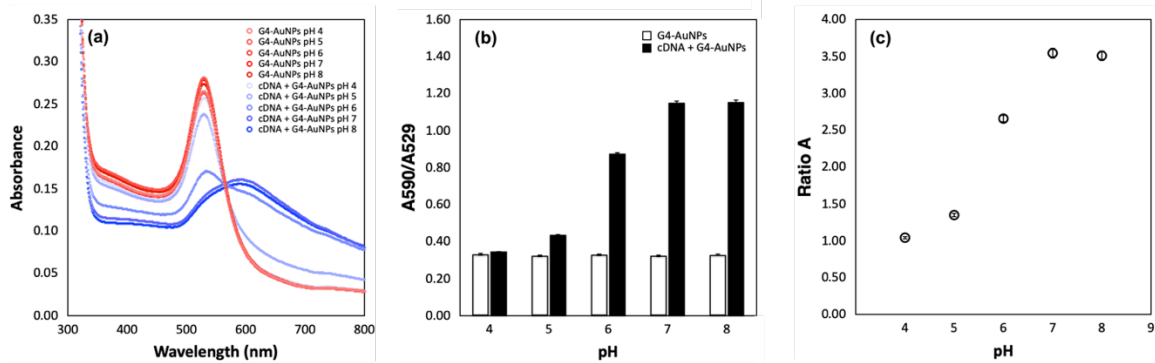


**Figure 4.4** (a) The UV-Vis spectra of 1.0 OD AuNPs with d(HS-(CH<sub>2</sub>)<sub>6</sub>-A<sub>15</sub>TCTCGGTTGGTGTGGTTGG) in presence and absence of its 19-nt complementary DNA (cDNA-6) (1.0 μM) in 0.1 M sodium buffer at various pH from 4 to 8, containing 0.25 M NaNO<sub>3</sub>. The corresponding A<sub>590</sub>/A<sub>529</sub> (b) and ratio absorption (ratio A) of sample (cDNA + G4-AuNPs) over control (G4-AuNPs) of its 19-nt complementary DNA (cDNA-6) (c).

#### 4.3.7 Detection Mechanism

The aggregation mechanism was clarified using small angle X-ray scattering (SAXS) technique, whether the partial hybridization of G4-AuNPs could be achieved and could induce an aggregation based on non-crosslinking behavior. On the one hand, the pH-dependency of 1.0 OD DNA probe-1-AuNPs (34-nucleotides (nt)) had been investigated with 1.0 μM cDNA-6 (19-nt) at various pH for the proof of the non-crosslinking phenomenon. On the other hand, 1.0 OD DNA probe-1-AuNPs (34-nt) had also been studied with 1.0 OD DNA probe-11-AuNPs (19-nt) for crosslinking aggregation. The intensity profiles of the colloidal solution of DNA probe-1 was found to associate with the notion that particles remained dispersed in all pHs since the profiles were well fitted, as shown in the red solid curves in Fig. 4.5a. However, the solution of

DNA probe-11-AuNPs, a complementary sequence of DNA probe-1, the aggregation was clearly noticed from the interferent peak arising in acidic solution while the colloidal solution displayed a good dispersion in basic solution Fig. 4.5d. In the presence of 1.0  $\mu\text{M}$  cDNA-6, partial hybridization was found to induce nucleation of particles toward non-crosslinking aggregation (Fig. 4.5b). Nevertheless, crosslinking aggregation was found to happen after adding DNA prob-11-AuNPs into DNA probe-1-AuNP solution (Fig. 4.5e). The corresponding scattering profiles of a spherical particle with a radius  $R$  could be fitted with Eq. 1 mentioned in section 2.3.4 of chapter 2, and the mean radius of gold colloid was calculated about 18.9 nm, afterward. This supports the notion of the dominant scattering noticeably belongs to heavier gold atoms<sup>5</sup>.

The aggregation was clearly noticed from the interferent peak arising, dependent on pH (Fig. 4.5b,e). The peak position around  $q = 0.14$  and  $0.17 \text{ nm}^{-1}$  were observed for non-crosslinking and crosslinking systems, respectively. The greater the peak position, the narrower interparticle distance between NPs was identified at the aggregation state. The SAXS profiles were analysed by considering the interference between the particles in terms of the structure factor  $S(q)$ , as shown in Eq. 2 ascribed in section 2.3.4 of chapter 2. Then curve fitting with the calculated  $S(q)$  was performed based on a paracrystalline theory using a disordered face-centered cubic structure<sup>6</sup>, showing in Fig. 4.5c,f. As expected, the center-to-center distance did not seem to depend on the pH. The gap between the particle surfaces was estimated using the calculated mean value from fitting analysis. The gap value between nanoparticle surfaces was *ca.* 19.0 and *ca.* 5.7 nm for non-crosslinking and crosslinking aggregations by partial inter-stranded hybridization, respectively. The larger estimated value was strong evidence to confirm that aggregation

was generated without crosslinking between the particles (Fig 4.6). Even if, the target hybridized partially to the DNA probe on the AuNP core.

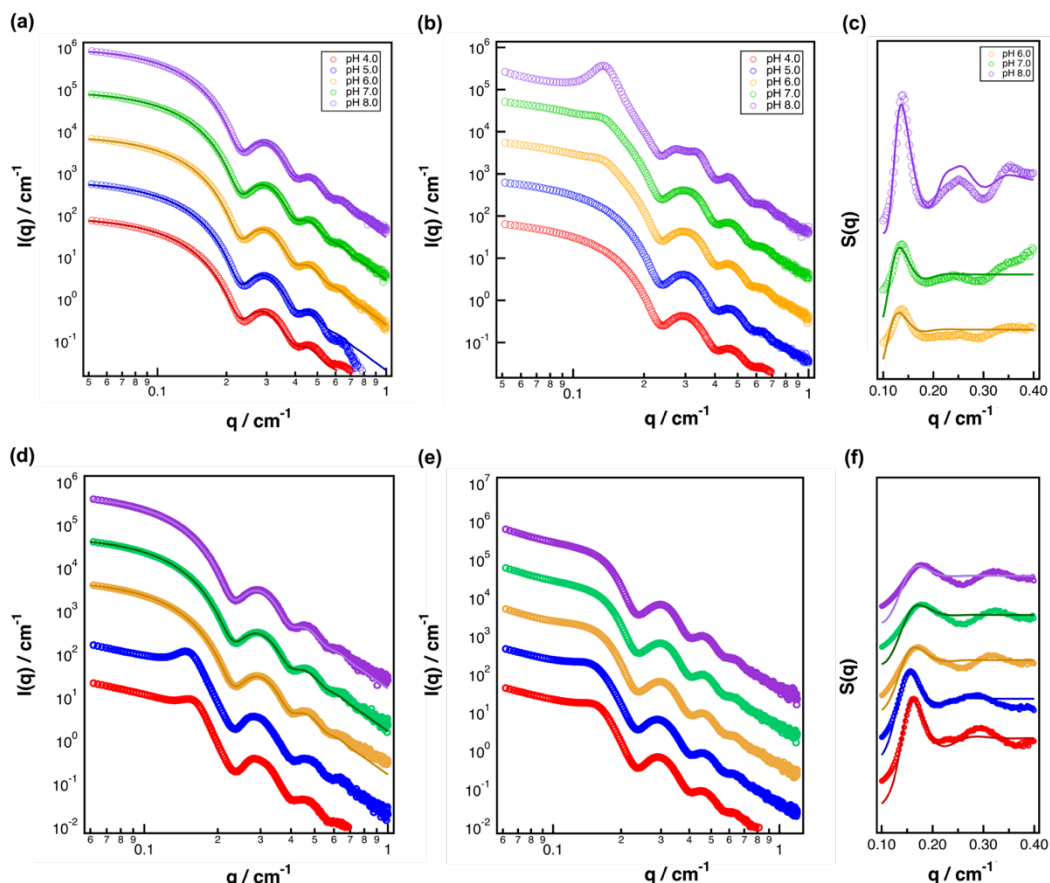


**Figure 4.5** SAXS intensity data of 1.0 OD AuNPs with d(HS-(CH<sub>2</sub>)<sub>6</sub>-A<sub>15</sub>TCTCGGTTGGTGTGGTTGG) in absence (a), and presence (b) of its 19-nt complementary DNA (cDNA-6) (1.0 μM), and in absence (d), and presence (e) of 1.0 OD AuNPs with (HS-(CH<sub>2</sub>)<sub>6</sub>-CCAACCACACCAACCGAGA) in 0.1 M sodium buffer, containing 0.25 M NaNO<sub>3</sub>. The data were taken at various pH: 4 (red), 5 (blue), 6 (yellow), 7 (green), and 8 (purple). The solid lines in (a) (d) and (c) (f) are the fitting curves of form and structure factors, respectively. The data of (a) (b) (c) is based on non-crosslinking aggregation. The data of

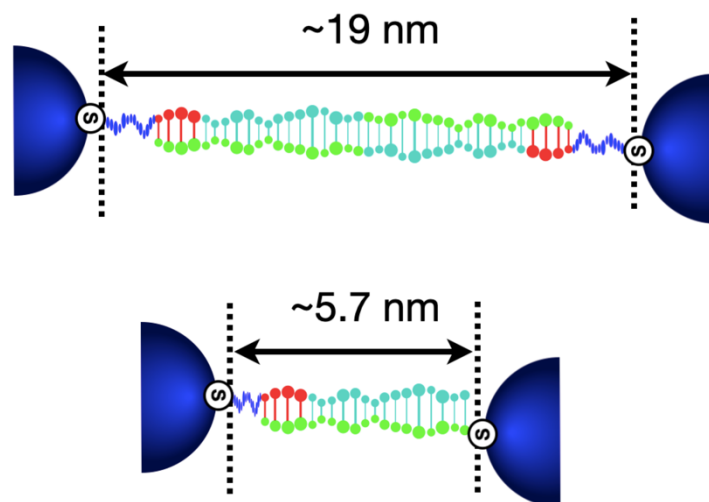


**Figure 4.6** The gap between nanoparticle surfaces of duplex-AuNPs by partial inter-stranded hybridization based on non-crosslinking (top) and crosslinking (bottom) phenomena.

## 4.4 Results and Discussion

### 4.4.1 Optimization of Involving Parameters

Five involving parameters have been studied. First, the number of linker bases directly affects the loop-like part of hairpin conformation. The linker part was varied from no-linker up to four linker bases. It was found that the more nucleotide numbers provide, the more stable of hairpin due to the greater increase of electrostatic repulsion in the loop. As shown in Fig 4.7, the relatively high degree of aggregation was shown for no-linker and one base of the linker, regarding no significant difference in aggregation amount among

pHs. On the other hand, two, three, and four linker bases provided a gradual aggregation in basic rather in acidic conditions. It is likely because the linker is long enough to maintain the hairpin-like structure (intrastranded duplex) in acidic solution, resulting in the difficulty of interstranded duplex formation. Even if in acidic conditions, no aggregation could be observed, but aggregation amount could be tuned in the next parameters. Hence, there are 3 candidate sequences that could be used in further experiments.

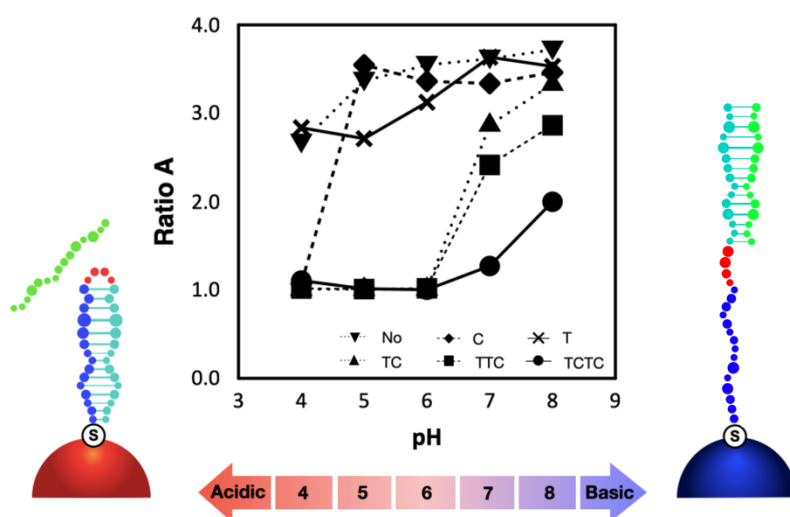


**Figure 4.7** (a) The absorption ratio of 1.0 OD AuNPs with d(HS-(CH<sub>2</sub>)<sub>6</sub>-A<sub>15</sub>linkerGGTTGGTGTGGTTGG) with various linkers: no, C, T, TC, TTC, and TCTC after adding 1.0 μM cDNA-3 (15-nt) in 0.1 M sodium buffer, containing 0.25 M NaNO<sub>3</sub>. The data were taken over a wide range of pH and collected at 10 min after adding cDNA-3. The hairpin-like (loop-like) intrastranded (left) and interstranded duplex formation (right) on AuNPs in acidic and basic solutions were shown, respectively.



Next, the effect of salt ( $\text{NaNO}_3$ ) on a partial hybridization toward non-crosslinking was examined (Fig 4.8). The interstrand duplex-induced aggregation was found to depend on salt concentration due to the screening of electrostatic repulsion. The results show that no aggregation was observed at all pHs at a low salt concentration of 0.1 M. The significant aggregation was shown in basic condition at 0.25 M. However, the particles aggregated with no significant difference in the degree of aggregation among pHs when the concentration of salt is higher than 0.5 M. Then 0.25 M was chosen as the optimum value. In addition, the effect of reaction time, elapsed from cDNA addition, was also studied. It was found that the aggregation amount increased with time up to 10 min. in basic condition. Then the aggregation reached a peak and remained constant (Fig 4.9). So, 10 min was chosen as the optimum time.

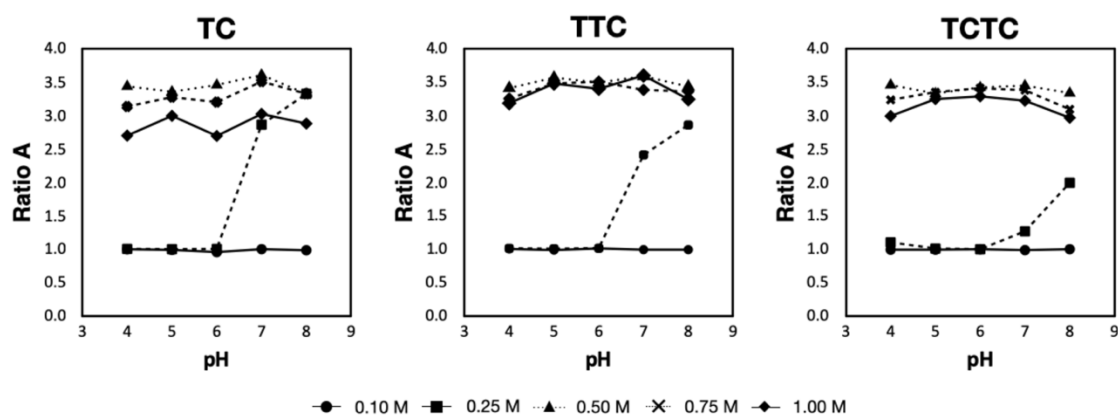


**Figure 4.8** The absorption ratio of 1.0 OD AuNPs with  $\text{d}(\text{HS}-(\text{CH}_2)_6-\text{A}_{15}\text{linkerGGTTGGTGTGGTTGG})$  with three different linkers: *TC* (left), *TTC* (middle), and *TCTC* (right) after adding 1.0  $\mu\text{M}$  cDNA-3 (15-nt) in 0.1 M sodium buffer, containing various salt ( $\text{NaNO}_3$ ) concentrations: 0.10 (●), 0.25 (■), 0.50 (▲), 0.75 (×), and 1.00 M (◆). The data were taken over a wide range of pH and collected at 10 min after adding cDNA-3.

The effect of the length of complementary DNA was investigated. The length of cDNA was varied, including each part of DNA probe— (i) G4, (ii) G4 and Linker, and (iii) G4, linker, and poly-A—with different length of cDNA (Fig 4.10). Noted, the hybridization starts from the bottom-up direction. It was hypothesized that different lengths of complementary strands would respond to the degree of aggregation differently due to duplex rigidity and hybridization affinity. The author noticed that the hybridized part should be covered the G4 (15-nt) and linker (2- for *TC*, 3- for *TTC*, and 4-nt for *TCTC*) parts (Fig 4.10d), at which 17-, 18- or 19-nt of complementary target strand, matching with the DNA probe, was proposed to use in order to initiate partial hybridization. As expected, the higher rigidity of double helix displayed a higher degree of aggregation, with a similar aggregation phenomenon of full-match and partial-match duplex formations.

The other factor is the types of a spacer, examining A, T, C, and G with the same length of 15-nt (Fig 4.11). Using SAXS, the AuNPs with  $d(\text{HS}-(\text{CH}_2)_6-\text{x}_{15}\text{TCTC}\underline{\text{GGTTGGTGTGGTTGG}})$  where x is a spacer: adenine (A), thymine (T), cytosine (C), guanine (G), and random base (R) were investigated in this experiment. The author hypothesized that the different nucleobase would respond to the ability of protonation in acidic conditions differently, resulting in the different properties of conformational arrangement. The partial hybridization-induced G4-AuNP aggregation was observed with all types of spacer except guanine-type due to the formation of the G4 structure at spacer part. Eventually, it was found that the only sequence, showing conformational arrangement depending on pH due to the ability of protonation in acidic condition, was

Poly-A-modified TBA on AuNP core (see Fig. 4.1b). Poly-T-, poly-C- and random spacer-modified G4-AuNPs, however, provided pH-independent aggregation.

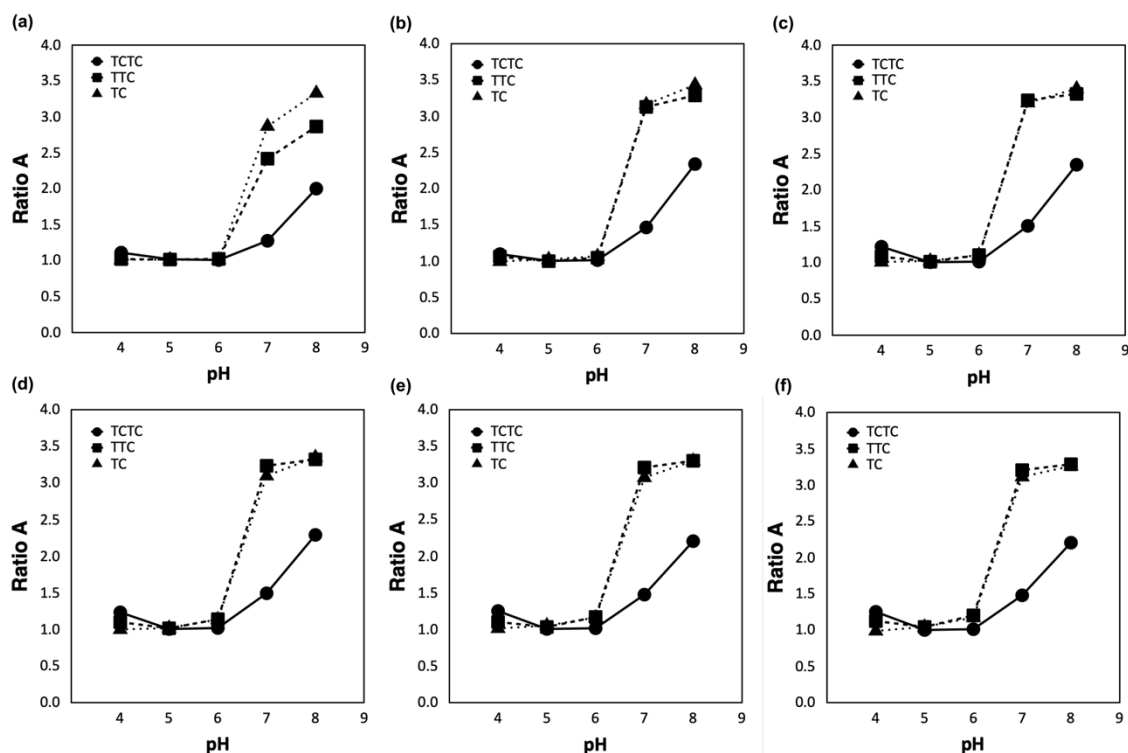


**Figure 4.9** The absorption ratio of AuNPs with  $d(\text{HS}-(\text{CH}_2)_6-\text{A}_{15}\text{linkerGGTTGGTGTGGTTGG})$  with three different linkers: TC ( $\blacktriangle$ ), TTC ( $\blacksquare$ ), and TCTC ( $\bullet$ ) after adding cDNA-3 (15-nt) in 0.1 M sodium buffer, containing 0.25 M  $\text{NaNO}_3$ . The data were taken over a wide range of pH and collected at 5 (a), 10 (b), 15 (c), 20 (d), 25 (e), and 30 min (f) after adding cDNA-

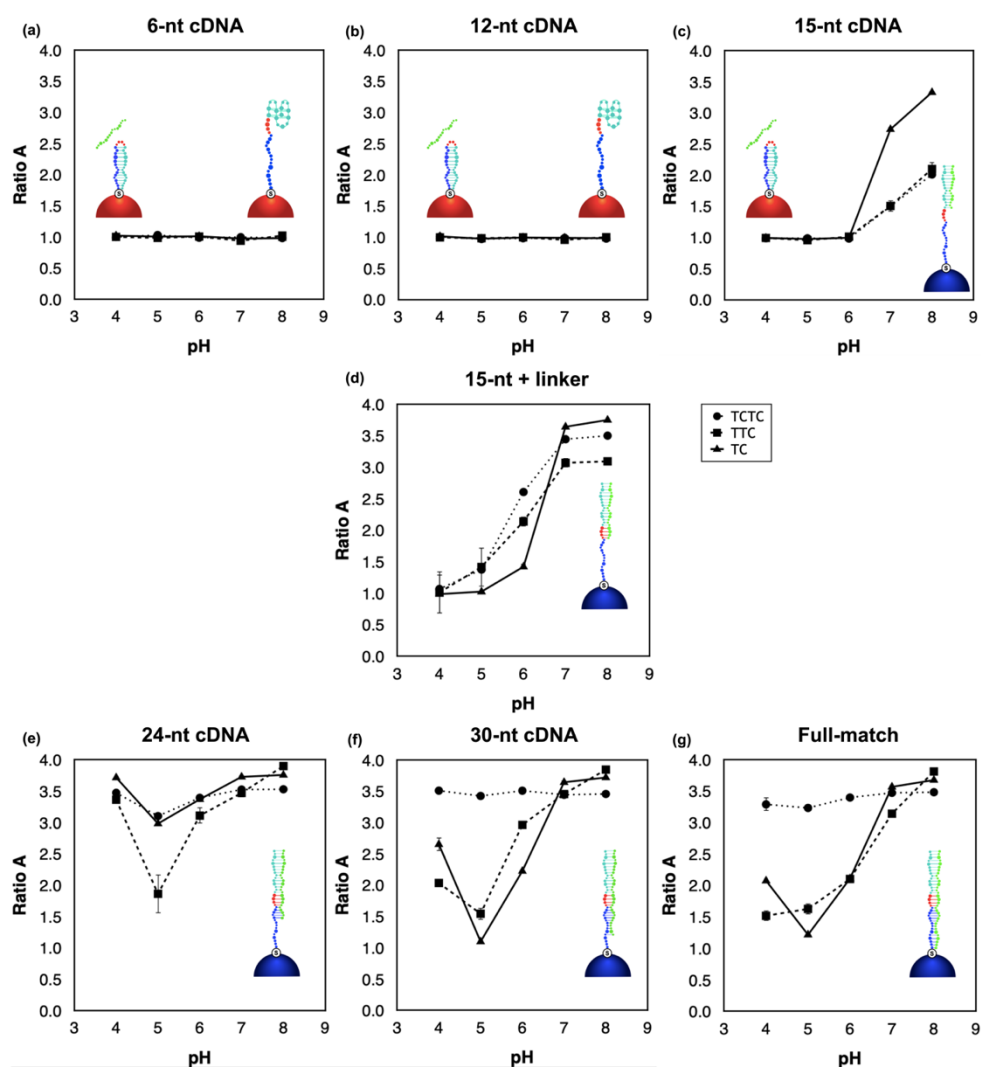


**Figure 4.10** The absorption ratio of 1.0 OD AuNPs with  $d(\text{HS}-(\text{CH}_2)_6-\text{A}_{15}\text{linkerGGTTGGTGTGGTTGG})$  with three different linkers: *TC* ( $\blacktriangle$ ), *TTC* ( $\blacksquare$ ), and *TCTC* ( $\bullet$ ) after adding different lengths of 1.0  $\mu\text{M}$  cDNA in 0.1 M sodium buffer, containing 0.25 M  $\text{NaNO}_3$ . The 6- (a), 12- (b), and 15-nt cDNA (c) hybridized “partially” to G4 (green part) of DNA probe. The 17- (for *TC*)/18- (for *TTC*)/19-nt (for *TCTC*) cDNA (d) hybridized “partially” to G4 and linker (green, and red parts) of DNA probe. The 24- (e), 30- (f), and 32- (for *TC*)/33- (for *TTC*)/34-nt (for *TCTC*) cDNA (g) hybridized “partially” or “fully” to whole DNA probe (green, red, and blue parts). The data were taken over a wide range of pH and collected at 10 min after adding cDNA.

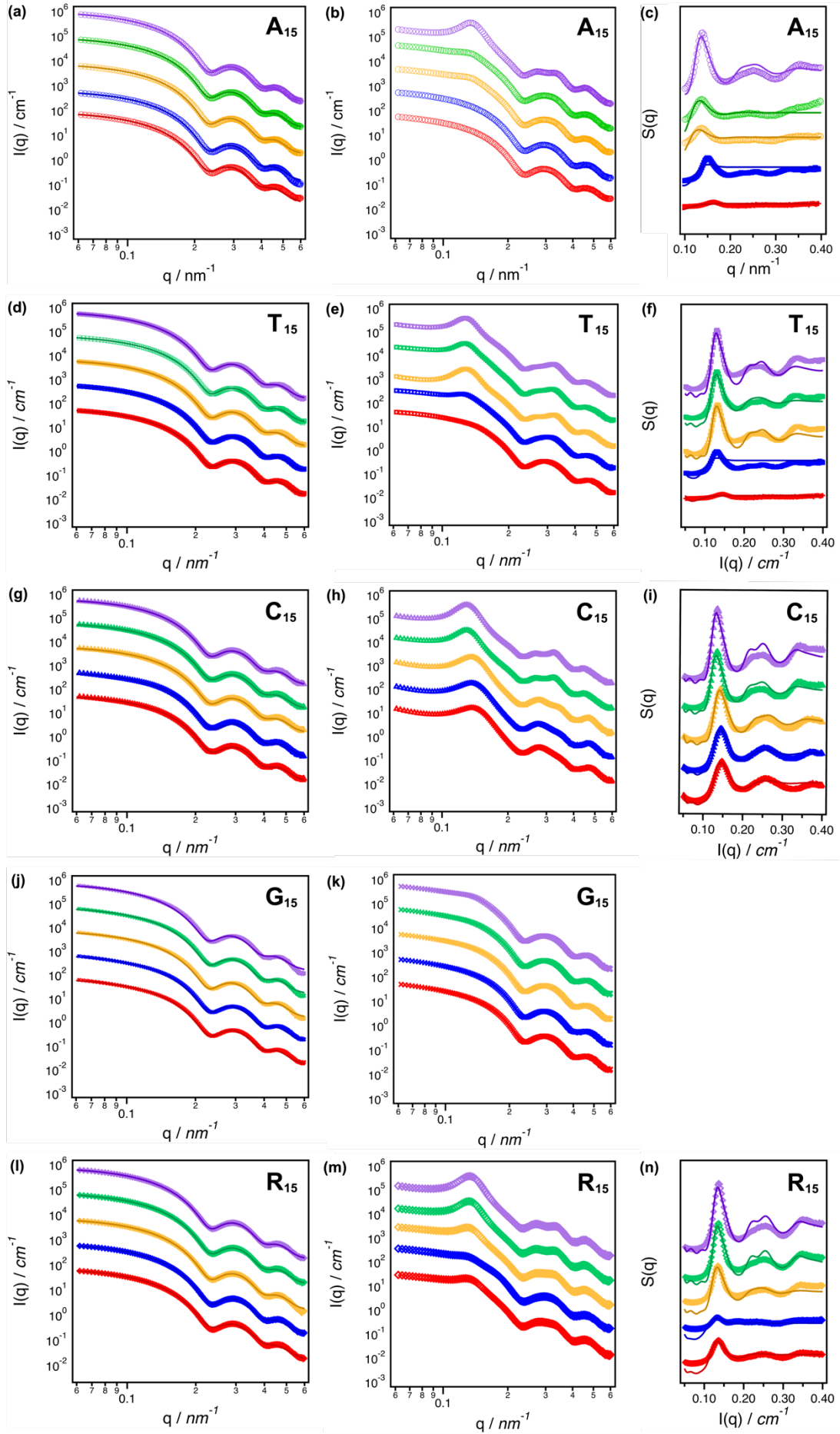


**Figure 4.11** SAXS intensity data for 1.0 OD AuNPs with d(HS-(CH<sub>2</sub>)<sub>6</sub>-x<sub>15</sub>TCTCGGTTGGTGTGGTTGG) where x is a spacer: adenine (A), thymine (T), cytosine (C), guanine (G), and random base (R) in 0.1 M sodium buffer, containing 0.25 M NaNO<sub>3</sub>. The intensity data for the particles without 1.0 μM 19-nt cDNA-6 were shown in (a), (d), (g), (j), and (l). The intensity data for the particles after adding 1.0 μM 19-nt cDNA-6 were shown in (b), (e), (h), (k), and (m). The corresponding structure factors for different spacers: adenine (c), thymine (f), cytosine (i), and random base (n). The data were taken at various pHs: 4 (red), 5 (blue), 6 (yellow), 7 (green), and 8 (purple). The solid lines in (a) (d) (g) (j) (l) and (c) (f) (i) (n) are the fitting curves of form and structure factors, respectively.

## 4.5 Conclusions

This work presents an inter-stranded partial hybridization as a new mechanism based on a non-crosslinking platform. The aggregation of G4-AuNPs was found to depend on pH using poly-A-modified G4-AuNPs, which made up the hairpin-like structure in acidic solution and made up the duplex formation in basic solution. The colloidal stability was measured at 10 min after the addition of complementary DNA to the colloidal system. This new platform of G4-AuNPs showed a good structural arrangement property with simple and fast aggregation, induced by partial hybridization. Last but not least, the author strongly believes that non-crosslinking aggregation via inter-stranded partial hybridization could apply to use as an alternative diagnostic tool, *e.g.*, pH sensor as well as it could be a basic idea for biosensors application of interests in future.

#### 4.6 References

- (1) Sato, K.; Hosokawa, K.; Maeda, M. Rapid Aggregation of Gold Nanoparticles Induced by Non-Cross-Linking DNA Hybridization. *J. Am. Chem. Soc.* **2003**, 125, 8102–8103.
- (2) McConnell, E. M.; Bolzon, R.; Mezin, P.; Frahm, G.; Johnston, M.; DeRosa, M. C. pHAST (pH-Driven Aptamer Switch for Thrombin) Catch-and-Release of Target Protein. *Bioconjugate Chem.* **2016**, 27, 1493–1499.
- (3) Demers, L. M.; Mirkin, C. A.; Mucic, R. C.; Reynolds III, R. A.; Letsinger, R. L.; Elghanian, R.; Viswanadham, G. A fluorescence-based method for determining the surface coverage and hybridization efficiency of thiol-capped oligonucleotides bound to gold thin films and nanoparticles, *Anal. Chem.*, 2000, 72, 5535–5541.
- (4) Chuaychob, S.; Thammakhet-Buranachai, C.; Kanatharana, P.; Thavarungkul, P.; Buranachai, C.; Fujita, M.; Maeda, M. A Nanobiosensor for the Simple Detection of Small Molecules using Non-Crosslinking Aggregation of Gold Nanoparticles with G-Quadruplexes. *Anal. Methods*. **2020**, 12, 230–238.
- (5) Sato, K.; Hosokawa, K.; Maeda, M. Rapid aggregation of gold nanoparticles induced by non-cross-linking DNA hybridization. *J. Am. Chem. Soc.* **2003**, 125, 8102–8103.
- (6) Fujita, M.; Katafuchi, Y.; Ito, K.; Kanayama, N.; Takarada, T.; Maeda, M. Structural study on gold nanoparticle functionalized with DNA and its non-cross-linking aggregation. *J. Colloid Interface Sci.* **2012**, 368, 629–35.
- (7) Smirnov, I; Shafer, R. H. Effect of Loop Sequence and Size on DNA Aptamer Stability. *Biochemistry* **2000**, 39, 1462–1468.



- (8) Schultze, P.; Smith, F. W.; Feigon, J. Refined Solution Structure of the Dimeric Quadruplex Formed From the Oxytricha Telomeric Oligonucleotide d(GGGGTTTTGGGG). *Structure* **1994**, 2, 221–233.
- (9) Haider, S.; Parkinson, G.N.; Neidle, S.; Crystal Structure of the Potassium Form of an Oxytricha Nova G-quadruplex. *J. Mol. Biol.* **2002**, 320, 189–200.

## **Chapter 5**

### **General Conclusions and Perspective**

## General Conclusions and Perspective

The present study demonstrates a biosensing platform based on G-quadruplex DNA-functionalized gold nanoparticles (G4-AuNPs) as an excellent sensing element which is cable to apply in biosensing applications for molecular detections of a hazardous small molecule “cisplatin” and a macromolecule “thrombin”, employed non-crosslinking phenomenon. Besides, the newly inter-stranded partial hybridization of the duplex on AuNP core has discovered the first time to induce non-crosslinking aggregation using the G4-AuNPs with an additional pH-dependent property.

The author illustrates the approach with the developed: (i) ultrasensitive colorimetric sensor for real-time cisplatin (5 min) and thrombin (10 min) test, which offers a wide dynamic range and acceptable limit of detection, (ii) on-demand turnability of the properties of interest: the degree of colloidal aggregation by the ease of space insertion of DNA probe, and the sensitivity of detection for high-performance biosensor, and (iii) high affinity and specificity for applicable determination in the real sample, *e.g.*, human serum.

Besides, the author elucidates the novel mechanism of duplex-induced non-crosslinking aggregation via inter-stranded “partial” hybridization toward a pH-dependent structural arrangement of G4-AuNPs. The discovered phenomenon allows non-canonical secondary structures (G4), which has a functionally important role in the human genome, to broaden a new avenue of DNA-functionalized AuNPs on the basis of non-crosslinking aggregation. The author strongly believes that the novel G4-AuNPs could be a fascinating platform for new generation nanodevices in various applications, especially biosensor and medical diagnosis in the future.

## Bibliography

### List of Publications

1. **S. Chuaychob**, C. Thammakhet-Buranachai, P. Kanatharana, P. Thavarungkul, C. Buranachai, M. Fujita, and M. Maeda, A Nanobiosensor for the Simple Detection of Small Molecules Using Non-crosslinking Aggregation of Gold Nanoparticles with G-quadruplexes, *Anal. Methods.*, 2020, 12, 230. (*The front cover of the issue*)



2. **S. Chuaychob**, M. Fujita, and M. Maeda, G-quadruplex-Gold Nanoparticles Based on Non-crosslinking Aggregation Platform: Real-time Biomolecule Sensor with On-demand Tunable Properties, *Manuscript in preparation*.
3. **S. Chuaychob**, M. Fujita, and M. Maeda, Partial Hybridization of DNA-Gold Nanoparticles Conjugated Material Induced Rapid Non-crosslinking Aggregation, *Manuscript in preparation*.

## List of Presentations

### *Invited Lecture*

**Colorimetric Thrombin Sensor using DNA Aptamer-modified Gold Nanoparticles.** *"Asian International Symposium - Colloid and Surface Chemistry-"* The 100th CSJ Annual Meeting, 22-25 March 2020. At Tokyo University of Science, Chiba, Japan.

### *International conferences*

#### **Poster presentations**

1. **S. Chuaychob**, C. Thammakhet-Buranachai, P. Kanatharana, P. Thavarungkul, C. Buranachai, M. Fujita, and M. Maeda, A Nanobiosensor for the Simple Detection of Small Molecules Using Non-crosslinking Aggregation of Gold Nanoparticles with G- quadruplexes. Trace Analysis and Biosensor International Symposium I, 10-11 February 2020. At Prince of Songkla University, Hat Yai, Songkhla, Thailand.
2. **S. Chuaychob**, M. Fujita, and M. Maeda, Development of G-quadruplex-Gold Nanoparticle Conjugate Material for Cisplatin Sensor. The 50th General Assembly and 47th IUPAC World Chemistry Congress, 5-12 July 2019. At Paris, France.

#### **Oral presentations**

1. **S. Chuaychob**, M. Fujita, and M. Maeda, DNA Aptamer-Gold Nanoparticles for Colorimetric Protein Assay. OKINAWA Colloids 2019, 3-8 November 2019. At Okinawa, Japan.

2. **S. Chuaychob**, M. Fujita, and M. Maeda, G-quadruplex-functionalized Gold Nanoparticles as a New Colorimetric pH Sensor. The 12th SPSJ International Polymer Conference (IPC2018), 4-7 December 2018. At Hiroshima, Japan.

### *National conferences*

#### **Poster presentations**

1. **S. Chuaychob**, M. Fujita, and M. Maeda, Non-crosslinking Aggregation of Gold Nanoparticles with G-quadruplexes for Simple Cisplatin Detection. The 69th SPSJ Annual Meeting, 27-29 May 2019. At Fukuoka, Japan.
2. **S. Chuaychob**, M. Fujita, and M. Maeda, Colorimetric Thrombin Sensor Based on G-quadruplex-grafted Gold Nanoparticles. RIKEN Summer School 2019, 7-8 October 2019. At Chiba, Japan.
3. **S. Chuaychob**, M. Fujita, and M. Maeda, pH Sensor via Tunable G-quadruplex Structure on Gold Nanoparticle Surface. The 40th Annual Meeting of the Japanese Society for Biomaterials, 12-13 November 2018. At Kobe, Japan.
4. **S. Chuaychob**, P. Thavarungkul, P. Kanatarana, C. Buranachai, C. Thammakhet-Buranachai, M. Fujita, and M. Maeda, G-quadruplex-Functionalized Gold Nanoparticles, A New Door for Cisplatin Detection. RIKEN Summer School 2018, 26-27 September 2018. At Tsukuba, Japan.

#### **Oral presentations**

1. **S. Chuaychob**, M. Fujita, and M. Maeda, G-quadruplex Aptamer-based Colorimetric Protein Sensor. The 41st Annual Meeting of the Japanese Society for Biomaterials, 24-26 November 2019. At Tsukuba, Japan.

2. **S. Chuaychob**, M. Fujita, and M. Maeda, Colorimetric Aptasensor-based Gold Nanoparticles for Thrombin Detection. The 68th Symposium on Macromolecules, 25-27 September 2019. At Fukui, Japan.
3. **S. Chuaychob**, M. Fujita, and M. Maeda, A Colorimetric Thrombin Sensor Using G-quadruplex-grafted Gold Nanoparticles. The 68th SPSJ Annual Meeting, 29-31 May 2019. At Osaka, Japan.
4. **S. Chuaychob**, M. Fujita, and M. Maeda, A Sensitive Colorimetric pH Sensor via G-quadruplex-conjugated Gold Nanoparticles. The 67th SPSJ Symposium on Macromolecules, 12-14 September 2018. At Sapporo, Japan.
5. **S. Chuaychob**, P. Thavarungkul, P. Kanatarana, C. Buranachai, C. Thammakhet-Buranachai, M. Fujita, and M. Maeda, G-quadruplex-Functionalized Gold Nanoparticles, A New Door for Cisplatin Detection. The 67th SPSJ Annual Meeting, 23-25 May 2018. At Nagoya, Japan.

## Awards

1. Trace Analysis and Biosensor International Symposium I, **Best Poster Presentation** (February 2020).  
“A Nanobiosensor for the Simple Detection of Small Molecules Using Non-crosslinking Aggregation of Gold Nanoparticles with G- quadruplexes.”
2. RIKEN Summer School 2019, **Poster Award Chemistry Prize** (October 2019).  
“Colorimetric Thrombin Sensor Based on G-quadruplex-grafted Gold Nanoparticles”
3. The 40th Annual Meeting of the Japanese Society for Biomaterials, **Poster Award** (November 2018).

“pH Sensor via Tunable G-quadruplex Structure on Gold Nanoparticle Surface.”

4. RIKEN Summer School 2018, **Poster Award Chemistry Prize** (September 2018).

“G-quadruplex-Functionalized Gold Nanoparticles, A New Door for Cisplatin Detection.”